

University of New Hampshire

University of New Hampshire Scholars' Repository

Doctoral Dissertations

Student Scholarship

Winter 2019

FATIGUE ASSESSMENT OF COMPLEX STRUCTURAL COMPONENTS OF STEEL BRIDGES INTEGRATING FINITE ELEMENT MODELS AND FIELD-COLLECTED DATA

Maryam Mashayekhizadeh
University of New Hampshire, Durham

Follow this and additional works at: <https://scholars.unh.edu/dissertation>

Recommended Citation

Mashayekhizadeh, Maryam, "FATIGUE ASSESSMENT OF COMPLEX STRUCTURAL COMPONENTS OF STEEL BRIDGES INTEGRATING FINITE ELEMENT MODELS AND FIELD-COLLECTED DATA" (2019).

Doctoral Dissertations. 2493.

<https://scholars.unh.edu/dissertation/2493>

This Dissertation is brought to you for free and open access by the Student Scholarship at University of New Hampshire Scholars' Repository. It has been accepted for inclusion in Doctoral Dissertations by an authorized administrator of University of New Hampshire Scholars' Repository. For more information, please contact Scholarly.Communication@unh.edu.

FATIGUE ASSESSMENT OF COMPLEX STRUCTURAL
COMPONENTS OF STEEL BRIDGES INTEGRATING FINITE
ELEMENT MODELS AND FIELD-COLLECTED DATA

BY

MARYAM MASHAYEKHIZADEH

BS, Shahid Rajaee Teacher Training University, 2008
MS, Isfahan University of Technology, 2012

DISSERTATION

Submitted to the University of New Hampshire
In Partial Fulfillment of
The Requirement for the Degree of

Doctor of Philosophy
in
Civil Engineering

December 2019

This thesis/dissertation was examined and approved in partial fulfillment of the requirements for the degree of
Doctor of Philosophy in Civil Engineering by:

Thesis/Dissertation Director, Erin Santini-Bell,
Professor Civil and Environmental Engineering

Raymond Cook, Associate Professor,
Civil and Environmental Engineering

John Leander,
Associate Professor Civil and Architectural Engineering
KTH Royal Institute of Technology, Sweden

Masoud Sanayeい,
Professor, Civil and Environmental Engineering
Tufts University

Martin Wosnik,
Associate Professor, Mechanical Engineering

On 12/10/2019

Approval signatures are on file with the University of New Hampshire Graduate School.

TABLE OF CONTENTS

ACKNOWLEDGMENTS	IX
DEDICATION.....	X
NOMENCLATURE	XI
LIST OF TABLES:.....	XIII
LIST OF FIGURES:	XIV
ABSTRACT.....	XVIII

CHAPTER	PAGE
INTRODUCTION	1
1.1 Motivation	2
1.2 Research contribution.....	4
1.2.1 Research tasks.....	6
1.3 Challenges and Limitations	7
1.4 Outline of the dissertation	8
REFERENCES	11
FATIGUE IN WELDED STRUCTURES.....	12
2.1 Introduction	12
2.2 Geometric impacts of welded structural components	12
2.3 Fatigue assessment methods.....	13
2.3.1 Nominal stress method	16
2.3.2 Hotspot stress method.....	19
2.3.3 Effective notch stress method	25
2.3.3 Linear elastic fracture mechanics method–LEFM.....	28
REFERENCES	33
THE CASE-STUDY: THE MEMORIAL BRIDGE	36

3.1	Introduction	36
3.3	The instrumentation plan of the Memorial Bridge	38
3.4	Data collection program at the Memorial Bridge.....	40
3.4.1	Field-collected SHM data for fatigue assessment	42
3.5	Truck load test at the Memorial Bridge.....	44
	REFERENCES	46
	THREE-DIMENSIONAL MULTISCALE FINITE ELEMENT MODELS FO IN-SERVICE PERFORMANCE ASSESSMENT OF BRIDGES.....	47
4.1	Abstract.....	47
4.2	Introduction	48
4.3	Multiscale methodology	51
4.3.1	Axial Load	54
4.3.2	Bending Moment	57
4.3.3	Torsion.....	59
4.3.4	Shear force	61
4.3.5	Verification of the developed constraint equations	63
4.4	The Case Study: The Memorial Bridge.....	67
4.5	Finite Element Model Categories.....	68
4.5.1	Beam element model (B-model).....	69
4.5.2	Shell element model (SH-model)	70
4.5.3	Multi-scale sub-structure model (S-S model).....	71
4.5.4	Multi-scale modeling (M-S model)	72
4.6	Model Verification	76
4.6.1	Comparison of the predicted and the field data natural frequencies	77
4.6.2	Comparison of the predicted and the field data strain response	78
4.6.3	Statistical post-processing	82
4.7	Conclusions	85

Acknowledgments.....	86
REFERENCES	87
FATIGUE ASSESSMENT OF THE GUSSET-LESS CONNECTION USING FIELD DATA AND NUMERICAL MODEL	90
5.1 Abstract.....	90
5.2 Introduction	91
5.3 Fatigue Assessment methods.....	93
5.3.1 The nominal stress method	94
5.3.2 The hot-spot stress method	94
5.4 The case study: The Memorial Bridge	97
5.4.1 The bridge specifications.....	97
5.4.2 The gusset-less connection	99
5.5 The numerical model of bridge	100
5.5.1 The global model of the long-span bridges	100
5.5.2 The FE model of the case-study bridge	100
5.5.3 Verification of the developed FE models	102
5.6 Fatigue assessment of the gusset-less connection	104
5.6.1 Using the field collected SHM data.....	104
5.6.2 The hot-spot stress at the gusset-less connection	106
5.6.3 Fatigue response of the gusset-less connection using the SCFs	110
5.7 Conclusion.....	112
REFERENCES	114
FATIGUE ASSESSMENT OF A COMPLEX WELDED STRUCTURAL CONNECTION STEEL VERTICAL LIFT BRIDGE USING A THREE-DIMENSIONAL MULTI-SCALE FINITE ELEMENT MODEL.....	116
6.1 Abstract:	116
6.2 Introduction:	117
6.3 Background.....	119

6.3.1	Hotspot stress method.....	119
6.1	The Case study: The Memorial Bridge	121
6.1.1	The bridge characteristics	121
6.1.2	Load Test at the Memorial Bridge.....	123
6.2	Finite Element Models of the Memorial Bridge.....	125
6.2.1	The shell element model.....	126
6.2.2	The sub-structure model	126
6.2.3	The multi-scale model	127
6.2.4	Verification of the FE models using the load test results	133
6.3	Numerical hotspot stresses of the gusset-less connection	135
6.3.1	Variation of the hotspot stresses under static loads	136
6.3.2	Variation of the hotspot stresses under dynamic loads.....	137
6.4	Fatigue assessment using nominal and hotspot stresses.....	140
6.4.1	The traffic scenarios defined through the M-S model	140
6.4.2	Predicted fatigue remaining Life	141
6.5	Conclusion and Recommended Future Work.....	143
	Acknowledgment	144
	REFERENCES	145
	FATIGUE CRACK PREDICTION IN COMPLEX WELDED COMPONENTS OF IN-SERVICE STEEL BRIDGES USING STRUCTURAL HEALTH MONITORING DATA AND NEURAL NETWORK METHOD	147
7.1	Abstract.....	147
7.2	Introduction	148
7.2	Proposed fatigue crack detection protocol	150
7.3	Methodology.....	151
7.3.1	Using long-term SHM data for fatigue assessment	151
7.3.2	Using numerical data for fatigue assessment.....	153

7.3.3	The Neural Network Method.....	154
7.4	The case study, the Memorial Bridge.....	155
7.4.1	Details, design and construction.....	155
7.4.2	Long-term SHM program of the bridge.....	156
7.5	Fatigue assessment of the case study bridge	157
7.5.1	Define a unique period of data collection.....	157
7.5.2	Correlation of measured fatigue damage indexes.....	159
7.5.3	Simulate fatigue cracks via FE model	161
7.5.4	Train NN model for fatigue crack detection.....	168
7.5.5	Damage detection via the NN models	171
7.6	Conclusion.....	174
	REFERENCES	176
	FATIGUE CRACK PROPAGATION PERFORMANCE ASSESSMENT OF COMPLEX STRUCTURAL COMPONENTS OF STEEL BRIDGES USING A MULTI-SCALE FINITE ELEMENT MODEL.....	178
8.1	Abstract.....	178
8.2	Introduction	179
8.3	Methodology.....	182
8.3.1	Fatigue crack under mixed mode loading.....	183
8.3.2	Estimating fatigue crack direction.....	185
8.3.3	Loading conditions during crack propagation	186
8.3.4	Crack propagation modeling using finite element method.....	187
8.4	The case-study bridge.....	187
8.5	FE modeling of Memorial Bridge	188
8.5.1	Multi-scale global FE model	188
8.6	The structural analysis results	191
8.7	Modeling fatigue crack via M-S model.....	193
8.7.1	Meshing layout	193

8.7.2	Crack initiation at weld toe of gusset-less connection.....	193
8.7.3	Crack propagation at weld toe of gusset-less connection.....	195
8.8	Numerical results under crack propagation.....	195
8.9	Fatigue life prediction results using numerical data.....	198
8.10	Conclusion.....	200
	REFERENCES	202
	CONCLUSIONS AND FUTURE WORK	204
9.1	Fatigue assessment using nominal stress method.....	204
9.1.1	Using SHM data	204
9.1.2	Using numerical data	205
9.2	Fatigue assessment using hotspot stress method	207
9.3	Fatigue response estimation due to an induced crack	208
9.3.1	Using SHM data	208
9.3.2	Using numerical model.....	208
9.4	Suggestions for future research	209

Acknowledgments

This dissertation is accomplished based upon work partially supported by the National Science Foundation under Grant No. 1430260, FHWA AID: DEMO Program and funding from the NHDOT Research Advisory Council.

I would like to appreciate my advisor, Professor Erin Santini-Bell for her invaluable support in overcoming numerous obstacles that I have encountered over the course of my research. I am also grateful to the members of my committee for their patience, support and technical feedbacks which were all crucial in my dissertation development.

I would like to thank my fellow graduate students for their feedbacks, cooperation and of course friendship. In addition, I would like to express my gratitude to the faculty and staff of the Department of Civil and Environmental Engineering at the University of New Hampshire for their invaluable assistance.

Dedication

عاشق شوار نه روزی کار جهان سر لید

ناخوانده نقش مقصود راز هرگاه هست

برای عزیز ترین شریعه

پدر، مادر

و

نوشینه و مهربوش

Nomenclature

General:

SHM	structural health monitoring
DOF	degree of freedom
FE	finite element
MPC	multi-point constraint
IIW	International Institute of Welding,
3D	three-dimensional
2D	two-dimensional
AASHTO	American Association of State Highway and Transportation Officials
CAFL	constant amplitude fatigue limit
LEFM	linear elastic fracture mechanics
C.O.V	coefficient of variable
MLP	multi-layer perceptron
MSE	Mean Square Error
NN	Neural Network
NDT	Non-destructive testing
RMSE	Root Mean Square Error
α	significant level

Fatigue

$\Delta\sigma_D$	fatigue limit
n_i	number of experienced stress ranges
S_i	experienced stress range in S-N curve
N_i	number of cycles to failure in S-N curve
S_{eq}	equivalent stress ranges
D	fatigue damage index
SIF	stress intensity factor
K_{eq}	equivalent stress intensity factor
K_{th}	threshold stress intensity factor
K_{Ic}	critical limit stress intensity factor
ΔK	stress intensity factor ranges
a	crack size
$\Delta\sigma$	cyclic stress range
$f(a)$	$f(a)$ geometry function to define stress intensity factor
ϑ	Poisson's ratio
K_I	stress intensity factor for crack mode I
K_{II}	stress intensity factor for crack mode II
K_{III}	stress intensity factor for crack mode III
J_I	J -integral for crack mode I
J_{II}	J -integral for crack mode II

J_{III}	<i>J</i> -integral for crack mode III
E	Young's modulus of a material

Multi-scale modeling

F_x	axial force in work equation
F_y	shear force (y direction) in work equation
F_z	shear force (z direction) in work equation
U, V, W	axial displacement for shell member, in x, y, z directions
u	displacement for beam member,
U_e, V_e, W_e	equivalent displacement of shell member in x, y, z directions
$[N]$	matrix of the quadratic shape functions
$\{U\}$	vector of the nodal axial displacements for shell elements
$[C]$	matrix of the constant coefficients defined by the shape functions
A	area of lateral edge plane of the shell member
t	thickness of the shell elements
l	length of the shell elements
J	Jackobian at Gauss points
w	weighting factors at Gauss points
B	beam element model
SH	shell element model
SS	multi-scale sub-structure model
M-S	multi-scale model
J^2	stress jump for bending and shear force
p	polynomial interpolation order
h	dimension of the shell element

List of Tables:

Table 3-1 Structural health monitoring sensors of the Memorial Bridge	39
Table 3-2 Data collection program at the Memorial Bridge.....	41
Table 3-3 Truck Load test specifications at the Memorial Bridge.	45
Table 4-1 Displacement comparison of the shell element model, multi-scale with the presented MPC equations.....	66
Table 4-2 Geometrical and material properties of the developed FE models.....	69
Table 4-3 Comparison between the natural frequencies of the FE models and field data.....	78
Table 4-4 Linear regression for validating the FE models compared to the field data.....	84
Table 5-1 Properties of the sub-structure and multi-scale finite element models.....	102
Table 5-2 Recoded stress ranges and the measured fatigue response over a year	106
Table 5-3 Hot-spot and nominal stress variations for six paths along the weld toe	111
Table 5-4 Application of multiple SCFs for fatigue assessment using field collected data	112
Table 6-1 Truck Load test specifications at the Memorial Bridge.	125
Table 6-2 Element properties for the three developed models in LUSAS.	133
Table 6-3 The nominal and hotspot stress and measured fatigue responses of simulated traffic scenarios.....	141
Table 6-4 Stress range and fatigue remaining life response at the six selected paths under the traffic scenario 8	142
Table 7-1 Number of samples for the NN models.....	169
Table 7-2 Summary of the NN model properties.....	170
Table 7-3 Variation of prediction performance for the five strain rosettes	171
Table 8-1 The characteristics of the M-S model.....	190
Table 8-2 The LEFM properties applied for fatigue assessment of the gusset-less connection.	199

List of Figures:

Figure 2-1 A representative S-N curve for steel material (6)	14
Figure 2-2 AASHTO S-N curve for all detail categories (6).....	15
Figure 2-3 Fatigue strength curves for normal stresses according to EN 1993-1-9 (7).....	15
Figure 2-4 Variations of global and local approaches for fatigue strength assessment (10)	16
Figure 2-5 Stress variation with distance to weld toe	17
Figure 2-6 A schematic single fatigue S-N curve (11)	18
Figure 2-7 Schematic hotspot S-N curves derivation from sample fatigue test results (1).....	20
Figure 2-8 Type 'A' and 'B' weld toes of the hotspot stress method (28).....	22
Figure 2-9 Linear extrapolation to calculate hotspot stresses at weld toe type 'A' and 'B'	22
Figure 2-10 FE modeling of the welded component (a) shell element, (b) solid element with weld geometry (22)	24
Figure 2-11 Rounding of weld toes and roots to measure the notch stress effects at weld toe (28)	26
Figure 2-12 Effective notch stress-based fatigue S-N curves recommended by the IIW (35)	27
Figure 2-13 Three crack regions in crack propagation	29
Figure 2-14 The three loading conditions/modes in fracture mechanics (43)	30
Figure 3-1 The Memorial Bridge, Portsmouth, NH.....	37
Figure 3-2 The gusset-less connection at the Memorial Bridge	38
Figure 3-3 Structural health monitoring instrumentation installed at the Memorial Bridge, Portsmouth, NH.	39
Figure 3-4 Sample time-history strain responses, a) collected event data, b) collected normal data	41
Figure 3-5 Defining the trigger program to collect the data during the lift events	42
Figure 3-6 Truck class statistics at the Memorial Bridge provided by NHDOT	43
Figure 3-7 The truck load test configuration at the Memorial Bridge.....	45
Figure 4-1 (a) Planar multi-scale coupling condition (b) Out-of-plane multi-scale coupling condition (beam to shell member).	54
Figure 4-2(a) Planar coupling condition (beam to shell element), b) Out-of-plane coupling condition (beam to shell element)-only representative connections is shown for clarity.....	59
Figure 4-4 (a) Multi-scale model with planar coupling beam to shell element (b) Single scale model with shell element (LUSAS®).....	65
Figure 4-5 The Memorial Bridge, Portsmouth, NH and the instrumentation plan.	68
Figure 4-6The gusset-less connection of the Memorial Bridge.....	68
Figure 4-7 FE global model of the Memorial Bridge made by beam elements, B-Model (Sap2000®).....	70
Figure 4-8 FE global model of the Memorial Bridge made by shell elements, SH-model (LUSAS®).	71

Figure 4-9 Coupling conditions for the (a) top connection, b) bottom connection (LUSAS®)...	75
Figure 4-10 Multi-scale model of the Memorial Bridge, connections and the deck are modeled with shell element (LUSAS®).....	76
Figure 4-11 Strain contour response of the multi-scale model under the truck load (LUSAS ®).	79
Figure 4-12 The field strain time-history response during the load test for the strain rosettes at the bottom connection, locations shown in Figure 4-13	79
Figure 4-13 The principal strain contours of the a) SH-model b) M-S model c) S-S model LUSAS ®) under the truck load	81
Figure 4-14 The comparison between the strain response of the FE models and field data a) bottom connection, and b) top connection.....	82
Figure 4-15 (a) Deviance strain response of SH, S-M and S-S from the field data with 95% confidence intervals	84
Figure 5-1 Hot-spot stress extrapolation at the weld toe (2).....	96
Figure 5-2 FE modeling of the welded component (a)shell element, (b) solid element with weld geometry (18).....	97
Figure 5-3 (a), The Memorial Bridge, Portsmouth, NH, (b), The gusset-less connection of the Memorial Bridge (20).	98
Figure 5-4 Instrumentation of the gusset-less connection at the bottom(left) and top chord (right)	99
Figure 5-5 Multi-scale global model of the Memorial Bridge in LUSAS.....	101
Figure 5-6 The sub-structure model of gusset-less connection at the Memorial Bridge in LUSAS	102
Figure 5-7 Comparison between the numerical result and field data at the load test for model verification	103
Figure 5-8 The strain contours of the gusset-less connection for the a) multi-scale model and b) the sub-.....	104
Figure 5-9 Examples of time history responses (a) SG5-A, (b) SG5-E.....	105
Figure 5-10 The selected paths along the curved weld toe for hot-spot stress measurements ...	107
Figure 5-11 The strain variation with the distance from the weld toe under the static truck load at the northbound (left) and southbound (right).....	108
Figure 5-12 SCF under the static truck load at the northbound and southbound	109
Figure 5-13 SCF under the dynamic truck load at the northbound and southbound	110
Figure 6-1 Hotspot stress extrapolation at the weld toe.....	121
Figure 6-2 (a) The Memorial Bridge, Portsmouth, NH, and (b) The gusset-less connection of the Memorial Bridge.....	122
Figure 6-3 Instrumentation of the bottom gusset-less.....	123
Figure 6-4 a) Truck stops at the quasi-static load test, b) the size and weight of the load test truck.	124
Figure 6-5 The SH global model of the Memorial Bridge created in LUSAS.	126
Figure 6-6 The SS global model of the Memorial Bridge created in LUSAS.....	127

Figure 6-7 The MS global model of the Memorial Bridge created in LUSAS.....	128
Figure 6-8 Coupling the nodal DOFs in a) shell elements b) solid elements.	131
Figure 6-9 Coupling the DOFs of the weld geometry modeled with the shell and solid elements.	
.....	132
Figure 6-10 Mesh configuration at the solid element part of the M-S model.....	133
Figure 6-11 Comparison of the numerical response of the FE models with the field data at the second stop of the Loadcase1(northbound).	134
Figure. 6-12 Comparing the principal strain contours of a) SH model, b) S-S model and M-S model in LUSAS, at the second stop of the Loadcase1(northbound).....	135
Figure 6-13 The selected paths to measure the hotspot and nominal stresses along the weld toe.	
.....	136
Figure 6-14 Variation of the numerical principal strain response with the distance to the weld toe for the six selected paths under the static truck load at a) northbound b) southbound.	137
Figure.6-15 Comparing the field collected strain response and the numerical time-history response of model in LUSAS, under the dynamic truck load, Loadcase2.	138
Figure 6-16 The numerical time history responses of the hotspot and nominal strain for the six selected paths under the dynamic truck load at the northbound (a and b), southbound (c and d).	
.....	139
Figure 7-1 The procedure to develop a NN model for fatigue crack detection	151
Figure 7-2 Schematic Multi-layer Perceptron Neural Network Architecture.....	155
Figure 7-3 (a) The Memorial Bridge, Portsmouth, NH, (b) The gusset-less connection of the Memorial Bridge.....	156
Figure 7-4 The trend of averaged fatigue damage index versus truck event cycles	158
Figure 7-5 Monthly averaged fatigue damage index for 12-month period of data collection at SG-A.....	159
Figure 7-6 The results of predicting the correlation between the measured fatigue.....	160
Figure 7-7 Calibrating the numerical responses of FE model corresponding	162
Figure 7-8 The simulated fatigue cracks at the gusset-less connection through FE model in LUSAS.....	164
Figure 7-9 The stress contours of the gusset-less connection healthy and three crack cases	165
Figure 7-10 Numerical time-history principal stress responses under the dynamic moving loads for a) healthy, b) crack case#1, c) crack case#2, d) crack case#3.....	166
Figure 7-11 Variability of the measured fatigue damage indexes with multiple crack sizes for a) crack case#1, b) crack case#2, c) crack case#3	167
Figure 7-12 Crack size versus p-values for five sensors and damage case 1, 2,3.	173
Figure 7-13 Minimum detected crack size through the NN models of the five strain rosettes for three crack cases	174
Figure 8-1 The three loading conditions/modes in fracture mechanics (112)	183
Figure 8-2 Determining Crack propagation direction in a radially meshed FE model.....	186
Figure 8-3 a) The Memorial Bridge, Portsmouth, NH(Left), b) The gusset-less connection of the Memorial Bridge (Right)	188

Figure 8-4 The MS global model of the Memorial Bridge created in LUSAS.....	190
Figure 8-5The connected members to the gusset-less connection.....	192
Figure 8-6 Meshing at the crack tip to predict fatigue crack direction.....	193
Figure 8-7 Selected location for crack initiation at weld toe of the gusset-less connection.....	194
Figure 8-8 Stress contours at the cracked area of the gusset-less connection for a)75 mm crack,b) 125mm crack.....	196
Figure 8-9 Time-history stress at the crack tip for four crack sizes.....	197
Figure 8-10 SIF variation in crack propagation considering mode I.....	198
Figure 8-11 Fatigue cycle variation in crack propagation for two crack modes	199

ABSTRACT

FATIGUE ASSESSMENT OF COMPLEX STRUCTURAL COMPONENTS OF
STEELBRIDGES INTERATING FINITE ELEMENT MODELS AND FIELD-
COLLECTED DATA

by

Maryam Mashayekhizadeh

University of New Hampshire

Fatigue damage in welded structural steel components has a complex presentation, which is influenced by the geometric configuration of the component and load path in a structural system. The classic fatigue assessment methods, using nominal stresses and S-N curves, may not capture nor predict the complicated performance of the component with respect to fatigue. Recent novel complex steel structural connections that experience multi-axial behavior or do not fit any conventional fatigue categories are not explicitly addressed in the existing fatigue design codes. An ideal fatigue estimation for the complex structural components is dependent on a thorough understanding of structural performance of the component within the global structural system and application of an appropriate fatigue assessment method.

This dissertation presents a fatigue assessment protocol for complex structural components of steel bridges, using numerical methods and field-collected structural response data. Multiple fatigue assessment methods are implemented, including the nominal stress method, hotspot stress method, and linear elastic fracture mechanics method to estimate fatigue performance of a complex

welded structural component. Accordingly, for each method, a set of computationally efficient finite element models of a large-scale bridge are created. Each model corresponds to the requirements of a specific fatigue assessment method and provides the required stress responses, under simulated dynamic traffic loads.

A major contribution of this research is the development of a novel a multi-scale modeling method to accommodate multiple dimensions of elements and multiple axes loading configurations. The multi-scale models are created for a case study, the Memorial Bridge in Portsmouth, NH, which is a vertical lift steel truss bridge and includes a novel gusset-less connection. The gusset-less connection includes a complex web geometry and curved fillet welds connecting the web to the flange. The bridge is also equipped with a long-term structural health monitoring program, with arrays of installed sensors. Field data are collected from the sensors to report the health status of the bridge. Additionally, field-collected data are utilized to validate the finite element models created for this study.

Due to the limited sensor location available, finite element models are used to predict structural responses that will supplement the field-collected data to appropriately provide stress-concentrated responses at the welded components of the bridge. The multi-scale model results illustrate that the geometric shape of the weld impacts the variability of the generated hotspot stresses along the weld toe. The changes in the stress state and estimated fatigue life are investigated during crack propagation procedure, using a multi-scale model with a simulated crack.

Chapter 1

1. INTRODUCTION

Fatigue can result in a local structural discontinuity in welded structural components (1). Fatigue cracks primarily emerge as a result of geometrical complexities, misalignments, and material imperfections, which can progress to cause a fracture in steel structural components. Given the repeated service loads in steel bridges, fatigue failure can jeopardize the health condition and shorten the service life (2). Fatigue-related failures can impose significant costs associated with repair or replacement of structural components. With increasing traffic loads, the prediction of the remaining life of steel bridge components is significant, given that traffic impact related to bridge construction negatively impacts the public. Fatigue condition assessment of welded fatigue-prone details is one of the crucial aspects of long-term management and maintenance programs of steel bridges (3). Fatigue induced fracture in steel truss bridges was firstly reported in Germany, Belgium, and France in the 1930s. In the late 1960s, the current approach for fatigue and fracture in the design and evaluation of steel bridges was first considered in bridge engineering (4).

Fatigue assessment of conventional structural components can be conveniently performed using the undisturbed far-field stress (nominal stress) responses of the component and developed Stress range vs Number of cycles to failure curves, more commonly known as S-N curves. The S-N curves are available for multiple connection details in the existing design codes (1). Some novel and complex structural components in signature steel bridges may not be documented in the

available fatigue design codes. Complex geometry and loading conditions of these structural components can play a significant role in the resulting stress and fatigue performance of the component (5). Therefore, more advanced fatigue assessment methods are required to address the fatigue performance of these components (6). This is the motivation of the work presented in this dissertation.

1.1 Motivation

Fatigue assessment in complex structural components relies on concentrated stresses at fatigue prone welded areas. Geometrical complexities and irregularities, as well as load transfer conditions of steel structures, can limit an accurate estimation of fatigue performance of structural components. Large steel structures such as signature bridges consist of multiple complex welded details that require careful estimation of traffic load-induced stresses and appropriate fatigue assessment methods (7). However, it is essential to determine the appropriate fatigue assessment method(s) that can appropriately predict the fatigue performance of the specific components. The existing fatigue design codes address fatigue specifications of numerous structural components for different fatigue assessment methods (3). Application of these specifications for the fatigue assessment of complex structural component (not-categorized) is dependent on a broad structural performance assessment of the component, and appropriate selection of advanced fatigue assessment methods as determined by the bridge engineer.

The objective stresses, specific to each fatigue assessment method, can be obtained through experimental efforts, numerical methods, field data collections or, a combination of these sources. Numerical methods are becoming one of the popular methods in obtaining the objective stresses through detailed and validated finite element (FE) models. Some fatigue assessment methods,

including the hotspot stress method, notch stress method, and linear elastic fracture mechanics methods, have documented guidelines for preparing the FE models to obtain the required stresses (8). However, the recommended guidelines are frequently documented for local FE models of a component. Application of these provisions in global FE models of large-scale bridges is limited, due to the required modeling skills and computational time. In addition, the development of FE models is dependent on a thorough review and understanding of the information related to the structural performance of a concerning component.

Validation of the FE models is a fundamental task in utilizing an FE model for fatigue assessment. The required information for the creation and validation of an FE model can be obtained through a review of existing information on the bridge structures, such as structural drawings, field inspection reports and, structural response data that are collected through installed sensors at a bridge. Collection and post-process of field data are frequently expressed as structural health monitoring (SHM) (9). SHM data can provide valuable information that reflects the current health status as well as the experiencing structural responses of structural components of in-service bridges (10).

Additionally, SHM data can be a useful source in providing data for the fatigue assessment of an objective component. However, access restrictions for instrumentation locations in an SHM program (for data collection at fracture critical welded areas) are one of the significant difficulties in obtaining the concentrated stresses for fatigue assessment (11). Therefore, the measured structural responses might not capture the required information to indicate the fatigue status of the welded connection appropriately. In this case, the collected stresses through SHM may not correspond to the selected fatigue assessment method. Therefore, the field-collected SHM data

may not create a complete database for the fatigue assessment of complex structural components and may require additional supplemental information from a validated FE model.

Large steel structures such as signature bridges consist of multiple complex welded details, which require precise prediction of traffic load-induced stresses for application to fatigue assessment methods (12). Therefore, it is essential to obtain a database of structural stresses, considering the geometrical complexities and irregularities, as well as load transfer conditions of steel bridges (13). In addition, an appropriate fatigue assessment method is required to be selected that can address the fatigue performance and consider the novel and complex structural characteristics of the specific element.

1.2 Research contribution

The main contribution of this work is a protocol for fatigue performance assessment of complex welded structural components of steel bridges that are not addressed in the existing design codes. This protocol includes creating a thorough database for structural performance predictions of a target component, appropriate selection of fatigue assessment methods corresponding to the structural performance assessment, and accurate estimation of the stress responses corresponding to the applied fatigue assessment methods.

The database for structural performance assessment is created by integrating an FE model and field-collected SHM data. The presented protocol provides a complete database of required structural responses through FE models that can supplement the field-collected SHM data. In this dissertation, long-term SHM data is collected to evaluate the traffic-induced stress amplitudes of a bridge. The collected SHM data are also utilized to validate a global FE model. The validated global FE model is then used to determine the stress concentrations at non-instrumented locations

of the bridge. Fatigue assessment methods are subsequently selected based on the component-specific features that are obtained through the numerical (from the FE models) and field-collected structural responses.

A set of global FE models are created, corresponding to the requirements of the selected fatigue assessment methods. These requirements can increase the modeling and computation efforts significantly, decreasing the efficiency of fatigue assessment applications. Therefore, the global FE models are modified to locally consider the specific fatigue assessment methods at the target component. A contribution of this work to fatigue assessment and structural performance prediction of large-scale structures with complex connections is the development of a set of multi-point constraint equations, used to create a multi-scale FE model. The multi-scale global FE model implements multiple dimensions of elements that are coupled in a single global model.

The modeling and fatigue protocol is implemented on a case-study steel bridge. The case-study, the Memorial Bridge, is in Portsmouth, NH, which includes a novel welded joint, the gusset-less connection. For coupling different dimensions of elements, novel constraint equations were required, due to the complex loading and geometry of the Memorial Bridge. An FE model is created through the developed constraint equations that would provide an accurate prediction of the structural response of the bridge at the targeted locations in the gusset-less connection. The required element types and dimensions correspond to the provisions of the selected fatigue assessment methods. The numerical results of the validated FE models are implemented to the associated fatigue assessment methods to evaluate fatigue performance of the complex gusset-less connection.

The bridge has equipped with a long-term SHM program since March 2017 (14). Long-term field-collected strain responses are implemented to obtain the stress range/cycles for fatigue

assessment. The obtained information related to the stress cycles is integrated with the numerical responses of the created FE model to estimate the fatigue performance of the gusset-less connection using multiple fatigue assessment methods. Additionally, SHM data is utilized for validating the created FE models of the bridge.

1.2.1 Research tasks

The gusset-less connection at the case-study Memorial Bridges is the focus for the application of the fatigue protocol discussed above based on its complex and novel geometric configuration. A representative gusset-less connection is equipped with five strain rosettes, collecting strain horizontal, vertical, and shear strain responses. The executed tasks in this dissertation are briefly expressed in the following:

- SHM data are collected through theses installed strain rosettes to inform the structural performance of the connection.
- A detailed global FE model of the bridge is created to supplement the sparse field-collected data. This global FE model considers all structural elements to represent the structural responses. The model is validated through an objectively designed load test.
- The field-collected SHM data are integrated with the numerical results of the FE model to determine the appropriate fatigue assessment methods.
- Fatigue assessment methods in this study include the Nominal stress method, the Hotspot stress method, and the linear elastic fracture mechanics method.
- Multiple detailed global FE models of the Memorial Bridge are created that meet the requirements of the selected fatigue assessment methods.

- A set of multi-scale global models of the Memorial Bridge are created. The existing multi-point constraint (MPC) equations are modified to obtain the required coupling conditions in creating a three-dimensional global FE model of the bridge.
- Field-collected SHM data and numerical results are implemented for fatigue assessment to highlight the advantages and restrictions of using each method.
- Machine learning tools are utilized for training the measured fatigue results for a fatigue crack prediction protocol.
- A global multi-scale FE model is created to investigate fatigue crack propagation in complex structural components under dynamic traffic loads

1.3 Challenges and Limitations

The challenges related to this work are primarily focused on the limited knowledge on the structural performance of a complex structural component. Some of these challenges limit the application of this work and create the opportunities of future work in this area of research. Complete structural information is required to create a detailed FE model for fatigue assessment. This information includes fabrication procedures, structural drawings and design calculations, field inspection reports and structural response data. While this information was readily available for the Memorial Bridge, which was constructed in 2013, this information may not be available for other fracture-critical bridges limiting the application of this protocol.

The selection of the appropriate fatigue assessment method is dependent upon a reasonable prediction of the structural performance of the target component. The prediction is directly related to the ability of the global FE model to reasonably predict the structural response. Geometric and access restrictions on the possible sensor locations on a SHM program also present a challenge for

fatigue assessment. Commonly, the critical point for fatigue assessment, such as a weld toe, is not a candidate for traditional sensor installment due to geometric constraints. Also, most SHM programs are limited in funding and, therefore, limited in sensor locations. This challenge was addressed in this work by the integration of structural response information predicted through a global FE model.

A significant limitation of this work is that the target structure is a new structure with no detectable fatigue cracks. Therefore, the simulated fatigue cracks and the fatigue crack propagation procedure of this work is entirely based on published information on crack propagation behavior and simulated structural performance. Also, the fatigue protocol was applied to only one case study, the Memorial Bridge. Additional case studies are required for broader application of the fatigue assessment methods presented in this work.

1.4 Outline of the dissertation

This dissertation consists of nine chapters. Five principal chapters that detail the technical contribution of this work include the journal articles that are published (Chapters 4, 5), under-review (Chapter 6), or in preparation for publication (Chapters 7, 8). Chapter 2 provides the literature survey associated with the fatigue assessment methods, and Chapter 3 details the structural properties of the case-study bridge. Chapter 9 is the concluding remarks and future works recommendations. The details of each chapter are explained in the following:

In Chapter 2, the dominant fatigue assessment methods and the background for each method are addressed. Also, a literature survey is included in this chapter which discusses fatigue assessment of plate-type welded structural components, using field data and FE model on steel bridges.

In Chapter 3, the case-study, the Memorial Bridge, and specifically the gusset-less connection is presented in detail. The long-term SHM program at the Memorial Bridge, including the instrumentation plan of the installed sensors, and initial investigations of the structural responses are detailed in this chapter.

Chapter 4, details the model creation, including a comparison of single-scale and multi-scale models and predicted structural responses. For the multi-scale models, a novel multi-point constraint t method is developed and utilized to couple the different dimensions of elements at the interface point under both in-plane and out-of-plane loading conditions. The developed FE models are verified using field-collected results of a truck load test. Chapter 4 is the first published peer-reviewed journal paper resulting from this work (15).

Chapter 5 details the fatigue assessment of the complex structural components using field-collected data integrated with FE model predictions. The long-term field strain responses of the Memorial Bridge are collected from the installed strain rosettes at the objective gusset-less connection. The collected data are utilized to compute fatigue remaining life of the component. Additionally, the validated FE model in Chapter 4, is used to determine the proportion of weld toe induced stress concentrations to the stresses at strain rosette locations (stress concentration factor). The stress concertation factor is implemented to the field-collected data to consider increased stresses for fatigue assessment. The fatigue remaining life of the gusset-less connection is estimated using the field-collected and modified stresses. Chapter 5 is the second published peer-review journal paper from this work (16).

Chapter 6 presents the fatigue assessment of complex structural components of a steel bridge using the hotspot stress fatigue assessment method. A global multi-scale FE model is created, which locally meets the FE modeling provisions of the hotspot stress method for the objective complex

component. The modeling process is implemented for the Memorial Bridge. Multiple traffic scenarios are simulated via the validated global multi-scale FE model to evaluate the hotspot stresses variations along the weld toe of the gusset-less connection. The numerical hotspot stress results are utilized to estimate the fatigue responses at weld toes of the component.

Chapter 7 presents a fatigue crack prediction protocol using data analytics. The validated FE model in Chapter 4 is used to produce the numerical crack-induced stresses and the resulting fatigue responses. Fatigue responses measured through field-collected SHM data and an FE model with simulated cracks are implemented for training a mathematical model, which can inform the deviant fatigue responses due to a possible fatigue crack.

Chapter 8 details the creation of a global FE multi-scale model of bridges considering a three-dimensional fatigue crack at weld toes of the component. A three-dimensional fatigue crack is simulated via three-dimensional solid elements in a global multi-scale FE model of the Memorial Bridge. The crack induced numerical stress responses of the model are obtained for multiple stages of crack progress. Multiple traffic scenarios are simulated for each step of crack size to determine the fatigue status of the cracked component appropriately. The linear elastic fracture mechanics (LEFM) method is applied to measure fatigue remaining life changes of the gusset-less connection due to crack propagation.

In Chapter 9, the most significant conclusions are explained, and concluding remarks of the study are expressed based on the results of the chapters. The suggestions for future studies are also included in this chapter.

References

- 1) Fisher, J.W., Roy, S. 2015. "Fatigue damage in steel bridges and extending their life." *Advanced Steel Research ,Advanced Steel Construction*, 11 (3): 250-268.
- 2) Fisher, J.W., Mertz, D.R. and Zhong, A. 1983. *Steel Bridge Members under Variable Amplitude Long Life Fatigue Loading, NCHRP Report 267*. T. Washington, D.C.: transportation Research Board,.
- 3) Administration, Federal Highway. December 2016. *Design and Evaluation of Steel Bridges for Fatigue and Fracture, Reference Manual*. Publication No. FHWA-NHI-16-016.
- 4) Barsom, J.M, Rolfe, S.T. 1999. *Fracture and Fatigue Control in Structures: Applications of Fracture Mechanics: 3rd Edition*. West Conshohocken, PA: ASTM International.
- 5) Martinsson, J. 2005. *Fatigue Assessment of Complex Welded Steel Structures*. KTH, School of Engineering Sciences (SCI), Aeronautical and Vehicle Engineering..
- 6) Hobbacher, A. 1996. *Fatigue Design of Welded Joints and Components: Recommendations of IIW Joint Working Group XIII - XV*. Woodhead publishing.
- 7) Leander, J. 2013. *Refining the fatigue assessment procedure of existing steel bridges* . Stockholm, Swede: KTH School of Architecture and Built Environment.
- 8) Radaj, D., Vormwald, M. 2013. *Advanced Methods of Fatigue Assessment*. Berlin, Heiderberg: Springer.
- 9) Li, Z.X., Chan, T.H.T., Ko, J.M. 2001. "Fatigue analysis and life prediction of bridges with structural health monitoring data-ParI: Methodology and strategy." , *International Journal of Fatigue*, 23 (1): 45-53.
- 10) Lund, R., and Alampalli, S. 2004. Estimating Fatigue Life of Patroon Island Bridge using Strain Measurement. New York: Transportation Research and Development Bureau.
- 11) Kwon, K., Frangopol, D.M.,. 2010. "Bridge fatigue reliability assessment using probability density functions of equivalent stress ranges based on field monitoring data." *International journal of fatigue*, 32 (8): 1221-1232.
- 12) Aygül, M. 2013. Fatigue evaluation of welded details – using the finite element method, Doctoral thesis. Gothenburg, Sweden : CHALMERS UNIVERSITY OF TECHNOLOGY.
- 13) Wang, W., Deng, L. 2016. "Fatigue Design of Steel Bridges Considering the Effect of Dynamic Vehicle Loading and Overloaded Trucks." *Journal of Bridge Engineering*, 21 (9).
- 14) NHDOT. 2016. "Memorial Bridge Project Innovations", New Hampshire Department of Transportation.
- 15) Mashayekhi, M., Santini-Bell, E. 2018. "Three-dimensional multiscale finite element models for in-service performance assessment of bridges. Computer-aided civil and infrastructure engineering";34(5):385-401.
- 16) Mashayekhi, M, Santini-Bell. 2019. "Fatigue assessment of the gusset-less connection using field data and numerical model. *Bridge Structures*";15(1-2):75-86.

Chapter 2

2 FATIGUE IN WELDED STRUCTURES

2.1 Introduction

Fatigue is a time-dependent damage mechanism, which can occur due to cyclic loadings in steel structural components. The physical process of fatigue damage can be divided into three phases, the crack-initiation phase, the subcritical crack propagation phase, and the fracture stage (1). A crack may initiate at stress-concentration locations of structural components, as a result of structural misalignments, imperfection or fabrication flaws. Material degradation is another influential factor in the crack initiation (e.g. in intrusion and extrusion welding).

Fatigue crack propagation, however, depends primarily on the induced tensile stresses at the cracked area. The fatigue crack propagation is also dependent on the resistance of a steel component under a cyclic applied load. Fatigue failure of a cracked component can occur under a continuous applied load that is greater than the material resistance. Multiple fatigue assessment methods are available to estimate the fatigue strength of steel structural components at different phases of fatigue. This chapter presents a fatigue definition in welded structural components and a literature review different fatigue assessment methods. The proficiencies and limitations of each method are also detailed.

2.2 Geometric impacts of welded structural components

Geometric shape, weld type, residual stresses generated during welding, possible defects in the welds and heat affected zones can trigger fatigue crack initiation in welded structural steel

components. In addition to the geometric impacts, structural details and loading conditions, are additional significant factors, which influence the fatigue performance of welded steel structures (2).

The geometric characteristics of welds includes the notch effects at weld toes and stress distribution changes at the fracture critical areas of a welded component. The geometric configuration of a structural component can impact crack initiation, and crack propagation phases of fatigue phenomena. In welded components with complex geometry, the induced stress concentrations at welded areas can cause stiffness degradation, which subsequently influences the stress distribution and damage nucleation (3). In addition, plate thickness is another source of geometric impacts to influence the characteristics of fatigue crack initiation and propagation. The rate of through-the-thickness stress dissipation is dependent on the thickness of plates, which adversely affects the induced residual tensile stresses. Therefore, the thickness of plates negatively contributes to the fatigue strength of welded components (4).

2.3 Fatigue assessment methods

Fatigue assessment methods are developed for different fatigue phases of welded structures. Since the early 19th century, experimental and theoretical studies were conducted to investigate fatigue in steel structures. In 20th century, numerous welded component details with different geometric properties were investigated and categorized in representative S-N curves, as shown in Figure 2-1. S-N curve can predict the remaining cycles to fatigue failure, N, under a cyclic stress range, S (5) for a given detail.

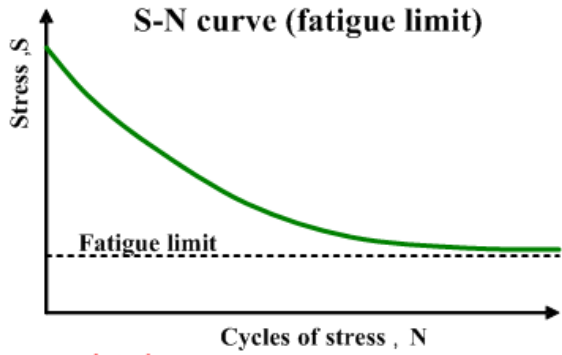


Figure 2-1 A representative S-N curve for steel material (6)

2.3.1 S-N curve

The S-N curves are documented in different design codes, which include Eurocode 3 (7), International Institute of Welding, IIW (8), and American Association of State Highway and Transportation Officials (AASHTO) (9). The S-N curves used in this research are from AASHTO. The AASHTO approach represents a 97.7% survival probability for the details that are associated with each curve, as shown in Figure 2-2. The fatigue strength S-N curves pertaining to the nominal stress method for welded structures. The developed S-N curves include the influence of material, geometry of a structural detail. Each S-N curve also considers weld type, weld geometry properties and local stress concentration effects due to weld geometry, which are unique to the categorized structural detail. In addition, the possibility of weld defects including porosity, lack of fusion or undercuts are included in the developed S-N curves. S-N curves are provided for a wide range of structural details through experimental efforts. The infinite fatigue life is defined for the stress ranges that are below the Constant Amplitude Fatigue Limit (CAFL), as shown in Figure 2-2.

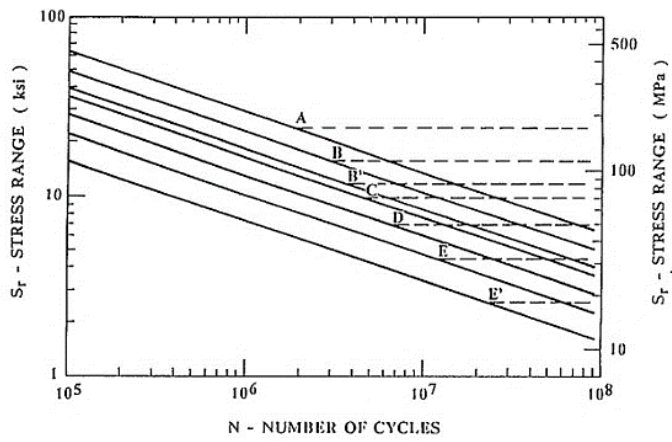


Figure 2-2 AASHTO S-N curve for all detail categories (9)

In addition, in some fatigue design codes including *EN 1993-1-9*, the cut-off limit is defined as the smallest values of stress ranges that do not contribute to crack propagation (7). In fatigue assessment of steel bridges, all the stress ranges that are lower than the cut-off limit can be neglected for damage accumulation. The cut-off limit is often fixed at 10^8 cycles, as shown in Figure 2-3. In addition, if the stress ranges are lower than the cut-off fatigue limit ($\Delta\sigma_D$), they do not contribute to the propagation of the crack until the crack reaches a certain size (10).

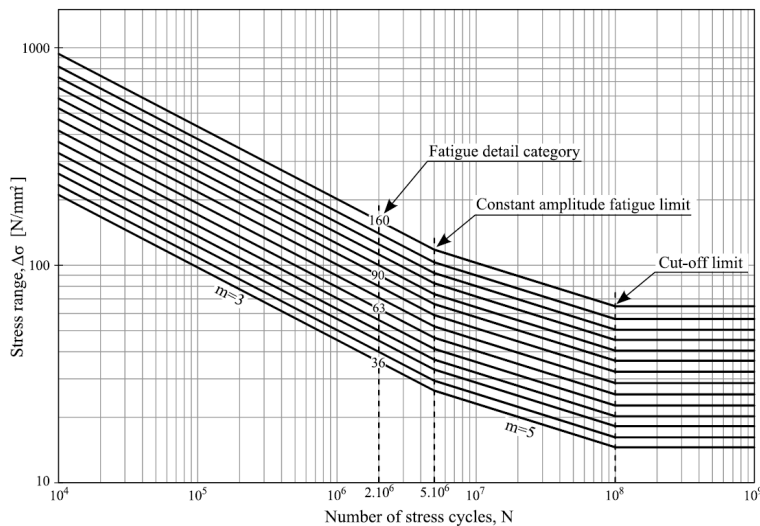


Figure 2-3 Fatigue strength curves for normal stresses according to EN 1993-1-9 (7)

Multiple fatigue assessment methods rely on the development of S-N curves. Variability of the documented S-N curves is dependent on the fatigue assessment method, as expressed in Figure 2-4. Application of the resulting S-N curve is restricted to the categorized structural details, which are expressed in the design codes (9). Therefore, using the S-N curve for the structural details that are not documented in the available codes can be based on the engineer's judgments, and therefore, may not result in an accurate fatigue response prediction. In the following, some of the conventional fatigue assessment methods are introduced, and categorized based on the applied stresses in each method.

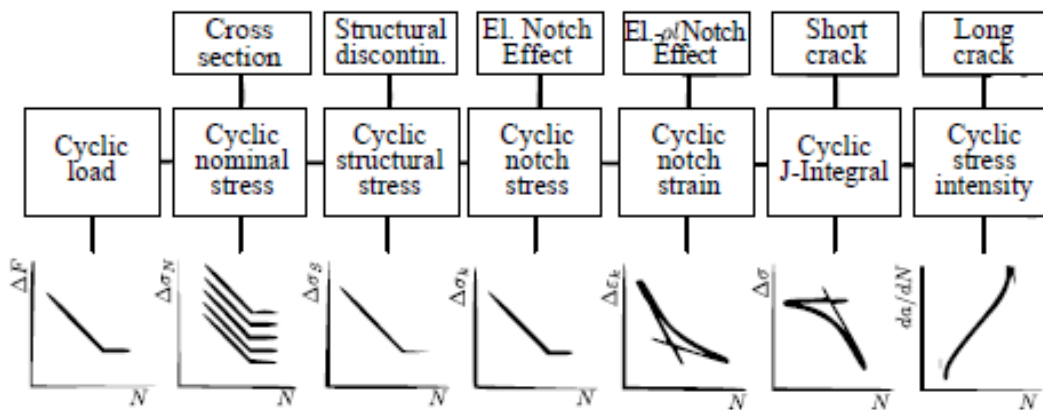


Figure 2-4 Variations of global and local approaches for fatigue strength assessment (11)

2.3.1 Nominal stress method

Nominal stress approach is the basic and most widely utilized method in fatigue design and assessment of structural component. Nominal stresses are obtained in distance to a weld toe, where the concentration stress effects are neglected in the responses, as shown in Figure 2-5. The applied nominal stresses frequently include the macro geometric effects, while stress concentration effects of welded details are excluded. In the complex structural components, nominal stresses are

influenced by complex loading, such as shear lag effect, which makes the stress estimation more complicated (2).

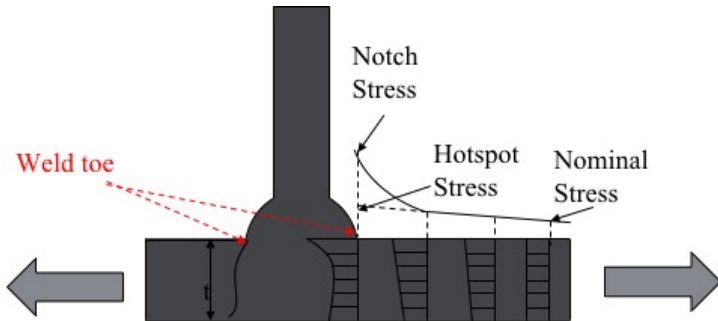


Figure 2-5 Stress variation with distance to weld toe

Therefore, with the limitations of the nominal stress method, local stress methods are the alternatives for a more precise estimation of the concentrated stresses at welded areas which consider the geometric impact of the component geometry. Using the S-N curve approach, the remaining fatigue life cycles are related to the cyclic-stress range through the following equations:

$$NS^m = A \quad \text{Eq. (2-1)}$$

$$\log N = -m \log S + \log A \quad \text{Eq. (2-2)}$$

where N shows number of fatigue cycles to failure, and S represents the stress ranges. m and A are the positive empirical material and structural component constants respectively. m represents the constant slope of the S-N curve, as shown in Figure 2-6.

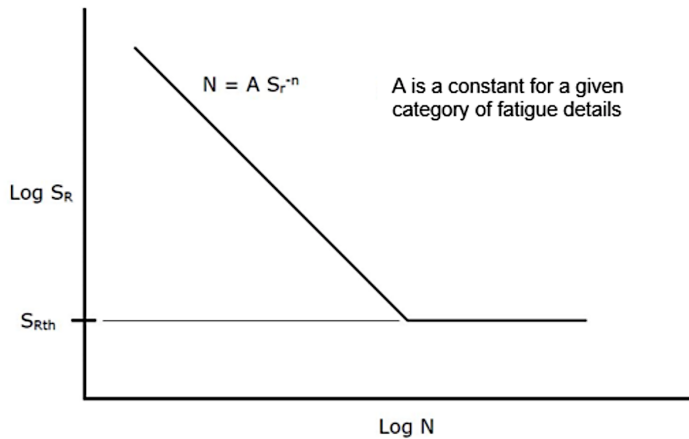


Figure 2-6 A schematic single fatigue S-N curve (12)

The S-N curve is developed under a constant amplitude axial loading condition, which amount of the applied load remains constant during a fatigue test. Fatigue damage can occur under variable amplitude loading conditions that are implemented at the structural components of in-service steel bridges (10). Variable amplitude stress ranges of a structural component can be considered in estimating fatigue responses using Miner's rule. Miner (13) proposed a linear fatigue-damage accumulation model to consider partial-fatigue damage at different stress-range levels. This linear damage-accumulation hypothesis can be expressed through Eq. (2-3).

$$D = \sum_{i=1}^k \Delta D_i = \sum_{i=1}^k \frac{n_i}{N_i} \quad \text{Eq. (2-3)}$$

where n_i denotes the number of experienced stress ranges, S_i . N_i represent the total number of cycles to failure under the constant stress range, S_i . D is a ratio between 0 to 1, which refers to the Miner's damage accumulation index.

The experienced strain time-histories at the structural components of steel bridges can have a scattered distribution, which is induced by variable amplitude traffic loads. Peaks of strain

(stress) time-history responses can be extracted to determine the cycle counts of all measured stress ranges. Rainflow cycle counting algorithm is one of the recognized methods, which extracts the cycles of stress ranges through time-history responses. A stress range histogram presents the number of cycles for each stress range magnitude which are captured during each measurement period. The resulting stress cycles are implemented in the selected S-N curve (input stress range, S, and extract N, remaining fatigue cycles) and, subsequently Miner's rule to measure fatigue damage index (14).

In recent decades, application of the nominal stress method has increased in monitoring-based fatigue assessment of steel bridges. DeWolf et al. (15) evaluated the fatigue life for a variety of bridges using field monitoring data by a portable computer-based strain gauge data acquisition system. Connor et al. (16) conducted a comprehensive fatigue evaluation for the replacement orthotropic bridge deck based on in-depth monitoring program. Others developed the approach for different types of bridges (17) (18) (19) (20). The nominal stress method, however, disregards any local stress redistribution due to the weld geometry and makes use of the “global stress field” away from the weld. Fatigue of welded structures is a localized phenomenon that is affected by local geometrical complexities. In the following, alternative methods are introduced to address issues relative to fatigue assessment in welded areas.

2.3.2 Hotspot stress method

The hotspot stress method is a local fatigue assessment method, which considers the stresses at the weld toe a welded component, as shown in Figure 2-4. The hotspot location is a fracture critical location at weld toe of a welded component, which is vulnerable to fatigue crack initiation. The hotspot stress method considers the induced stress concentration due to the

geometric impacts of the welded component. The hotspot stress fatigue assessment method is also based on application of S-N curves, however, the diversity of S-N curves are limited, as compared to the nominal stress method (21).

The hotspot stresses at weld toe includes the stress increasing effects due to geometric discontinuities or complex loading conditions, which are of particular concern in complex structural components. Therefore, the hotspot S-N curves exclusively consider the stress raising effects and weld defects in a limited number of weld details. The hotspot or structural stress method was primarily developed for the fatigue assessment of the tubular joints in offshore structures (22) (23) (24). In recent years, application of the hotspot method is also extended to plate-type structures (25). In addition, linear elastic behavior of material is assumed in the hotspots stress method, while the method excludes the non-linear peak stress effects at the weld toe (shown in Figure 2-5).

IIW provided hotspot stress design S-N curves similar to the nominal design S-N curves as shown in Figure 2-7 (8). In the hotspot stress S-N curve, the fatigue category (FAT class) refers to the hotspot stress range. The hotspot S-N curves are obtained through fatigue test data which are correspond to approximately 2.3% probability of failure. In the developed S-N curves, the effect of tensile residual stresses has been considered (26). In some theoretical approaches, tensile stresses are frequently increased to yield point to consider the residual stress effects. In addition, the compressive residual stress is not directly considered. Alternatively, a bonus factor is recommended to be applied to the fatigue strength. The favorable compressive residual stress can occur for example in the longitudinal shrinkage of the fillet welds of I-beams, which is not considered in the hotspot stress method (27).

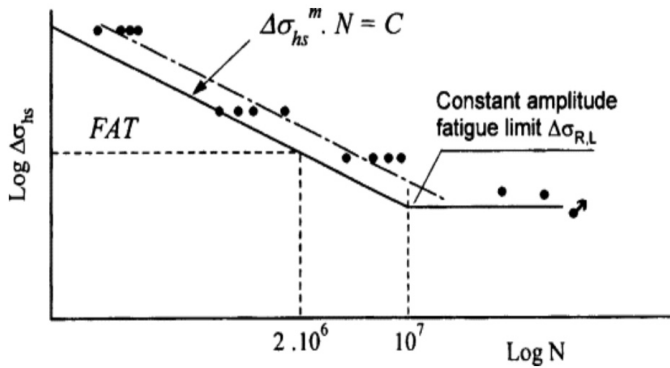


Figure 2-7 Schematic hot spot S-N curves derivation from sample fatigue test results (26)

Fatigue strength of welded structural components can be influenced by misalignments that may occur in manufacturing process (28). Misalignment can cause local stress distribution at weld area due to additional bending moment. In IIW guideline, the effects of misalignment are presented for plate type structures, through theoretical efforts (29). The IIW guideline considers the effect of weld location, the ratio of length over width of the weld in the hotspot stress. Also, misalignment impact on fatigue performance of welded structural component is considered using finite element method and hotspot stress method (30).

2.3.2.1 Hotspot stress measurements using reference points

The stress concentration at weld toe consists of bending, membrane and notch effects. The hotspot stress method does not consider the notch stress effects at the weld toe. Through linearization efforts, the membrane and bending stress components at a weld toe are separated from the non-linear stress peaks due to notch effect. Multiple linearization methods are developed to calculate the hotspot stress, depending on the type of the weld. Two types of weld toes are defined in linear extrapolation estimation of hotspot stress. Type ‘A’ and type ‘B’ weld toes as shown in Figure 2-8.

For each weld type, the hotspot stress is calculated through the measured stresses at the reference points. The resulting hotspot stress in Type “A” are more sensitive to the plate thickness and through the thickness stress reduction, in comparison with Type “B”. The stresses at the reference points can be either obtained through numerical or experimental methods. In the experimental efforts, sensors are required to be installed at the reference points, which might not be feasible for all structural component. The distance of the reference points to the weld toe is defined based on the required distance for dissipation of the non-linear notch effects. The number and location of reference points, also, depends on the stress extrapolation method. The extrapolation relationships can be either linear or quadratic method for a surface extrapolation.

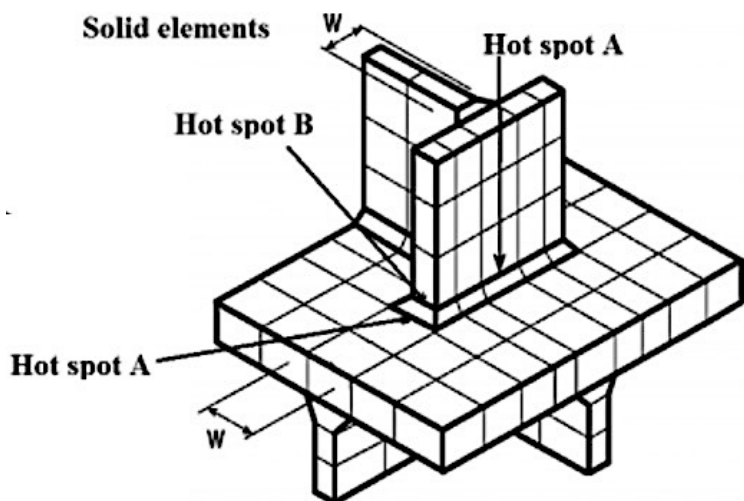


Figure 2-8 Type 'A' and 'B' weld toes of the hotspot stress method (31)

Two reference point are required for linear extrapolation, as shown in Figure 2-9. Using linear extrapolation method, in type “A” weld toe, the distances of $0.4t$ and $1.0t$ from the weld toe are the reference point locations, expressed in Eq (3.4), where t is the plate thickness. The reference points for type “B” are not established as the proportion of plate thickness. Therefore, the reference pointes are determined based on absolute distances of 4mm, 8mm, and 12mm from weld toe, expressed via Eq. (3.5).

$$\sigma_{hs} = 1.67\sigma_{0.4t} - 0.67\sigma_{1.0t} \quad \text{Eq. (3.4)}$$

$$\sigma_{hs} = 3\sigma_{4mm} - 3\sigma_{8mm} + \sigma_{12mm} \quad \text{Eq. (3.5)}$$

In a quadratic extrapolation, three reference points are required, as expressed in Eq.3.6.

$$\sigma_{hs} = 2.52\sigma_{0.4t} - 2.24\sigma_{0.9t} + 0.72\sigma_{1.4t} \quad \text{Eq. (3.6)}$$

0.4t, 0.9t, and 1.4t denote the distance of the reference points from weld toe.

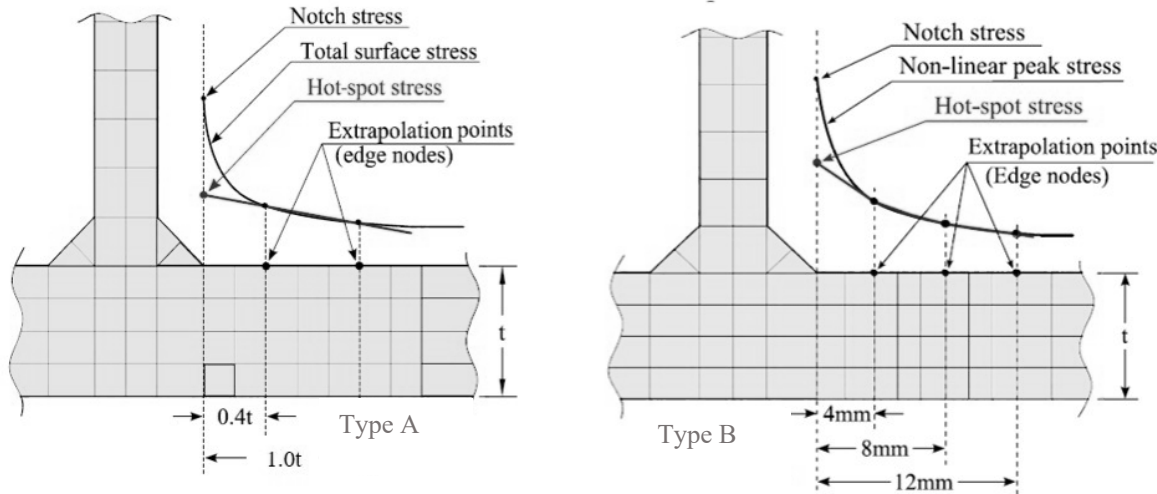


Figure 2-9 Linear extrapolation to calculate hotspot stresses at weld toe type 'A' and 'B'

The hotspot stress is frequently determined through developing a well-detailed FE model.

To accurately compute the hotspot stress at weld toes, the FE model must be created based on the stipulated specifications, including the geometry of the component and mesh configurations that correspond to element type, and size (32). In numerical methods, the applied FE model is required to include the geometric properties of an investigating detail. Possible imperfections or weld defects are considered in the S-N curve. The numerical hotspot stress obtained through the FE model can be dependent on the element size and type. In addition, the mesh layout is required to be adjusted based on the type of weld toe and location of the reference points.

In the available literature, an extensive research effort has been dedicated to establishing the detailed provisions for modeling procedure and the required characteristics of the FE model (32). The modeling instructions include type of elements and mesh size selection. FE models are created through either shell elements or solid elements (33). Solid elements are often preferred, since the weld geometry can be included in the model, as shown in Figure 2-10. However, past research demonstrates acceptable responses may be obtained, using shell element models.

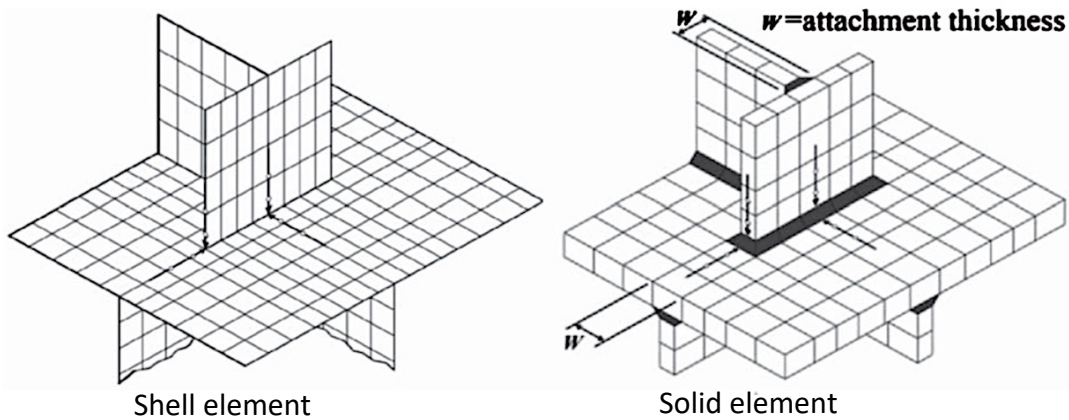


Figure 2-10 FE modeling of the welded component (a) shell element, (b) solid element with weld geometry (23)

The provisions for measuring hotspot stresses of the curved welds have been considered in several studies, which are specifically applied in tubular joints, hollow sections, and welded components of ships, (23) (34). Dong et al. extensively studied the requirements for the mesh size, and element-type of the continuous welds, such as curved fillet welds (35) (36). Dong proposed the hotspot stress measurement procedure, which is based on the work equations of the nodal force of the elements along the weld toe, through a linear equation system. Additional information about hotspot fatigue assessment of curved welds will be addressed in Chapter 5 and Chapter 6.

2.3.3 Effective notch stress method

Sharp local changes due to weld geometry or other geometric discontinuities, such as holes have stress raising effects at the weld areas, which impact fatigue performance of a welded component. The notch stress is the total stress at a local notch that is induced due to structural discontinuity in a linear elastic material, as shown in Figure 2-5. This stress concept includes all the stress raisers effects at the local notch, which considers incorporation of geometrical stress and non-linear stress peak. Fatigue life assessment based on the notch stress is known as the effective notch stress method. The resulting fatigue responses relies on the highest computed elastic stress at the critical points, i.e. weld toe and weld root. However, the effective notch stress method focuses on fatigue strength at the root or toe of a notch, while the method does not consider the elastic-plastic material behavior at the crack tip. Notch stress are exclusively obtained using FE method.

The effective notch stress method was first introduced by Radaj and Sonsino (37). These authors applied Neuber rule and suggested with a fictitious radius of 1 mm for plate thicknesses of 5 mm and more to evaluate high-cycle fatigue strength for samples with crack initiation and early growth phase, as shown in Figure 2-11. IIW provided some guidelines for fatigue analysis of welded components using the effective notch stress method (31).

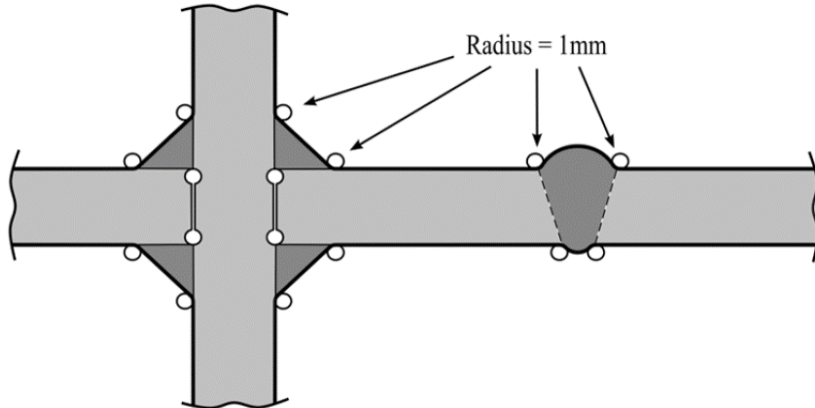


Figure 2-11 Rounding of weld toes and roots to measure the notch stress effects at weld toe (31)

In creating FE models for the notch stress method, the existing sharp notches at weld toes are rounded with a fictitious radius, the reference notch radius. The round weld toe aids to avoid stress singularities and obtain the stress responses at anticipated crack initiation location (at weld toe or weld root) (31). Therefore, the effective notch stress method requires a well-defined FE model and high-density mesh sizes at the stress concentration areas (weld toe and weld root) (33) (8). In fatigue assessment using the notch stress method, a single S-N curve is utilized to estimate the fatigue strength of a welded component. IIW considers four different S-N curves for the notch stress method, which vary based on the plate thickness and type of stresses, shown in Figure 2-12.

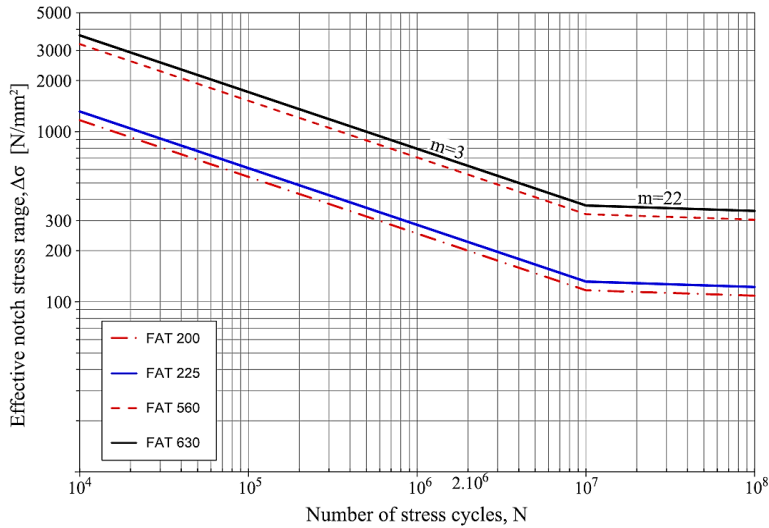


Figure 2-12 Effective notch stress-based fatigue S-N curves recommended by the IIW (8)

The development of the notch stress method has been the focus of significant research efforts in recent years. Lawrence et al. (38) proposed a procedure for the evaluation of fatigue notch factor, based on Peterson's hypothesis (39). In their study, the authors considered an approximate radius of 0.25mm at weld toe, as the worst-case condition. Köttgen et al. (40) proposed a notch stress approach for welded joints, which uses a toe radius of 1 mm for steel components, based on the mean of values obtained through experimental samples. Multiple welded T and Y joints with variable plate thicknesses (between 8 and 40mm) were investigated to obtain the characteristic values of the notch stress $S-N$ curve.

Zhang and Richter (41), developed a new approach for numerical fatigue life prediction of spot-welded structures, considering the relationship between the stress intensity factor and the notch stress with the fictitious radius of 0.05 mm. Sonsino et al. (42) investigated notch stress concept for four structural components from different industrial sectors, considering the reference radius of 1 mm and 0.05 mm for thick walled steel and thin walled welded steel connections, respectively.

Aygul et al. (43) conducted a comparative study on five selected common welded joints in steel bridges to investigate the fatigue strength results of three different fatigue assessment methods. They concluded that the effective notch stress method, provides an inconspicuous improvement in estimation of the fatigue strength, while more efforts for modeling and computation is required. Sonsino applied the notch stress method to obtain the maximum principal stress at weld toe, when the direction of the principal stress might be constant (proportional loading conditions). Also, the method was applied in multiaxial stress condition, in non-proportional loading condition (44).

2.3.3 Linear elastic fracture mechanics method–LEFM

Under cyclic applied stresses, an initiated crack can start to propagate and cause fracture in the cracked component. Fatigue assessment of cracked welded component are frequently executed, using fracture mechanics methods. Linear elastic fracture mechanics (LEFM) is a recognized method in estimating fatigue strength variations with the progress of an initiated crack in a linear elastic material, while the method does not reflect the plasticity effects (45). LEFM method considers the stress state at a crack tip to estimate the fatigue strength of the cracked component, through linear elastic relationship. LEFM method is applied for fatigue assessment of welded structural components, which include an initiated crack at the welded area (can initiate from 0.05 to 1 mm) (46).

The stress intensity factor (SIF) is defined as the state stress at a crack tip. The LEFM method also reflects the process of fatigue crack propagation in three different phases. As shown in Figure 2-13, the crack progress per stress cycles, is related to the corresponding SIF variations (in a logarithmic scale). The first phase represents the material resistance for crack initiation, which

is called threshold region. In this phase, the crack propagation may negligibly occur, while the rate of progress is very slow.

The second phase will take place, when the initiated crack starts to propagate. The crack propagation can occur, when the measured SIF exceeds the threshold value, K_{th} . The K_{th} , can be determined through experimental material toughness tests (47). In the second phase, the crack propagation has a linear trend until the SIF increases to the critical limit, K_{IC} . The critical limit is the end of the second phase, which separates the phase II and phase III. Phase III describes fracture of the cracked component, when the resulting SIF exceeds the critical limit in the third phase.

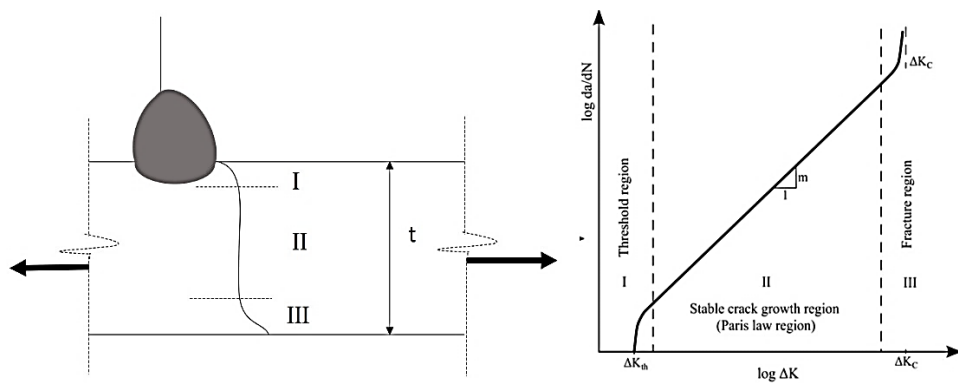


Figure 2-13 Three crack regions in crack propagation

The LEFM method relationships are developed for different crack types, which are classified in three dominant crack-type categories. The crack-types are categorized based on the loading conditions as well as the resulting crack. Shown in Figure 2-14, Mode I crack is induced due to tensile stresses, which causes an opening crack mode. Mode II crack occurs due to in-plane shear stresses, which causes sliding between the crack faces. Mode III expresses tearing mode, which can be induced with torsion. In welded structures, the induced crack may follow one of these three patterns, depending on loading condition. In addition, mixed-mode cracks can occur in

a complex loading situation which may happen in welded structural components of large-scale steel bridges.

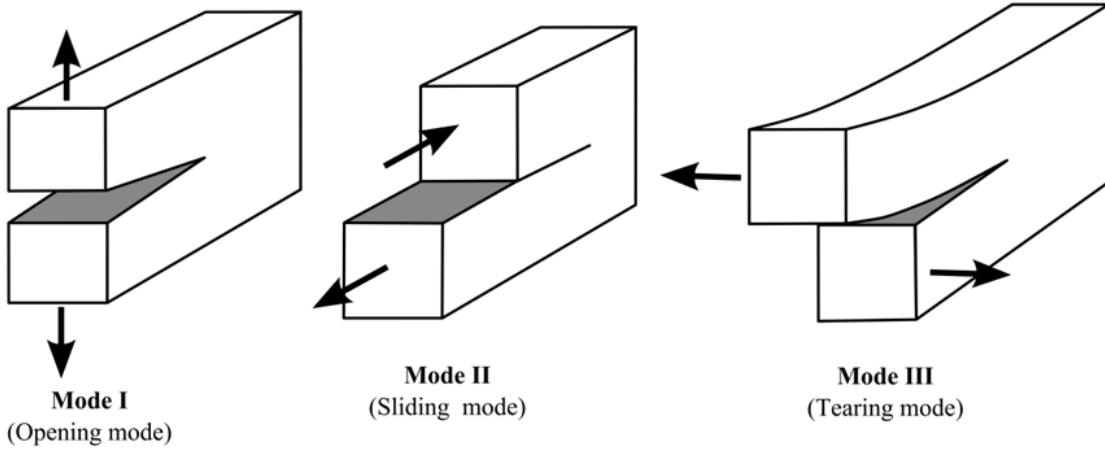


Figure 2-14 The three loading conditions/modes in fracture mechanics (45)

Fatigue remaining life cycles due to an initiated crack in welded structural components can be estimated using Paris's Law (48), as expressed in Eq. (3.6):

$$\frac{da}{dN} = C(\Delta K)^m , \quad \text{Eq. (2.6)}$$

where C and m are the constants that define the material properties (determined experimentally). For most of the materials m varies from 2 to 4 in cyclic-loaded structural components (45). The remaining fatigue life cycles can be extracted, using Eq. (3.7).

$$N = \frac{1}{C} \cdot \int_{a_0}^{a_f} \frac{da}{\Delta K^m} \quad \text{Eq. (2.7)}$$

SIF range (ΔK) is obtained through Eq. (3.8)

$$\Delta K = K_{max} - K_{min} = f(a) \cdot \Delta \sigma \cdot \sqrt{\pi \cdot a} , \quad \text{Eq.(2.8)}$$

where a denotes the crack size. $\Delta\sigma$ is the cyclic stress range at the crack tip, and $f(a)$ is a function which is dependent on the geometry, loading condition, and crack shape. The $f(a)$ can be found in the literature for a variety of the stress components. The Paris law is implemented to the linear elastic materials that include an initiated fatigue crack, while the final crack size can be defined by assumption. In (11) the minimum size of 0.1 mm is described as the short crack, where the application of LEFM is prohibited for the smaller crack size. BS 7910:1999 recommends to estimate the initial crack size, based on the thickness of a cracked material (49). In the available literature, the thickness of a cracked material is considered as the final crack size (50). However, in reasonably thick materials, smaller sizes of crack shall be applied.

Paris's law and the existing constants are obtained based on the Mode I crack. However, for the combinations of the three modes, the Paris's law is modified, using the equivalent SIF of the existing crack modes (K_{eq}), expressed in Eq. (2-9) by IIW (29).

$$\Delta K_{eq} = \sqrt{K_I^2 + K_{II}^2 + (1 + \vartheta)K_{III}^2}, \quad \text{Eq. (2.9)}$$

where ϑ is the Poisson's ratio. Accurate computation of SIF is one of the fundamental steps in LEFM method. There are multiple methods for calculating the SIF, which include crack tip opening displacement method, crack tip stress field method and *J-integral* (46). The relationship between the *J-integral* and SIF of different modes can be expressed as:

$$\begin{aligned} J_I &= \frac{K_I^2}{E'} \\ J_{II} &= \frac{K_{II}^2}{E'} \\ J_{III} &= K_{III}^2 \left(\frac{1 + \vartheta}{E'} \right) \end{aligned} \quad \text{Eq. (2.10)}$$

where E' denotes the Young's modulus of the material, which is equal to E and $(1 - \vartheta^2)/E$ for plane stress and plan strain materials, respectively. Theoretical relationships are also available in BS 7910:1999 (49). The *J-integral* method is utilized for complex details that experience mixed-mode crack conditions. For the mixed crack mode, the corresponding *J-integral* can be expressed as Eq. (2.11).

$$J = \frac{1}{E} (K_I^2 + K_I^2) + \frac{1}{2E} (K_{III}^2) \quad \text{Eq. (2.11)}$$

Additional details for fatigue crack propagation estimation using, are addressed in Chapter 8.

References

- 1) ASCE. 1982. "ASCE committee on fatigue and fracture reliability ." *Fatigue reliability:Journal of Structural Division* 3-23.
- 2) Fisher, J. W. Albrecht, P., Yen, B. T., Klingerman, D. J., McNamee, B. M. 1974. *Fatigue strength of steel beams with welded stiffeners and attachments*. Washington, DC : NCHRP report, Transportation Research Board.
- 3) Nussbaumer, A., Borges, L., and Davaine, L. 2011. *Fatigue Design of Steel and Composite Structures*. Berlin: ECCS – European Convention for Constructional Steelwork.
- 4) Gurney, T.R. 1979. *Fatigue of welded structures*. Cambridge: Cambridge University Press.
- 5) American Society for Testing and Materials. Committee E08 on Fatigue and Fracture. 2007. *Standard practice for conducting force controlled constant amplitude axial fatigue tests of metallic materials*. ASTM.
- 6) Sinnet, B. 2013. <http://www.substech.com/dokuwiki/doku.php?id=fatigue>.
- 7) EN1993-1-9. 2005. *Eurocode 3: Design of Steel Structures - Part 1-9: Fatigue*. Brussels: European Committee for Standardization.
- 8) IIW. 2008. *Recommendation for fatigue design of welded joints and components*. Cambridge, England: IIW-1823-07 ex. XIII-2151r4-07/XV-1254r4-07, The international Institute of Welding.
- 9) AASHTO. 2012. *Specifications for fatigue evaluation of existing steel bridges*. Washington, DC: American Association of State Highway and Transportation Officials.
- 10) Fatemi, A., and Yang, L. 1997. "Cumulative fatigue damage and life prediction: a survey of the state of the art for homogenous materials." *International Journal of Fatigue* 9-34.
- 11) Radaj, D., Sonsino, C. M., and Fricke, W. 2006. *Fatigue Assessment of Welded Joints by Local Approaches*. Cambridge: 2. Edition: Woodhead Publishing.
- 12) Administration, Federal Highway. December 2016. *Design and Evaluation of Steel Bridges for Fatigue and Fracture, Reference Manual*. Publication No. FHWA-NHI-16-016.
- 13) Miner, M.A. 1945. "Cumulative damage in fatigue." *Journal of Applied Mechanics* 12 (3): A159-A164.
- 14) Downing S.D., and Socie D.F. 1984. "Simple Rainflow Counting Algorithms." *International Journal of Fatigue* 31-40.
- 15) DeWolf, J. T., Lauzon, R. G., and Culmo,M. P. 2002. "Monitoring bridge performance." *Structural HealthMonitoring* 129-138.
- 16) Connor, R. J., Richards, S. O., and Fisher, J. W. 2003. *Long-term Remote Monitoring of Prototype Orthotropic Deck Panels on the Bronx-Whitestone Bridge for fatigue evaluation*. Balkema, Lisse, The Netherlands: Recent Developments in Bridge Engineering, K. M. Mahmoud ed.
- 17) Lund, R., and Alampalli, S. 2004. *Estimating Fatigue Life of Patroon Island Bridge using Strain Measurement*. New York: Transportation Research and Development Bureau.
- 18) Imam, B., Rightinotis, T. D., and Chryssanthopoulos, M. K. 2005. "Remaining fatigue life estimated for riveted railway bridges." *Journal of Engineering Bridge management* 417-423.
- 19) Frýba, S., and Urushadze, L. 2012. "Improvement of fatigue properties of orthotropic decks." *Journal of Engineering Structures* 1166-1169.
- 20) Wang, W. , Deng, L. and Shao, X. 2016. "Number of stress cycles for fatigue design of simply-supported steel I-girder bridges considering the dynamic effect of vehicle loading." *Engineering Structures* 70-78.
- 21) Neimi, E., Marquis, G.,. 2002. "Introduction to the structural stress approach to fatigue analysis of plate structures." *Proceedings of the IIW fatigue seminar, 2002*.

- 22) De Back, J. 1987. "The design aspects and fatigue behaviour of tubular." *Proceedings of the Third International ECSC Offshore Conference on Steel in Marine Structures*. Amsterdam: Noordhoek C, de Back J, editors. 205-240.
- 23) Fricke, W. 2001. "Recommended hot spot analysis procedure for structural details of FPSO's and ships based on round-robin FE analyses." *International Journal of Polar Engineering* 12 (1): 1-8.
- 24) Maddox, S.L. 2002. "Hot-spot stress design curves for fatigue assessment of welded structures." *International Journal of Polar Structures* 12 (2): 134-141.
- 25) Lotsberg, I. 2004. "Recommended methodology for analysis of structural stress for fatigue assessment of plated structures." Houston, USA: Proceedings of OMAE specialty symposium on integrity of FPSO system.
- 26) Niemi, E., Fricke, W. Maddox, S.J., Fatigue Analysis of Welded Components Designer's Guide to the Structural Hot-Spot Stress Approach. s.l. : Woodhead Publishing, 2006.
- 27) Fricke, W., Fatigue Design and Structural Hot-Spot Stress Determination for Welded Joints. s.l. : 9th Portugues Conference of Fracture, 2004.
- 28) Lotsberg, I. 2009. "Stress concentrations due to misalignment at butt welds in plated structures and at girth welds in tubulars." (*International Journal of Fatigue*) 31 (8-9): 1337-1345.
- 29) Hobbacher, A.F. 2016. *Recommendation for fatigue design of welded joints and component*. Springer International PublishingSpringer, 978-3-319-23757-2 .
- 30) Marquis, G.B., Barsoum ,Z . 2016. *IIW recommendations for the HFMI treatment*, Singapore, Singapore: Springer 9789811025037.
- 31) Fricke, W. 2010. *IIW Recommendations for the Fatigue Assessment by Notch Stress Analysis for Notch Stress Analysis for Welded Structures*. International Institute of Welding.
- 32) Dong, P. 2001. "A structural stress definition and numerical implementation for fatigue analysis of welded joints." *International Journal of Fatigue* 23 (10): 865-876.
- 33) Niemi, E., Fricke, W. and Maddox, S.J. 2016. *Structural hot-spot stress approach to fatigue analysis of welded components-Designer's guide*. IIW-XIII-2639r3-16,XV- 1521r3-16.
- 34) Connolly, M. P., Helier, A. K., and Sutomo, J.,. 1990. "A parametric study of the ratio of bending to membrane stress in tubular Y- and T-joints." *International Journal of Fatigue* 12 (1): 3-11.
- 35) Dong, P. and Hong, J. K. 2002. *A Structural Stress Based Master S-N Curve*,55th International Institute of Welding (IIW). Doc. XIII-1930-02/XV-1119-02, Copenhagen, Denmark: IIW.
- 36) Dong, P., Hong, J. K., and Cao, Z. 2003. "Stress and Stress Intensities at Notches: Anomalous Short Crack Growth." *Intenrational Journal of Fatigue* 25: 811-825.
- 37) Radaj, D. and Sonsino, C.M. 1998. *Fatigue Assessment of Weldd Joints b Local Approaches*. Woodhead Publishing.
- 38) Lawrence, F.V., Burk, J.D., and Yung, Y.K. 1982. *Influence of residual stress on the predicted fatigue life of weldments*. Philadelphia: ASTM STP 776. Residual stress effects in fatigue.
- 39) Peterson, R. E. 1974. *Stress Concentration Factors*. USA: John Wiley & Sons.
- 40) Köttgen, V.B., Olivier, R., and Seeger, T. 1991. *Fatigue analysis of welded connections based on local stresses (English Translation)*. Dusseldorf: IIW-doc. XIII-1408-91/XV-802-92,International Institute of Welding.
- 41) Zhang G, Richter B. 2000. "New approach to the numerical fatigue-life prediction of spot-welded structures." *Fatigue and Fracture of Engineering Materials and Structures* 23: 499-508
- 42) Sonsino, C. M., Fricke, W., De Bruyne, F., Hoppe, A., Ahmadi, A., and Zhang, G. 2012. "Notch stress concepts for the fatigue assessment of welded joints—background and applications." *International Journal of fatigue* 2-16.
- 43) Ayg"ul, M., Bokesj, M., Heshmati, M. and Mohammad. M. 2013. "A comparative study of different fatigue failure assessments of welded bridge details." *International Journal of Fatigue* 62-72.
- 44) Sonsino, C.M. 2009. "Multiaxial fatigue assessment of welded joints – Recommendations for design codes." *International Journal of Fatigue* 31: 173-187.

- 45) Andersson, T.L. 2017. *Fracture Mechanics: Fundamentals and Applications, Fourth edition*. New York, USA: CRC Press Taylor and Francis Group.
- 46) Schijve, J. 2009. *Fatigue of structures and materials* . Netherlands: Springer.
- 47) BS7608:1993. 1999. *Code of Practice for Fatigue Design and Assessment of Steel Structures* . London, United Kingdom: British Standard Institution.
- 48) Paris, P.C., and Erdogan, F. 1963. "A Critical Analysis of Crack Propagation Laws." *Journal of Basic Engineering* (Transaction ASME), 85 (4): 528-534.
- 49) BS7910:1999. 2000. *Guide on methods for assessing the acceptability of flaws in fusion welded structures*. London, United Kingdom: British Standard Institution.
- 50) Maddox, S. J. 1974. "Assessing the significance of flaws in welds subject to." *Welding Journal Research Supplement* 401-409.

Chapter 3

3 THE CASE-STUDY: THE MEMORIAL BRIDGE

3.1 Introduction

In this section, the case-study bridge, the Memorial Bridge is introduced. The geometric details of the structural components are briefly presented, as well as the structural sensor layout, load test plan and data acquisition system. The target structural component of the Memorial Bridge, the gusset-less connection, and the requirements for fatigue assessment are presented. The Memorial Bridge is equipped with a long-term structural health monitoring (SHM) program. The instrumentation plan, the data type and frequency of each type is also discussed in this chapter. The long-term collected data sets at the Memorial Bridge are utilized for the fatigue assessment goal of this research.

3.2 The case-study, the New Memorial Bridge

The Memorial Bridge carries US Route 1 across the Piscataqua River connecting Portsmouth, NH with Kittery, ME, (see Figure 3-1). The bridge is also the only pedestrian link between the two communities, which was opened to traffic in July 2013 (1). The new Memorial Bridge is a vertical lift truss bridge, which includes an innovative “gusset-less” truss connection and a metalized corrosion protective coating (2). Each span has a 297 ft (91 m) length. The vertical lift tower has 158 feet (48 m) height. The truss elements consist of W14 section diagonals ranging in size from a W14x90 to a W14x211 depending on location along the span and built-up chord

elements with integral knuckle connection. The chord elements are constructed with 1-inch and 1-1/4-inch (2.5-cm and 3.2-cm) thick web plates. The top chord web plates are 24 inches (0.61m) tall and the bottom chord web plates are 36 inches (91 cm) tall. The flange plates range in thickness from 1-1/4-inch (3.2-cm) to 2-3/4 inches (7.0 cm) and are 26 inches (66 cm) to 36 inches (91 cm) wide. The web-flange connection is a 5/8-inch (1.6 cm) weld.



Figure 3-1 The Memorial Bridge, Portsmouth, NH.

The gusset-less truss connection is shown in Figure 3-2. This connection is unique to the Memorial Bridge and is the only connection of its kind in a vehicular bridge, which makes the verification of the design procedure vital for future applications of this connection type. The complex geometry of the curved fillet weld, the impact on creation stress concentrated areas at the weld toe and on the induced hotspot stresses, make the connection an appropriate example for the fatigue assessment goals of the study.



Figure 3-2 The gusset-less connection at the Memorial Bridge

3.3 The instrumentation plan of the Memorial Bridge

The long-term structural health monitoring of the Memorial Bridge is implemented through an array of sensors, which are permanently installed at the bridge. The south span and south lift tower are the instrumented parts of the bridge. The sensors are installed through an instrumentation plan, which is designed based on the initial observations and a numerical model (3). The sensor network is a valuable tool to capture the response of critical bridge elements under traffic loads. In addition to the traffic, the life action of the bridge is another source of excitations, which provides a unique opportunity to obtain the structural response due to the vertical lift operations. Through a long-term continues data collection program, the influence of environmental variations on the recorded structural responses are also investigated, due to the coastal location of the bridge. In Table 3-1, the details of the instrumentation plan of bridges is expressed. The structural sensors and the current instrumentation layout are shown in Figure 3-3.

Table 3-1 Structural health monitoring sensors of the Memorial Bridge

Type of SHM Sensors	Number of Sensors		Total Number of Sensor Channels
	East Face	West Face	
Uniaxial Accelerometer (1 channel)	9	3	12
Rosette Strain Gage (3 channels)	14	2	48
Uniaxial Strain Gage (1 channel)	5	5	10
Biaxial Tiltmeter (2 channels)	2	0	4

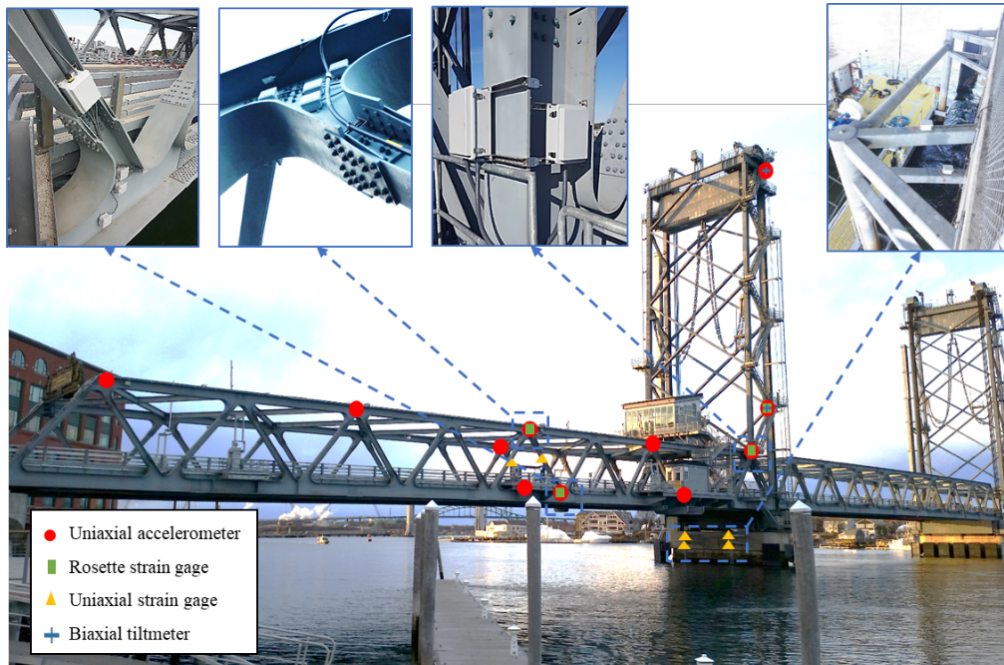


Figure 3-3 Structural health monitoring instrumentation installed at the Memorial Bridge, Portsmouth, NH.

The information collected from the structural sensors will be used to calibrate the bridge's structural FE models. The resulting numerical responses from validated FE models are also utilized to supplement the field collected SHM data for fatigue assessment. In addition, the SHM data continuously collects information about the in-service performance of the bridge, related to the structural performance.

3.4 Data collection program at the Memorial Bridge

In the SHM program of the Memorial Bridge, three types of strain data are collected, including decimated, normal, and event data (expressed in Table 3-2). The decimated data, and the high-speed normal data are collected continuously to study the daily trends and the detailed performance of the bridge respectively. In Figure 3-4, the samples of event and normal strain data are shown, respectively. It can be observed that the decimated data notices a daily change in the trend of structural responses, while the normal data reflects the detailed variations. In this study, the normal data is utilized for fatigue assessment of the gusset-less connection. The changes in the traffic load and/or environmental impacts can be investigated using the normal data.

The event data is collected via a triggered program. Event data collection starts with lift action and continues for a 20-minutes period after each lift. This time interval was selected based on the initial observations of the monitoring data, which ensures to collect the data during a considerable traffic volume congested after each lift action. Consequently, the number of the event samples per day have a variable property, corresponding to the number of experienced lift actions in each day. In addition, the duration of the rise and fall of the midspan is identical for all of the collected lift events. However, the height and duration of lift depends on the naval traffic. In Table 3-2, the details of data collection program of the Memorial Bridge are expressed.

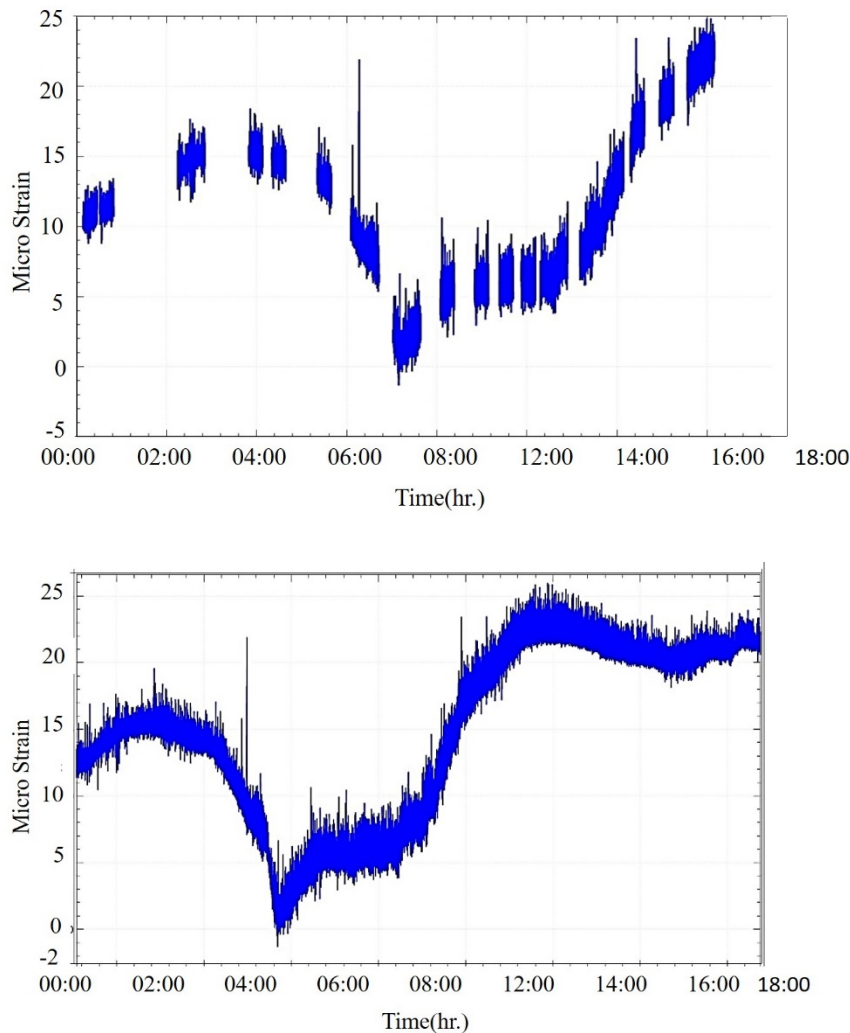


Figure 3-4 Sample time-history strain responses, a) collected event data, b) collected normal data

Table 3-2 Data collection program at the Memorial Bridge.

Type of data	Sample rate (Hz)	Daily data collection	Objective
Decimated	600	Continuous (24 hour)	The overall trend
Normal	50	Continuous (24 hour)	Condition Assessment
Event	50	Lift Event triggered (20 Minutes)	Lift operation assessment

In Figure 3-5, the time-history acceleration responses of the accelerometer at the bottom of the tower is shown. The responses of this sensor are investigated to be the most sensitive data to

the lift action, which is obtained through the observations. The acceleration threshold for the trigger program is defined based on the acceleration responses of this accelerometer. The 20-minutes duration of data collection after lift action is defined based on the traffic records by the video camera, installed at the bridge. However, it is observed that the lift events that occur at less traffic hours may not significantly include traffic-induced stress cycles.

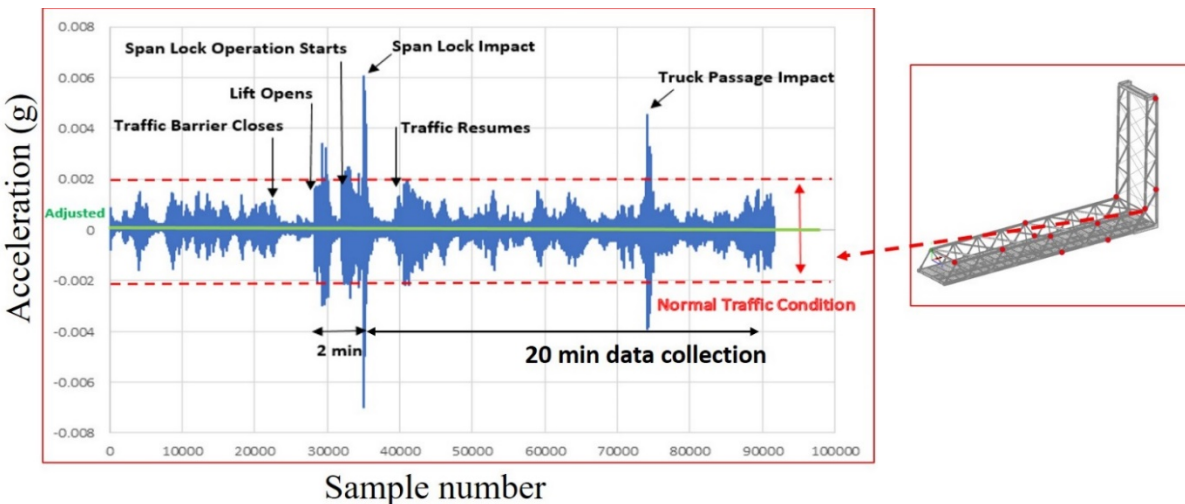


Figure 3-5 Defining the trigger program to collect the data during the lift events

3.4.1 Field-collected SHM data for fatigue assessment

In this study, only the normal and the event strain data are utilized for fatigue measurements (the nominal strain responses at the gusset-less connection). The collected strain responses less than 20 micro strain are considered as outliers and removed from fatigue calculations. Initial investigations were performed through synchronizing the traffic video camera records of the bridge with field-collected strain responses. It was observed that the strain responses that are induced under passenger cars and small trucks traffics are below the defined threshold (20 micro strain). The statistics of vehicle classes and related average daily truck traffic (ADTT) rates at the Memorial Bridge was reported by New Hampshire Department of Transportation (NHDOT).

Based on the reported vehicle classes, Class 6-10 are only considered for fatigue assessment goal of this study, as shown in Figure 3-6. It is also observed that the lift operation excitations cause a negligible stress response at the south span (below 20 micro strain) of the bridge. Therefore, the lift-induced strain responses are excluded for fatigue assessment of the target gusset-less connection in this work. In addition, the field collected strain responses are filtered to remove the outliers, which may influence the results. For this purpose, Hanning window with 60% overlap and bandpass Butterworth IIR filter is used using MATLAB® filtering tools. The lower cutoff frequency of 1 Hz and higher cutoff frequency of 5 Hz were used.

2018 AADT = **10,000** (Source: MS2 - NHDOT TDMS) US1 Memorial Bridge Functional Classification - Other Principal Arterial Urban (3U)

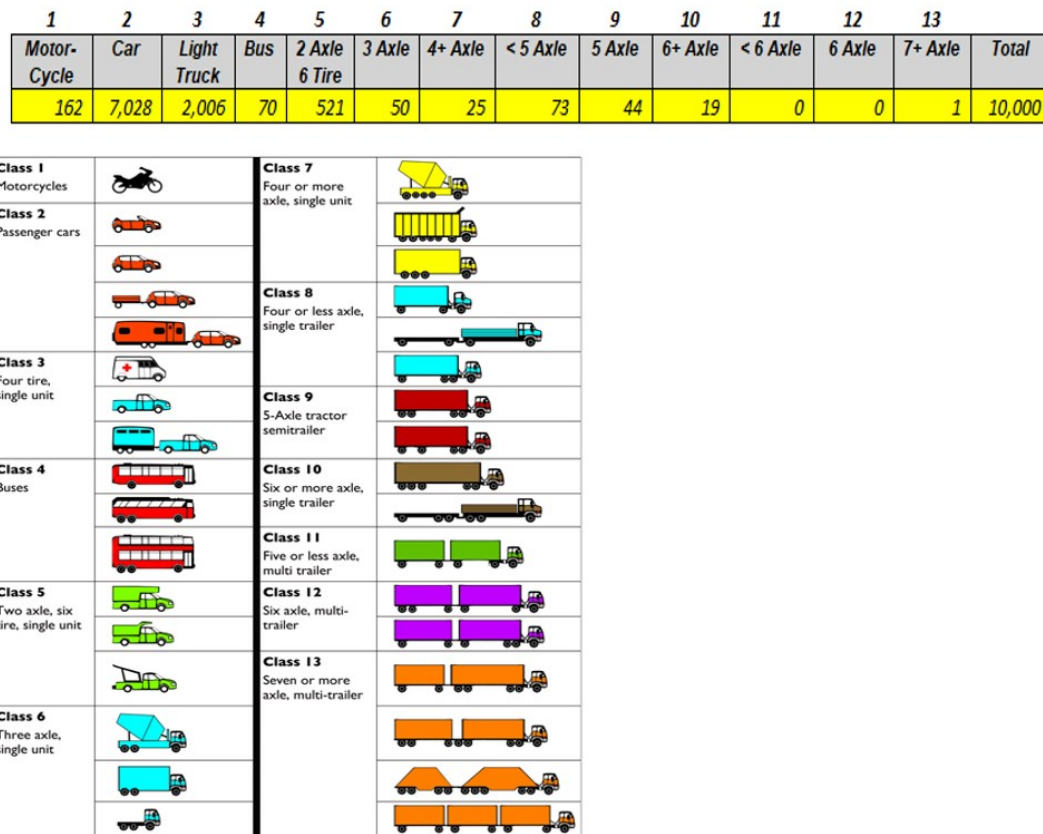


Figure 3-6 Truck class statistics at the Memorial Bridge provided by NHDOT

In addition to the long-term field collected strain data, numerical data is another source that will be employed for fatigue assessment goal of the study. The numerical data are obtained via validated FE models of the bridge. The FE models are validated using the field data that was collected during a truck load test.

3.5 Truck load test at the Memorial Bridge

A truck load test was designed and conducted at the Memorial Bridge, which includes multiple controlled pseudo-static and dynamic load tests. A tri-axial dump truck carrying jersey barriers was provided by NHDOT to load the bridge (see Figure 3-7). The measured load of the truck was reported 165KN (37 kips). Each run of the load test consists of a series of individual truck passes to ensure collection of high-quality data with minimized measurement errors. The pseudo-static tests were designed with two stop positions on both northbound and southbound of the bridge, see Figure 3-7. The pseudo-static results are applied for validating the FE models of the bridge.

The dynamic truck tests were conducted with the approximate speed of 48 KM/h, the maximum speed limits of each lane on the bridge. Two dynamic tests were conducted during the load test, which includes the individual truck with closed traffic and the individual truck with open traffic. These dynamic tests were designed to verify the numerical models in simulating multiple traffic scenarios. Using a validated FE model of the bridge, the time-history numerical responses are obtained under the simulated traffic scenarios. The resulting numerical time-history strain responses will be utilized for model-based fatigue assessment purpose of this study. In the following chapters, the details of validating the FE models through the load test results are explained.

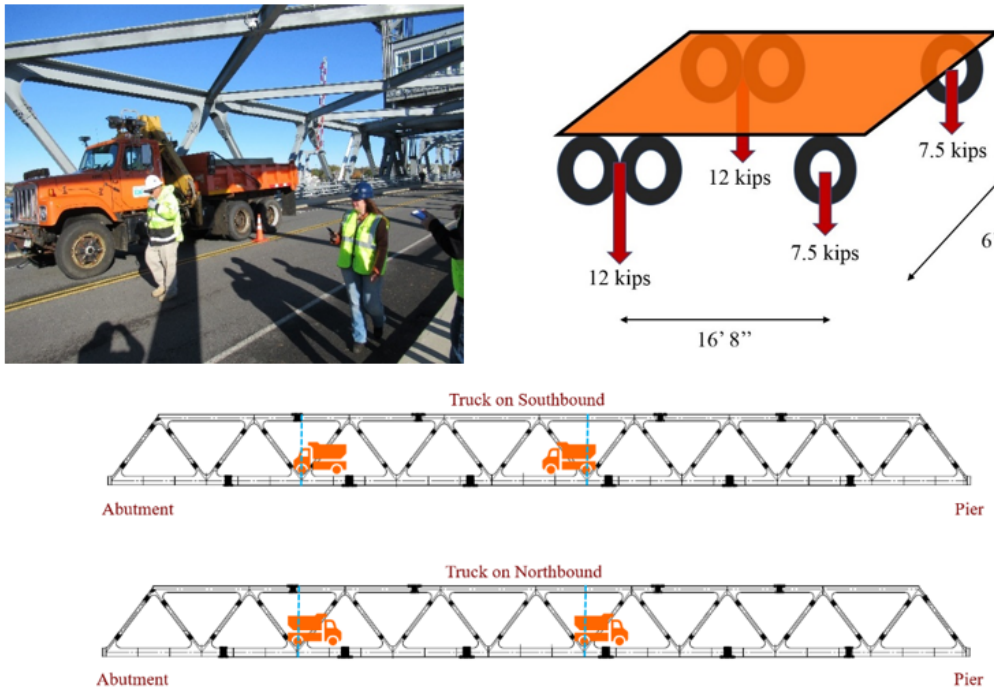


Figure 3-7 The truck load test configuration at the Memorial Bridge.

Table 3-3 Truck Load test specifications at the Memorial Bridge.

Load test	Load test description	Traffic condition	Speed (KM/h)	Objective
1	Quasi static/two stops	Single truck	10	Model verification
2	Dynamic	Single truck	48	Model verification
3	Dynamic	Multiple vehicles plus truck	48	Traffic simulation/fatigue assessment

The three load tests are applied in this study for model validation and simulation of the traffic scenarios.

References

- 1) Adams, T., Mashayekhizadeh, M. Santini-Bell, E., Wosnik, M., Baldwin, K., and Fu, T. 2017, "Structural Response Monitoring of a Vertical Lift Truss Bridge." *96th Annual Meeting, Transportation Research Board*. Washington, D.C.
- 2) NHDOT., 2016, "Memorial Bridge Project Innovations". New Hampshire Department of Transportation.
- 3) Mashayekhizadeh, M., Santini-Bell, E. and Adams, T. 2017," Instrumentation and Structural Health Monitoring of a Vertical Lift Bridge." *Proceedings of 27th ASNT Research Symposium*. Jacksonville, Fl.,

Chapter 4

4 THREE-DIMENSIONAL MULTISCALE FINITE ELEMENT MODELS FOR IN-SERVICE PERFORMANCE ASSESSMENT OF BRIDGES

Mashayekhi, M., Santini-Bell, E. 2018. Three-dimensional multiscale finite element models for in-service performance assessment of bridges. *Computer-aided civil and infrastructure engineering*, doi: <https://doi.org/10.1111/mice.12424>.

4.1 Abstract

Accurate representation of the structural performance of civil engineering structures, specifically complex bridge structures, may be achieved through an efficient multi-scale finite element (FE) model. Multiscale FE modeling couples multiple dimensions of elements in a single model. In this study, the selected existing multipoint constraint equations applied in planar coupling conditions are modified and refined for out-of-plane coupling conditions in a single three-dimensional FE model. Also, the optimum location for the interface points of different elements is determined to improve the model's accuracy and efficiency. The present case study, the Memorial Bridge in Portsmouth, NH, is a vertical lift bridge, which includes novel gusset-less connections. These connections have complex geometries and therefore require finer dimension elements to represent the structural behavior, while the remainder of the structure is modeled with coarser dimension elements. To achieve an accurate and efficient multiscale model of the

Memorial Bridge, multiple global FE models are developed, and the predicted structural responses are verified with respect to the field- collected structural responses of the bridge.

4.2 Introduction

Structural deficiencies including construction defects, fatigue cracks, or material degradation in critical structural members of bridges can create local performance abnormalities and, in some cases, influence the overall global performance of the structure (1). A finite element (FE) model calibrated with respect to structural health monitoring (SHM) data can facilitate the investigation of the influence of local impacts on global performance (2). The ability to include the impact of small physical or material changes in FE modeling requires high-dimensional property elements with fine mesh sizes to accurately represent the structural properties of the critical members (3) (4). In the global FE models of complex bridges, application of finer dimension elements can generate additional degrees of freedom (DOFs), which significantly increases the computational cost and decreases the ease of use of the model (5). In the global FE modeling of structures, there are less critical members that can be sufficiently modeled through coarser dimension elements to capture the global structural performance. A successful multiscale approach must accurately couple multiple element types in a single FE model to reduce the number of DOFs, and subsequently, the cost of analysis. This method requires an appropriate coupling system (constraint equation) to provide a uniform stress distribution and continuous displacement at the interface point of multiple element types (6).

In the early stages of applying mixed dimensions in FE modeling, numerous methods were proposed. Surana (7) proposed a method developing isoperimetric transition elements for various cross-sectional properties and stress analysis, which was further expanded to connect the

axisymmetric shell to solid elements (8). Gong applied multiple transition elements for local and global structural elements through providing the criterion for differentiating the local and global areas (9). Application of the transition elements was extended by Liao et al. for geometrically nonlinear laminated composite elements (10). Gumur and Kauten also applied the transition elements in the dynamic analysis (11). More developments were implemented by Guzelbey and Kanber who derived practical shape functions for two-dimensional (2D) transition elements using the Pascal triangle (12). The transition element relationships are highly dependent on the number of the applied nodes and the defined mesh pattern for each multiscale application that may not be reusable when the mesh patterns change.

The kinematic coupling method, an alternative approach for the multiscale modeling, applies rigid links to couple the translational and rotational DOFs of multiple element types at the interface point as a function of the nodal displacements. However, the rigid links used in this method can restrict the deformation at the interface point that makes the method less desirable for the multiscale modeling (13). Carrera et al., developed a variable kinematic FE to combine multiple elements in a one-dimensional (1D) domain using Lagrange multipliers (14).

Another approach in developing multiscale models is known as the multipoint constraint (MPC) equation method, which couples the displacements of multiple dimensions at the interface point (15) (16). McCune employed the Reissner bending theory of elastic plates to couple beam-to-shell and shell-to-solid elements (17). Further developments were implemented by Monaghan et al. for multiple cross sections of the shell-to-solid and beam-to-solid elements (18). The developed MPC equation method in this research equates the work performed by different element types on either side of the interface point to provide a compatible displacement and continuous stress distribution in the multiscale FE models. The MPC method can be applied to couple

numerous dimensional elements and is extensively utilized by researchers for model-updating and damage assessment purposes (19) (20). Furthermore, in recent years, other multiscale approaches were also developed to increase the ease of application. Wang et al. developed a coupling method using the virtual work principle in providing the displacement compatibility and stress equilibrium (21). Izzuddin and Jokhio recently developed a mixed-dimensional method, which is based on the transition element and MPC equation methods for partitioned nonlinear FE analysis (22). In recent years, the application of the multiscale approach has also been expanded in multiple fields including historic masonry restoration (23) (24).

Advances in available FE commercial software increase the ease of the FE model development of complex structures. In this study, a three-dimensional (3D) multiscale global FE model of a complex bridge is developed using the MPC equations originally presented by McCune (17) and Monaghan (25). This method was applied to a 2D multiscale model of structures where both element dimensions have a planar alignment (26). The 3D geometry of a global FE model requires the coupling of multiple dimensions including planar as well as out-of-plane conditions. In this study, the existing MPC equations are modified to account for the out-of-plane coupling behavior where the different element types have non-planar directions. Multiple global FE models are developed to determine the optimal multiscale model through the comparison of the calculated structural responses and the field- collected SHM data. The multiple developed models in this study support a protocol for the 3D multiscale modeling of complex bridge structures.

Also included in this article is the optimum location for the interface point of the intersecting elements, representing the optimum ratio of the finer to the coarser dimensions in a global multiscale FE model. The optimum location for the interface point is defined by minimizing the difference between the results of the developed multiscale model and other models, as well as

the field collected SHM data. It is illustrated that in a global FE model, the optimum location of the interface points surrounding the finer dimension components will enhance the accuracy and efficiency of the model.

4.3 Multiscale methodology

Developing multiscale FE models is becoming more popular in aviation, automotive, and civil structure designs. In this study, the multiscale modeling approach is applied to develop a 3D model of a bridge structure. In 3D multiscale modeling, multiple element types can intersect in the planar and nonplanar directions. The demand for coupling of multiple dimensions in arbitrary alignments requires to apply the constraint equations in the planar as well as nonplanar coupling conditions. The out-of-plane coupling condition in the multi- scale modeling is less studied. The MPC equation method is developed and applied in the planar coupling condition for a variety of multiple elements. The MPC equations developed by McCune rely on the equivalence of the work performed by multiple elements types at the interface point (27). The method applies the Reissner bending theory of plates for linear elastic plates that considers the through thickness shear effect of the shell elements (28). This method is proficient in the multiscale model development for a variety of elements and cross-section properties coupled in the planar conditions, as demonstrated in the previous researches (29). In the planar coupling condition, where two different dimensions of elements have the same alignment at the inter- face point, the assumption of the long and slender property for the member modeled with the finer dimension element results in similar behavior for the members at each side of the interface point. In the out-of-plane coupling condition, where different dimensions do not have identical alignments, the assumption of a long, slender member is invalid. This limitation restricts the application of the method in the modeling of a 3D structure

where two different dimensions can have nonplanar alignments. In the out-of-plane coupling condition, the unequal performance of the coupled dimensions under a single load at each side of the interface point can be expected. Consequently, in the out-of-plane coupling conditions, providing a continuous displacement at the interface point between the intersecting elements having incompatible alignments and performance is rather complex. The work-based MPC method aids to develop the constraint equations that are not exclusively dependent on the displacement of the intersecting elements. In this method, developing the constraint equations relies on the work equation that considers the stress as well as the displacement distribution. This approach can ensure a more compatible displacement and continuous stress distribution at the interface point for the out-of-plane coupling condition.

In this section, the development of the required constraint equations for the out-of-plane coupling through the extrapolation of the existing MPC equation applied for the planar coupling is presented. The constraint equations in this study are developed to couple a 2D member modeled with shell elements (shell member) to a 1D member modeled with beam elements (beam member) under various loading conditions. As shown in Figure 4-1a, in the planar coupling, the lateral edge plane of the shell member is coupled to the end point of the beam member at the interface point. In Figure 4-1b, the lateral plane is replaced by the face edge plane for the out-of-plane coupling condition. In addition, shown in Figure 4-2a, in the planar coupling condition, only the shell elements situated at the lateral edge plane of the shell member are involved in the coupling. In the out-of-plane coupling condition, all the shell elements placed at the face edge plane of the shell member are coupled, as shown in Figure 4-2b. This can increase the number of DOFs and computation time, which is required to determine the optimum area of coupling for the shell elements.

The beam and the shell elements considered in developing the constraint equations, in this study, are the 3D thick beam and thick shell elements, each having six nodal DOFs. Therefore, six constraint equations are required to entirely couple multiple element types at the interface point. Correspondingly, six loading conditions are also required to develop the six constraint equations, while the load is applied at the interface point. The work of the beam member is measured as a product of the applied load and the induced displacement at the interface point. Similarly, the work of the shell member is measured using the induced nodal stresses and displacements at the edge plane of the shell member.

The general form of the work equation for the beam member, Π_B , with six nodal DOFs and six analogous loadings is expressed as:

$$\Pi_B = (F_x u + F_y v + F_z w + m_x \theta_x + m_y \theta_y + m_z \theta_z) \quad \text{Eq. (4-1)}$$

where F_x is the axial force, F_y and F_z are the shear forces in y and z directions respectively, m_x is the torsional moment around the x axis, and m_y and m_z are the bending moments in the xz and xy directions respectively. For the shell member, the work equation, Π_S , under the identical loading conditions is written as:

$$\Pi_S = (F_x U + F_y V + F_z W + M_x \theta_x + M_y \theta_y + M_z \theta_z) \quad \text{Eq. (4-2)}$$

The lower-case displacements, u , v , w , θ_x , θ_y , θ_z expressed in the Eq. (4-1), are the translational and rotational DOFs of the beam member with respect to the Cartesian coordinate system at the interface point. The upper-case displacements, U , V , W , θ_x , θ_y , θ_z in Eq. (4-2) are the equivalent translational and rotational DOFs at the edge of the shell member with respect to the Cartesian coordinate system at the interface point. In the following, the constraint equations for multiple loading conditions, including the axial load, bending moment, torsion moment and shear

force, are addressed. In each loading condition, the planar constraint equations are initially expressed to illustrate the refinements required to develop the corresponding out-of-plane constraint equation.

The planar relations expressed for each loading condition are based on the previous efforts by Monaghan (25), who developed the method for the circular sections modeled with solid elements to be coupled with beam elements, and later by Yu et al. (30) who considered the pipe and box cross-sections modeled with shell elements to be coupled with beam elements. The procedure of developing the planar constraint equation is explained in detail in the addressed references and is not repeated in this paper.

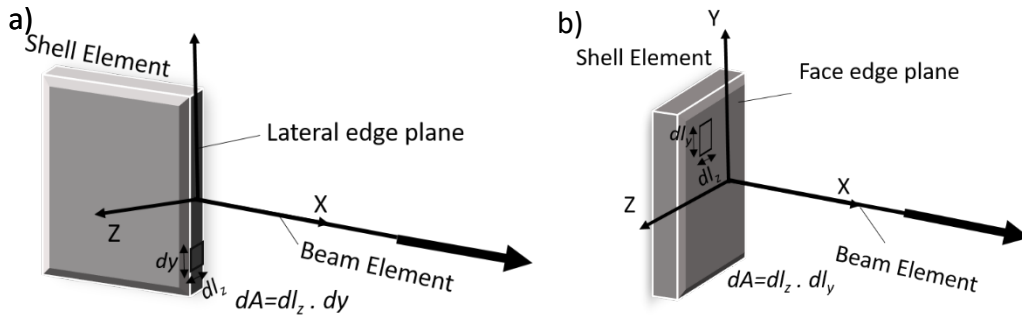


Figure 4-1(a) Planar multi-scale coupling condition (b) Out-of-plane multi-scale coupling condition (beam to shell member).

4.3.1 Axial Load

The axial load applied to the end point of the beam member causes axial displacements in the beam as well as the shell member. The axial displacement creates normal stress at the edge plane of the shell member. The constraint equation at the interface point can be expressed as Eq. (4-3):

$$F_x u = \int_A \sigma_x U dA \quad \text{Eq. (4-3)}$$

where F_x and u are the applied axial force and axial displacement of the beam element respectively. σ_x and U are the equivalent normal stress and displacement at the edge plane of the shell member respectively. Eq. (4-3) is the general form of the constraint equation of the beam to shell member under an axial load that must be refined for the planar as well as the out-of-plane coupling conditions.

In-plane. For the planar coupling condition, the equivalent displacement of the shell member at the interface point can be expressed as the sum of all nodal displacements generated at the edge nodes shown in Figure 4-2(a) as:

$$U_e = \sum_{i=1}^{N_{\text{element}}} [N_i] \{U_i\} \quad \text{Eq. (4-4)}$$

where U_e is the equivalent displacement, $[N]$ is the matrix of the quadratic shape functions for a four-nodded shell element, and $\{U\}$ is the vector of the nodal axial displacements for the edge shell elements at the interface point. Using the FE relationship shown in Eq. (4-4) for the equivalent axial displacement of the shell member, the constraint equation is shown in Eq. (4-5):

$$F_x u = \sum_{i=1}^{N_{\text{element}}} \int_A \sigma_x [N_i] dA \{U_i\} = [B] \{U\} \quad \text{Eq. (4-5)}$$

where $[B]$ is the matrix of the constant coefficients which is defined through the shape functions as well as the geometrical and material properties of the shell elements. In addition, with the assumption of a long, slender, two-dimensional member in the planar coupling condition, uniform stress distribution can be assumed all over the edge plane of the shell member. The area for the lateral edge plane of the shell member, A , can be expressed as the sum of the areas of the edge shell elements, as shown in Eq. (4-6)

$$A = \sum_{i=1}^{N_{\text{element}}} t_i l_i \quad \text{Eq. (4-6)}$$

where t and l are the thickness and the length of the shell elements respectively, shown in Figure 1(a). The double integral over the area of the shell member can be decreased into a single integral by assuming a constant thickness at the lateral edge plane. The constraint equation Eq. (4-5) which is developed by a single integral over the length of the edge shell elements is shown in Eq. (4-7).

$$u = \frac{1}{A} \sum_{i=1}^{N_{\text{element}}} t_i \int_0^l [N_i] dy \{U_i\} \quad \text{Eq. (4-7)}$$

Out-of-plane. For the out-of-plane coupling condition, shown in Figure 4-1(b), the axial load applied to the end point of the beam member, causes axial displacement in the beam member and induces an out-of-plane displacement at the intersecting shell member. Depending on the plate geometries, the classical theory of plates (Kirchhoff-Love theory) for the thin shells, or the Reissner bending theory of plates for the elastic plates can be considered to develop the constraint equations (31). In the multi-scale modeling of bridge structures, the critical members modeled with thick shell or solid elements, are expected to experience small out-of-plane displacements. Therefore, the Reissner bending theory of plates is appropriate due to the assumed small out-of-plane deformations for the thick shell elements (28). In this case, the induced normal stress at the edge face of the shell member can be expressed as Eq. (4-8):

$$\sigma_x = \frac{3F_x}{4} \left[\frac{2}{3} + \frac{U}{t/2} - \frac{1}{3} \left(\frac{U}{t/2} \right)^3 \right] \quad \text{Eq. (4-8)}$$

where σ_x and U are the normal stress and the out-of-plane displacement of the shell member at the interface point respectively. The relationship for the axial constraint equation, Eq. (4-5) shall be considered for the out-of-plane coupling condition. However, the assumption of a uniform stress

distribution at the edge plane of the shell member is invalid. In this case, the work equation of the shell member is determined using the nodal displacements and stresses of the shell elements at the face edge plane shown in Figure 4-2(b). The constraint equation can also be solved at the Gauss points and then be extrapolated to the nodes of each element, as shown in Eq. (4-9):

$$F_x u = \sum_{i=1}^{N_{element}} \left\{ \sum_{j=1}^4 \sum_{k=1}^4 \sigma_x^{(k, j)} w_j \cdot w_k |J| [N_i] \{U_i\} \right\} \\ = [B] \{U\} \quad \text{Eq. (4-9)}$$

where J and w are the Jacobian and the weighting factors at the Gauss points, k and j respectively (32). In the out-of-plane coupling condition, four Gauss points are required to be considered in the equation.

4.3.2 Bending Moment

The bending moment applied to the end point of the beam member generates an out-of-plane rotation in the beam member, while it creates the equivalent normal stress and displacement at the edge plane of the shell member. The constraint equation is acquired by equating the work done by the bending moment for the beam member to the work done by the equivalent normal stress for the shell member at the interface point expressed as Eq. (4.10):

$$M_z \theta_z = \int_A \sigma_x y dA \quad \text{Eq. (4.10)}$$

where θ_z is the out-of-plane rotational displacement of the beam element at the interface point around z axis. Eq. (4-10) is applicable for the planar and out-of-plane coupling while required to be solved in different ways.

In-plane. For the planar coupling, the applied bending moment generates normal stresses at the lateral edge plane of the shell member. For the symmetric cross-sections of this study (I-shape and

rectangular), the induced normal stress can vary linearly along the edge shell elements shown in Eq. (4.11).

$$\sigma_x = \frac{M_z y}{I_z} \quad \text{Eq. (4-11)}$$

Using Eq. (4.11), the constraint equation Eq. (4.10) is solved at the Gauss points of the edge shell elements which can be written as Eq. (4.12):

$$\begin{aligned} \theta_z &= \frac{1}{I_z} \sum_{i=1}^{N_{element}} \left\{ \sum_{k=1}^2 y_i w_k |J| [N_i] \{U_i\} \right\} \\ &= [C] \{U\} \end{aligned} \quad \text{Eq. (4-12)}$$

where $[C]$ is the matrix of the constant coefficients defined by the shape functions and the physical properties of the shell elements.

Out-of-plane. For the out-of-plane coupling, the applied bending moment at the end point of the beam member causes normal stresses as well as out-of-plane displacements at the edge face plane of the shell member. The equivalent out-of-plane displacements can be assumed to vary linearly along the length of the coupling area as Eq. (4-13):

$$U_e = U + \theta_z \cdot y \quad \text{Eq. (4.13)}$$

where U_e is the equivalent out-of-plane displacement of the shell member. Eq. (4-13) can be expressed using the nodal displacement vector and the shape functions of the shell elements as shown in Eq. (4-14).

$$U_e = \sum_{i=1}^{N_{element}} [N_i] \{U_i\} + [N'_i] y_i \{\theta_{z_i}\} \quad \text{Eq. (4.14)}$$

The constraint equation Eq. (4-10) can be modified to couple the nodal displacements at the edge face plane of the shell member to the end point of the beam member at the interface point by substituting Eq. (4.14) and Eq. (4.11) which is shown in Eq. (4.15).

$$\theta_z = \frac{1}{I_z} \sum_{i=1}^{N_{element}} \int_{A_i} \left\{ y_i [N_i] \{U_i\} + y_i^2 [N'_i] \{\theta_{z_i}\} \right\} dA_i \quad \text{Eq. (4-15)}$$

Eq. (4-15) can also be solved at the Gauss points, shown in Eq. (4.16).

$$\begin{aligned} \theta_z &= \frac{1}{I_z} \sum_{i=1}^{N_{element}} \left\{ \sum_{j=1}^4 \sum_{k=1}^4 y_i w_j w_k |J| [N_i] \{U_i\} \right\} + \\ &\left\{ \sum_{j=1}^4 \sum_{k=1}^4 y_i^2 w_j w_k |J| [N'_i] \{\theta_{z_i}\} \right\} = [D] \{U\} + [E] \{\theta_z\} \end{aligned} \quad \text{Eq. (4.16)}$$

A similar relationship can be developed for the bending moment applied around y axis.

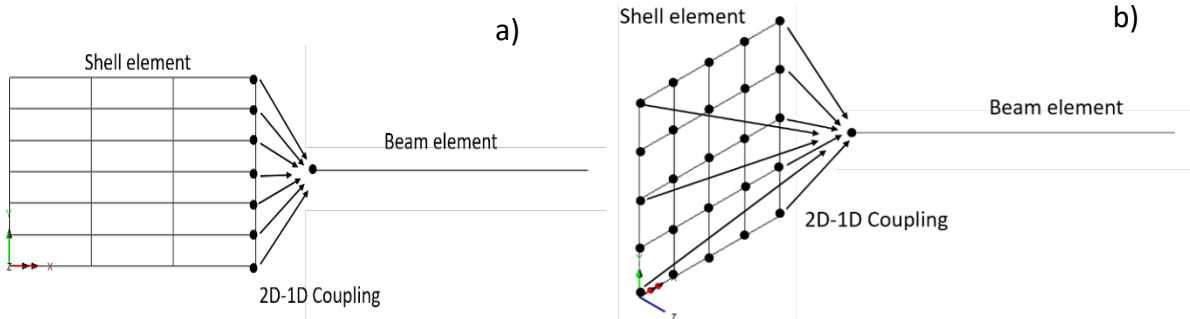


Figure 4-2(a) Planar coupling condition (beam to shell element), b) Out-of-plane coupling condition (beam to shell element)-only representative connections is shown for clarity

4.3.3 Torsion

The torsional moment, applied to the end point of the beam member, generates a rotational displacement for the beam member. Also, the in-plane displacements and induced shear stresses at the edge plane of the shell member are created. The constraint equation under the torsional moments can be expressed as Eq. (4.17) (29):

$$m_x \theta_x = \int_A (\tau_{xz} V_e + \tau_{xy} W_e) dA \quad \text{Eq. (4.17)}$$

where V_e and W_e are the equivalent in-plane displacements and τ_{xz} and τ_{xy} are the in-plane shear stresses at the edge plane of the shell member in the xz and xy-plane, respectively.

In-plane. For the planar coupling condition, the applied torsional moment generates shear stresses and in-plane displacements at the lateral edge plane of the shell member. The equivalent in-plane displacements, V_e and W_e can be expressed through the nodal displacements of the shell elements at the interface point, shown in Eq. (4.18a) and Eq. (4.18b).

$$W_e = \sum_{i=1}^{N_{\text{element}}} [N_i] \{W_i\} + [N'_i] \{\theta_{x_i}\} y_i \quad \text{Eq. (4.18a)}$$

$$V_e = \sum_{i=1}^{N_{\text{element}}} [N_i] \{V_i\} + [N'_i] \{\theta_{x_i}\} z_i \quad \text{Eq. (4.18b)}$$

Substituting the nodal displacement relations Eq.(4-18a), Eq.(4-18b) into Eq. (4-17), the constraint equation under the torsional moment, at the Gauss point can be expressed as Eq. (4-19).

$$\begin{aligned} m_x \theta_x &= \sum_{i=1}^{N_{\text{element}}} \left\{ \sum_{k=1}^2 \tau_{xz}^{(k)} w_k |J| [N_i] \{V_i\} \right\} + \\ &\quad \left\{ \sum_{k=1}^2 z_i \tau_{xz}^{(k)} w_k |J| [N'_i] \{\theta_{x_i}\} \right\} + \\ &\quad \left\{ \sum_{k=1}^2 \tau_{xy}^{(k)} w_k |J| [N_i] \{W_i\} \right\} + \\ &\quad \left\{ \sum_{k=1}^2 y_i \tau_{xz}^{(k)} w_k |J| [N'_i] \{\theta_{x_i}\} \right\} \end{aligned} \quad \text{Eq. (4-19)}$$

In developing the torsional constraint equation, the warping effect shall be considered. In case the torsional constraint equation is required for coupling, the selected elements must essentially consider the warping effect. This can influence the selection of both types of elements.

Out-of-plane. For the out of plane coupling condition, the shear stresses, τ_{xz} and τ_{xy} induced by the torsional moment, have a parabolic variation with respect to the center of the rectangular edge plane. Based on the Reissner plate bending theory, similar behavior of the through thickness shear distribution can be also assumed for the edge face shear stresses. Therefore, the constraint equation Eq. (4.19) shall be applicable for the out-of-plane coupling condition. The constraint equation at the Gauss points of the shell elements can be expressed as Eq. (4.20):

$$m_x \theta_x = \sum_{i=1}^{N_{\text{element}}} \left\{ \sum_{j=1}^4 \sum_{k=1}^4 \tau_{xz}^{(j,k)} w_k \cdot w_j |J| [N_i] \{V_i\} \right\} + \\ \left\{ \sum_{j=1}^4 \sum_{k=1}^4 z_i \tau_{xz}^{(j,k)} w_k \cdot w_j |J| [N'_i] \{\theta_{x_i}\} \right\} + \\ \left\{ \sum_{j=1}^4 \sum_{k=1}^4 \tau_{xy}^{(j,k)} w_k \cdot w_j |J| [N_i] \{W_i\} \right\} + \\ \left\{ \sum_{j=1}^4 \sum_{k=1}^4 y_i \tau_{xz}^{(j,k)} w_k \cdot w_j |J| [N'_i] \{\theta_{x_i}\} \right\} \quad \text{Eq. (4.20)}$$

where τ_{xz} and τ_{xy} are the shear stresses of the elements at the edge face plane of the shell member considered at the Gauss points.

4.3.4 Shear force

The applied shear force to the end point of the beam member creates translational displacements along the shear load direction at the beam member while generating in-plane shear stresses and displacements at the edge plane of the shell member. The constraint equation under the applied shear load at the interface point is shown in Eq. (4.21a) and Eq. (4.21b):

$$F_y v = \int_A (\tau_{xz} V + \tau_{xy} W) dA \quad \text{Eq. (4-21a)}$$

$$F_z w = \int_A (\tau_{xz} V + \tau_{xy} W) dA \quad \text{Eq. (4-21b)}$$

where F_y and F_z are the applied shear loads at the end point of the beam member respectively.

In-plane. For the planar coupling condition, the equivalent displacements at the lateral edge plane of the shell member, V_e and W_e can be considered as the sum of the nodal displacements at the edge shell elements shown in Eq. (4.22a) and Eq. (4.22b).

$$V_e = \sum_{i=1}^{N_{\text{element}}} [N_i] \{V\}_i \quad \text{Eq. (4-22a)}$$

$$W_e = \sum_{i=1}^{N_{\text{element}}} [N_i] \{W\}_i \quad \text{Eq. (4-22b)}$$

The constraint Eq. (4-21a) can be solved at the Gauss points by considering Eq. (4.22a) and Eq. (4.22b) as shown in Eq. (4.23).

$$F_y v = \sum_{i=1}^{N_{\text{element}}} \left\{ \sum_{k=1}^2 \tau_{xz}(k) w_k |J| [N_i] \{V\}_i \right\} + \left\{ \sum_{k=1}^2 \tau_{xy}(k) w_k |J| [N_i] \{W\}_i \right\} \quad \text{Eq. (4-23)}$$

A similar equation can be acquired for the shear force in the z direction.

Out-of-plane. For the out-of-plane coupling condition, the shear loads applied at the end point of the beam member generate shear stresses as well as a torsional moment at the edge face plane of the shell member shown in Eq. (4.24).

$$F_y v = \int_A (\tau_{xz} V + \tau_{xy} W + M_x \theta_x) dA \quad \text{Eq. (4-24)}$$

Eq. (4.24) can also be solved at the Gauss points expressed in Eq. (4.25).

An identical constraint can be expected for the shear force in the z -direction.

$$\begin{aligned}
F_y v = & \sum_{i=1}^{N_{element}} \left\{ \sum_{j=1}^4 \sum_{k=1}^4 \tau_{xz}^{(k,j)} w_j \cdot w_k \cdot |J| [N_i] \{V_i\} \right\} + \\
& \left\{ \sum_{j=1}^4 \sum_{k=1}^4 \tau_{xy}^{(k,j)} w_j \cdot w_k \cdot |J| [N_i] \{W_i\} \right\} + \\
& \left\{ \sum_{j=1}^4 \sum_{k=1}^4 M_x^{(k,j)} w_j \cdot w_k \cdot |J| [N'_i] \{\theta_{x_i}\} \right\}
\end{aligned} \tag{4-25}$$

The developed equations shall be applicable for the other types of elements having a different number of DOFs and geometrical properties while the appropriateness of the elements is required to be evaluated before application. The selected elements for the beam and shell element in this study do consider all the DOFs to adequately represent the three-dimensional structural performance of the members modeled in the multi-scale model. However, in the coupling of multiple elements with dissimilar DOFs, the compatibility between the nodal DOFs of multiple elements at each side of the interface point is required to be provided. This ensures that all of the DOFs of the multiple elements are appropriately coupled. The MPC equations developed in this work require evaluation and verification prior to application to the multi-scale modeling of the case study bridge.

4.3.5 Verification of the developed constraint equations

This work presents a validation protocol for the appropriate- ness of the developed MPC equations for the intended use. Two cantilever beams are modeled using multiscale modeling method showing the examples of the planar and out-of-plane coupling systems. In each example, the geometric and material properties for all of the models are identical. The FE models are developed in the FE package, LUSAS®, shown in Figure 4-3 and Figure 4-4. In the planar coupling example, a multiscale cantilever I-beam, where half of the beam is modeled with beam

elements and the other half of the beam is modeled with shell elements, is developed to evaluate the planar constraint equations shown in Figure 4-3a.

In addition, an identical cantilever model made of shell elements is developed to compare the results shown in Figure 4-3b. For the out-of-plane coupling example, a beam element with I-cross section is perpendicularly connected to a 2D plate shown in Figure 4-4a. Similar to the planar example, an identical model made of shell elements shown in Figure 4-4b is also developed for verification purposes. In each example, the coupling of the beam to shell element at the interface point is provided through implementing the appropriate constraint equations as the matrices of the constant coefficients to the nodes of the shell elements.

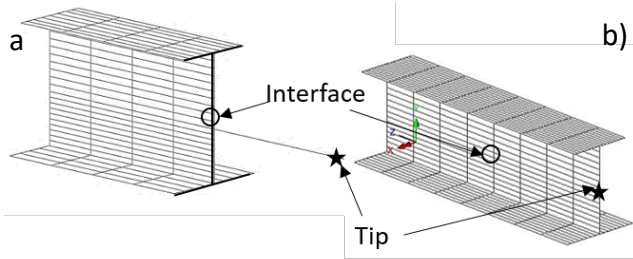


Figure 4-3 (a) Multi-scale model with planar coupling beam to shell element (b) Single scale model with shell element (LUSAS®).

The matrices of the constants are developed in MATLAB® using the developed equations in this study as well as considering the element properties. The applied locations of the constraint equations are highlighted for the planar coupling (the I-cross section) shown in Figure 4-3 and for the out-of-plane coupling (the specified rectangle) shown in Figure 4-4a.

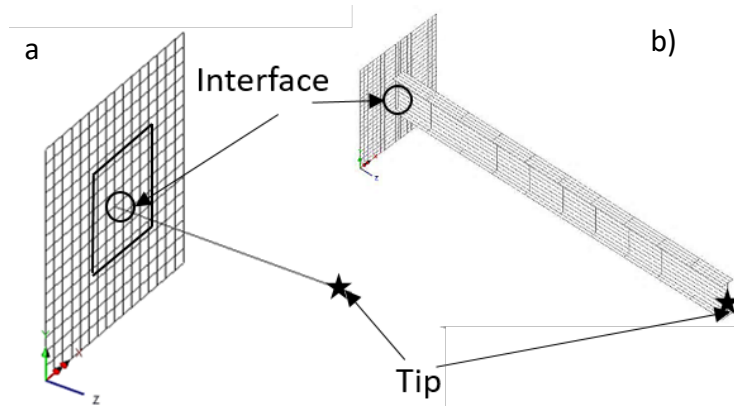


Figure 4-4 (a) Multi-scale model with planar coupling beam to shell element (b) Single scale model with shell element (LUSAS®)

The evaluation of the revised MPC for the multiscale models includes the comparison of the displacements of the shell model, the multiscale model using the default software setting (Kinematic Coupling) and the presented MPC method for both planar and out-of-plane conditions. In Table 4-1, for each example, the results of the three FE models (two multiscale and one shell element model) are expressed for the vertical displacements under a 10 kN shear load applied to the free end of the cantilever beams. Two specified locations, at the tip and the interface point of the beam members as shown in Figure 4-3 and Figure 4-4, are considered for the comparison. The displacement of the MPC-multiscale model illustrates a more favorable agreement to the shell element model, as compared to the displacement results of the default multiscale model. The displacements of the default multiscale model are less than the shell element model, which indicates that the model is highly constrained. It is also observed that in the out-of-plane coupling condition, the accuracy of the default multiscale model is more dependent on the appropriate selection of the area for coupling.

Expanded application of the developed constraint equations requires the simultaneous consideration of all potential loading conditions to create a set of matrices of constant coefficients. In this study, the matrices are developed for the different groups of members having identical geometric conditions in the planar and out-of-plane coupling conditions. For the out-of-plane coupling condition, an appropriate area of the shell elements is considered for all cases. The developed matrices of constant coefficients can be applied in FE commercial software packages for multiscale modeling.

Table 4-1 Displacement comparison of the shell element model, multi-scale with the presented MPC equations and Lusas® constraint default in multi-scale modeling

Multi-scale	Constraint	Tip	Difference	Interface	Difference
situation	Equation	(m)	(%)	(mm)	(%)
Planar	Shell	-0.79	-	-3.89E-6	-
	MPC	-0.79	0.50	-3.62E-6	6.94
	Default constraint	-0.81	2.13	-3.29E-6	15.40
Out-of-plane	Shell	-20.20	-	-0.98E-5	-
	MPC	-20.19	0.07	-0.92E-5	6.88
	Default constraint	-20.32	0.55	-0.87E-6	11.91

4.4 The Case Study: The Memorial Bridge

The case study in this paper is the newly reconstructed Memorial Bridge in Portsmouth, NH. The Memorial Bridge is a vertical lift bridge on US Route 1 over the Piscataqua River is shown in Figure 4-5. The bridge includes three identical spans each with a length of 91 m, and two vertical lift towers each with a height of 48 m (33). To alleviate some of the long-term maintenance related issues of the typical gusset-plate connections, an innovative gusset-less connection was used in the Memorial Bridge shown in Figure 4-6. The cold-bent plate flanges of the gusset-less connection are welded to the web plates with a five-pass fillet weld. The complex geometry of the gusset-less connection can increase fatigue vulnerability due to high-stress concentrations.

The lifting operation at the Memorial Bridge has an on-demand schedule which can increase to every half hour due to the naval traffic. The repetitive lifting operations of the bridge as well as the uncertain performance of the gusset-less connection raise the need for a design verification protocol and subsequently a SHM plan. A long-term objective-based monitoring program has been designed and applied at the south span and south tower of the Memorial Bridge to provide real-time data for condition assessment and design verification purposes (91) (92). The instrumentation plan includes sixteen tri-axial strain rosettes, two uni-axial strain gages, sixteen uni-axial accelerometers, four biaxial tiltmeters, and a weather station, as shown in Figure 4-5. This instrumentation plan provides inadequate structural performance information due to the installation restrictions agreed upon with the bridge owner's maintenance team. Therefore, a set of global FE models of the bridge is created and verified with the field data to represent the accurate structural performance of the bridge. The instrumented parts of the bridge, the south span and south tower, are considered in the FE model.

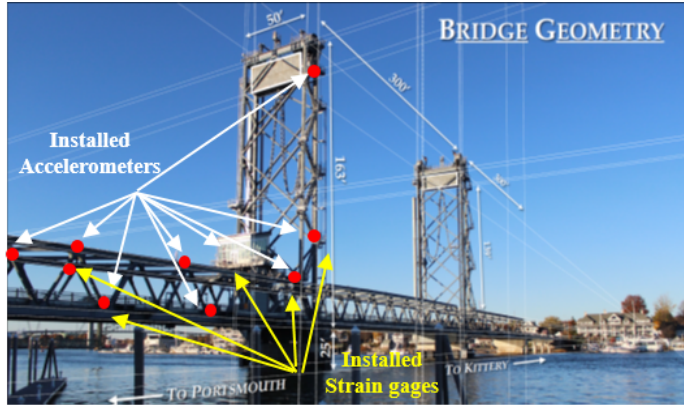


Figure 4-5 The Memorial Bridge, Portsmouth, NH and the instrumentation plan.



Figure 4-6 The gusset-less connection of the Memorial Bridge.

This project aims to combine the information acquired through the collected monitoring data with the analytical results of an efficiently detailed FE global model of the Memorial Bridge to create a complete performance profile for further conditions assessments.

4.5 Finite Element Model Categories

In this study, four different FE models of the bridge, each meeting a specific goal of this work, are developed to determine the multi-scale model which is capable of representing the structural performance of the bridge. These models which vary in terms of complexity from a simplified beam element model to a detailed shell element model are beam element (B) model,

shell element (SH) model, multi-scale sub-structure (S-S) model and multi-scale global (M-S) model.

All models accurately reflect the global geometry of the bridge. Boundary condition representations and section properties of the structural elements are based on the as-built structural plans and the field observations. The boundary conditions are considered to be simply supported at the four corners of the truss representing the bearings which constraint the truss to the bridge's piers. In the following sections, the procedure for the development as well as the objective of each model is explained in detail. The properties of each model, including the material properties, the type of and the number of elements, as well as the time of analysis, are expressed in Table 4-2.

Table 4-2 Geometrical and material properties of the developed FE models

Model properties	B-Model	SH-Model	M-S Model
Type of elements	3D linear beam element	Linear thick shell	Linear quadrilateral thick shell
Number of elements	Beam elements: 265	Shell elements:297418	3D linear thick beam Shell elements:158993 Beam elements:5160
Computational time:			
Static Analysis (min)	0.033	2	0.81
Dynamic Analysis (min)	0.033	40	16

4.5.1 Beam element model (B-model)

A simplified global FE model consisting only of beam elements, the B-model, is developed in SAP2000®, as shown in Figure 4-7(35). This model is unable to consider the features of the gusset-less connection. The B-model represents the gusset-less connection with a single node that considers a full moment transfer, which is applied at all joints. This model includes only 265 elements and is efficient in terms of the computation cost and effort (shown in Table 4-2) while it has limited ability to capture the local behavior of the connection.

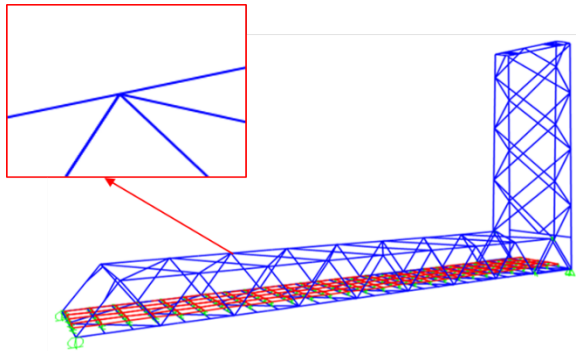


Figure 4-7 FE global model of the Memorial Bridge made by beam elements, B-Model (Sap2000®).

4.5.2 Shell element model (SH-model)

A global single-scale shell-element model, the SH-model, is developed as a benchmark to adequately represent the performance of each member (shown in Figure 4-8). The SH-model is developed in the FE software LUSAS®. The developed SH- model and B-model will provide the upper and lower bounds for the structural responses of the investigating multiscale model, respectively. Thick shell elements are utilized for all members considering membrane, shear, and flexural deformations to provide more analytical information of the members. To have an identical mesh in all gusset-less connections and make the model mesh insensitive, the perimeters of the connection's webs are equally divided into appropriate sections. The mesh size of the deck is selected based on the travel path and the characteristics of the load test vehicle used in the model verification process. The SH-model is beneficial to provide continuous stress contours in all members, which will aid in the development of the efficient multiscale FE model.

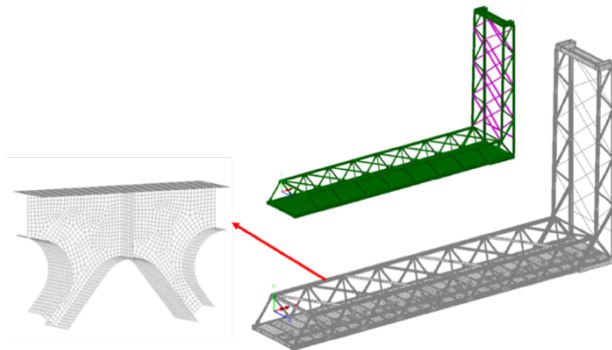


Figure 4-8 FE global model of the Memorial Bridge made by shell elements, SH-model (LUSAS®).

4.5.3 Multi-scale sub-structure model (S-S model)

Developing a local FE model of the identified critical components using finer-dimension elements associated with a global FE model using coarser-dimension elements is known as the sub-structuring method. The method provides detailed information on the local performance of the objective components while representing the overall performance of the structure through the global FE model. The MPC equation method has been applied to link the local sub-structure models to the global model (30). In this study, the local model of the gusset-less connection is developed as the sub-structure (S-S) of the B-model. The developed constraint equations of this study are applied to the boundaries of the S-S model for the association to the global B-model.

The S-S-model is developed to evaluate the efficiency and the preference of applying the MPC equations to create a single multi-scale model versus a multi-scale sub-structure model. An identical number and type of shell elements are used for the local S-S model and the gusset-less part of the M-S model to provide a reasonable comparison between the two modeling approaches.

4.5.4 Multi-scale modeling (M-S model)

The multi-scale model (M-S model) of the Memorial Bridge is created through a stepwise procedure, where the groups of members that were initially modeled with the shell elements in the SH-model are replaced with a single beam element to develop an efficient M-S model. This stepwise procedure for the M-S model development started with the least critical to the most critical groups of members.

After the dimensional reduction of each group, a comprehensive comparison is made between the structural responses of the M-S model to the SH-model and B-model and ultimately to the field-collected data. The optimum location for the interface point of different dimensions is determined through minimizing the difference between the structural response of the M-S model to the other FE models and the field-collected data. The error estimations are performed using the second term of the energy norm expressed through the following equation (36):

$$\delta_{error} = \frac{h(1-\nu)t}{24Ep} \int J^2 dy \quad \text{Eq.(4.26)}$$

$$J^2 = \delta\sigma^2 + \delta\tau^2$$

where J^2 is the stress jump for bending and shear force, p is defined as the polynomial interpolation order, h and t are the dimension and the thickness of the shell element respectively (37). In the following, the procedure and the criteria for the selection of the members including braces, floor beams, diagonals and, chords, for dimensional change are discussed.

4.5.4.1 Braces

Initial evaluation of the SH-model indicated that the braces are one of the least stressed group of the bridge's members, which make them the leading candidates for the dimensional reduction. The braces of the Memorial Bridge are connected through the bolted joints to the web

of the gusset-less connection. The developed out-of-plane constraint equations are applied at the bolted area to couple the braces to the gusset-less connections shown in Figure 4-9a. The results of the SH-model show that the axial performance of the braces does not generate significant stress concentration at the connected gusset-less connection as it dissipates around the bolted area.

4.5.4.2 Floor Beams

Floor beams connecting the eastern and the western trusses of the bridge at the bottom chords are the highest stressed members due to the traffic loads. The initial results of the SH-model show that the floor beams can be replaced by a single beam element when they are coupled to the shell element with an appropriate interface location. In this model, the floor beams are coupled to the edge of the stiffeners at the bottom chord representing the bolted connection between the floor beam and the stiffener shown in Figure 4-9b. This modeling approach provides a planar coupling to the floor beams along the stiffeners. There are also skewed beams tying the floor beams to the bottom gusset-less connections.

The procedure for reducing the dimension of the skewed beams is similar to the braces as they have significant axial performance. However, due to the high transferred load from the floor beam to the gusset-less connection, the concentrated stresses may require a larger area of coupling at the gusset-less connection compared to the actual bolted area. This larger area allows for stress concentration dissipation while it increases the time of analysis by increasing the number of DOFs involved in the constraint equations.

4.5.4.3 Diagonals

The diagonals connect the gusset-less connections at the top chord to the bottom chord, as shown in Figures 4-9a and 4-9b, respectively, through the bolted joints and have a dominant axial

performance. The initial analysis of the SH-model showed that in the multiscale modeling of the diagonals with the beam elements, the interface point location is less influential on the global performance of the model. The coupling between the different dimensions is performed at the bolted end of the diagonals.

4.5.4.4 Top and bottom chord

Top and bottom chord plate girders at the Memorial Bridge are uniformly connected to the gusset-less connections, as shown in Figures 4-9a and 4-9b. The initial structural analysis results of the SH-model showed that these members are the high-stressed regions that require careful considerations for dimensional reduction. The error estimation procedure in Eq. (4.26) is applied to find the appropriate location for the interface point. The results of the estimated error show that the interface location for the top and bottom chord may not be identical. This difference originates from the unequal performance of the chord members as well as the connected members to them.

The complex geometry of the gusset-less connection also requires more consideration in selecting the interface location (Saint Venant principle). The appropriate position of the interface point is determined through minimizing the estimated error in Eq. (4.26) between the structural response of the M-S model as compared with the SH-model and the field-collected data. In the developed M-S model, the interface location at the bottom chord is located at a distance equal to three times the depth of the cross-section from the connection center point. The interface distance can be reduced to two times the depth of the cross-section for the top chord connection to ensure that the interface point will not conflict with the flange curvature. The defined interface location depends on the geometric properties and the structural performance of the component as well as the connected members that may require either planar or out-of-plane coupling conditions. In the

less complex bridges requiring the planar coupling condition, the distance for the interface point can be considerably decreased, which reduces the number of higher dimension elements (e.g., shell element) required for an appropriate M-S model.

Shown in Figure 4-9a and Figure 4-9b, are the coupling conditions of the members modeled with beam elements and coupled to the gusset-less connections modeled with shell elements for the top and bottom chord, respectively. Similar efforts are performed for the gusset-less connections at the tower. The finalized multiscale model is shown in Figure 4-10. In the next section, all four developed models are compared to the field- collected data for model verification purposes and to highlight the advantage and disadvantage of each developed model. In addition, the comparisons are quantified using statistical postprocessing.

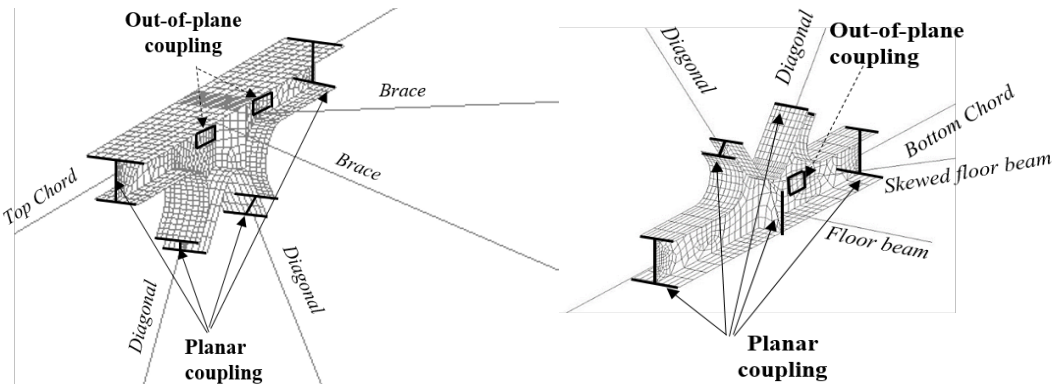


Figure 4-9 Coupling conditions for the (a) top connection, b) bottom connection (LUSAS®).

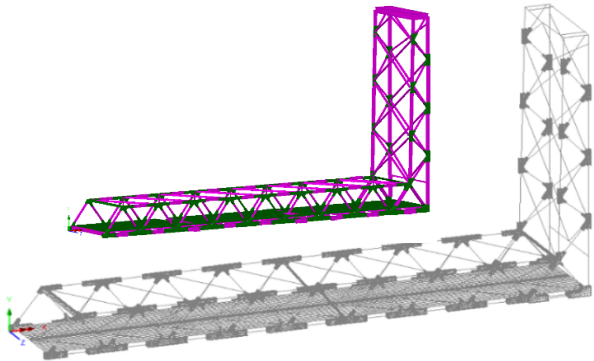


Figure 4-10 Multi-scale model of the Memorial Bridge, connections and the deck are modeled with shell element (LUSAS®).

4.6 Model Verification

The accuracies of the developed FE models are evaluated through model verification efforts in this section. A load test was designed to provide a comparison tool between the responses of the bridge to the analytical response of the FE models. The load test was performed at the crawl speed (8 km/h) with two stops part way across the bridge and at normal speed (48 km/h) with no other vehicular traffic. The location of the truck stops was selected based on the influence line results of the FE model drawn for the strain response of the bridge at the diagonal (at the installed strain gage location).

Application of the two different speed conditions provides the opportunity to compare both static and dynamic response of the bridge with the developed FE models. Each test was repeated three times, and the results were averaged to reduce the probability of error in the comparison. The field data collected during the load test includes the acceleration and strain responses acquired from all installed sensors shown in Figure 4-5.

4.6.1 Comparison of the predicted and the field data natural frequencies

The natural frequencies of the bridge are determined through the postprocessing of the recorded acceleration response of the installed accelerometers. The natural frequency results of the bridge are compared to the natural frequencies of the developed B, SH, and M-S models. The natural frequency response for the S-S model is acquired through the associated global B-model, which is not repeated. The comparison is made for the first five transverse natural frequencies shown in Table 4-3. In evaluating the difference between the field data and the analytical responses, there are multiple sources of uncertainty that influence the response of the analytical models (4). In the FE analysis, the dynamic response of the model highly depends on the defined boundary conditions, material properties, and element interfaces.

The first natural frequencies of the Memorial Bridge observed in the numerical analysis are influenced by the global deformation of the deck. Also, the difference between the field and numerical responses of the natural frequencies can be raised due to the location of the accelerometers, uncertain concrete material properties, as well as the deck geometrical details, which are not considered in the FE models (38) (39). However, the higher modes of all three models correlated well with the field data verifying the accuracy of the models. Additional model updating will be conducted based on the expanded field-collected information. However, successful model updating must start with a reasonable priori model of the structure, which is shown in the M-S model (40).

Table 4-3 Comparison between the natural frequencies of the FE models and field data

Mode Number	B Model (Hz)	SH Model (Hz)	M-S Model (Hz)	Field Data (Hz)
1	1.23	1.49	1.56	1.45
2	2.04	2.41	2.51	2.36
3	3.11	3.03	3.13	2.97
4	3.66	3.65	3.70	3.6
5	4.17	4.04	4.07	3.97

4.6.2 Comparison of the predicted and the field data strain response

The verification of the developed FE models including the SH, M-S, and S-S models are also performed by comparing the field strain response collected during the load test, to the analytical strain results at the installed strain gages' locations. Having a cluster of five strain rosettes in a single gusset-less connection provides the opportunity to compare the strain distribution (strain contours) of the developed models under the truck load to the field strain rosettes' responses. The B-model is not included in this comparison as it does not capture the local strain response of the gusset-less connection. The differences between the field strain response and the predicted response by FE models can result from the modeling assumptions, including the material properties and the modeling simplifications, such as ignoring the weld geometry and the bolted connection in the model.

In Figure 4-11, the strain contours of the global M-S model are shown under the testing truck load at the second stop. It is observed that the M-S model can sufficiently provide the required information related to the local performance of the connections modeled with shell elements while providing the global behavior of the bridge modeled with beam and shell elements with an efficient reduction in the computational time shown in Table 4-2. In Figure 4-12, the time history for the principal strain response of the four strain rosettes installed at the bottom connection

is shown. The graphs belong to the quasi-static load test with two stops at the northbound (toward the tower).

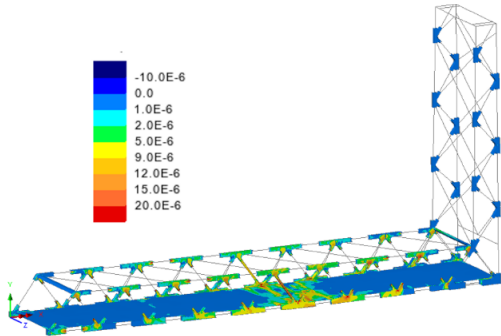


Figure 4-11 Strain contour response of the multi-scale model under the truck load (LUSAS ®).

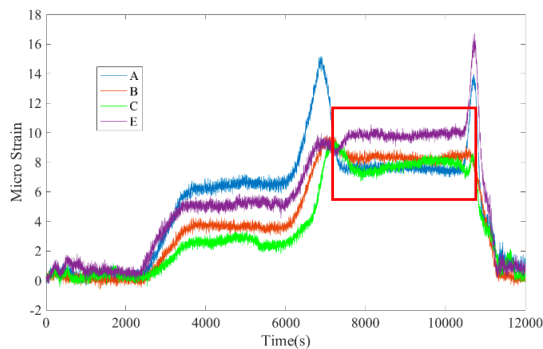


Figure 4-12 The field strain time-history response during the load test for the strain rosettes at the bottom connection, locations shown in Figure 4-13

As shown in Figure 4-12, the specified part showing the truck stop is considered for model verification purposes. The time- history response data collection was started from zero for each load test. Therefore, the resulting structural responses are only due to the excitation of the test truck, as the impact of environmental demands was minimal over each ~120-s test run. Shown in Figure 4-13 are the principal strain contours of the SH, S-M, and S-S models at the bottom gusset-less connection. In addition, the locations of the five strain rosettes installed at the bottom

connection are specified (A-E). For each model, the presence of the stress concentrations, strain response magnitude, and the agreement with the field data are evaluated. Comparing the strain distribution of the three models, it is illustrated that the SH-model, which is shown in Figure 4-13a, has the most uniform strain distribution with minimum concentrated strain. For the M-S model shown in Figure 4-13b, minor strain concentrations are observed at the location of the floor beam attachment. The S-S model also includes more strain concentrations as compared to the two other models shown in Figure 4-13c.

The concentrated stress areas for the M-S and S-S models are due to the application of the beam element for the floor beams, which indicates a single beam element might not appropriately represent the whole floor beam causing strain concentrations at the gusset-less connection. In the planar coupling conditions, this can be addressed by changing the interface point along the beam element. In the out-of-plane coupling conditions, the problem can be solved by considering a larger area of coupling. However, the strain concentration is less observed in the area where the skewed beam is coupled to the gusset-less connection, proving the efficiency of the out-of-plane constraint equations developed in this study.

In evaluating the magnitude of the strain response of the FE models, the SH-model has a higher strain value due to the flexible property of the shell element compared to the beam element. Therefore, the M-S model has lower strain response due to the higher stiffness of the model compared to the SH-model. The S-S model has the highest strain response values compared to the other models due to the applied loads that were determined from the global model. The comparison between the strain contours of the S-S and M-S models also demonstrates that application of the developed MPC equations in a single global model may result in a more accurate response compared to the sub-structuring method. Presence of the concentrated stress areas, as well as the

higher strain response of the S-S model, can result in over-estimations for further damage assessments.

The focus of this study is to develop an efficient FE global model which provides the required information on the local as well as the global performance of the bridge. The concentrated regions observed in the strain contours of the M-S model do not warrant the modeling of the floor beam with shell elements. Including more shell elements in the M-S model will significantly increase the number of DOFs, and therefore, the time of analysis. However, this information provides the intuition about the causes of the difference between the developed FE models and the acquired field data in the model calibration and validation process.

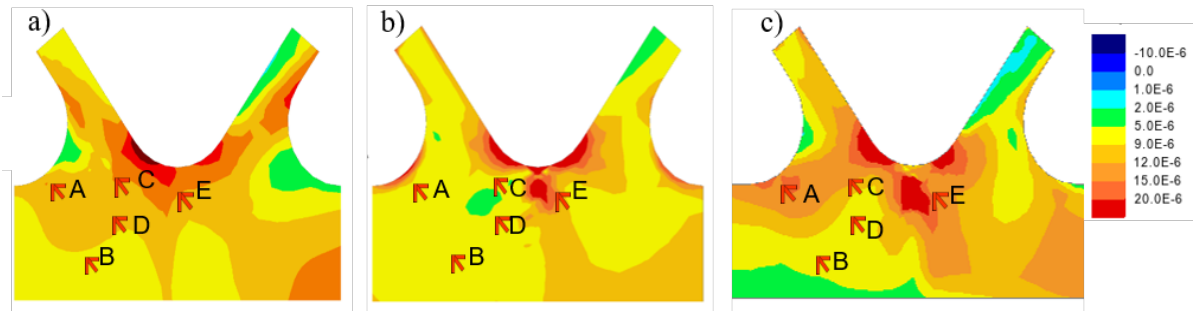


Figure 4-13 The principal strain contours of the a) SH-model b) M-S model c) S-S model LUSAS ® under the truck load

A numerical comparison between the strain results of the FE models and the strain gages' response is performed through some statistical efforts. The results are shown in the bars for all five-installed strain rosettes (A to E, shown in Figure 4-13) at the bottom and top gusset-less connection, shown in Figure 4-14(a) and Figure 4-14(b) respectively. It is demonstrated that at most of the strain gage's locations, the S-S model has more difference to the field data. In the next section, the difference between the results are quantified.

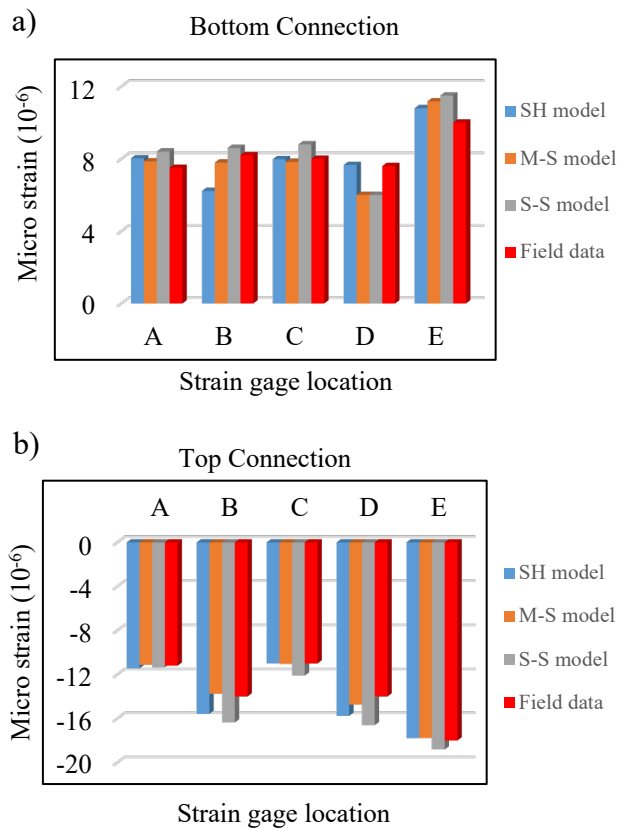


Figure 4-14 The comparison between the strain response of the FE models and field data a) bottom connection, and b) top connection.

4.6.3 Statistical post-processing

In model verification of the FE models, statistical comparisons aid to quantify the discrepancies between the field data and the analytical responses to select an appropriate model for the design verification and performance assessment protocol. In this study, the linear regression approach is applied using JMP® to evaluate the fitness of the strain responses of the investigating FE models to the field data. The data applied to develop the bar charts in Figure 4-14 are utilized for regression analysis shown in Figure 4-15. The five negative principal strain values belong to the top chord at the strain gage' location while the five positive values belong to the strain gages located at the bottom chord. In Figure 4-15 (a), a regression line is fitted to the strain response for

the bottom chord (negative strains) and the top chord (positive strains) from the three presented FE models. In each comparison, a 95% curved confidence interval for the data is drawn to show the relationship between the strain responses. It is illustrated that the M-S model shows a better agreement with the field data.

In Figure 4-15 (b), the comparison is clarified through fitting a linear regression line to the field data to investigate the deviance response of each FE models with respect to the field data. In each graph, the field data are shown with crosses, and the analytical results are shown with circles. It is observed that the analytical responses of the M-S model are more compatible with the fitted line of the field data showing a stronger agreement with the bridge's performance. The quantitative results of the regression analysis are shown in Table 4-4. The accuracy of the models is evaluated through the measurement of R^2 , RMSE, and the difference between the mean values of the field data and the analytical results. It is observed that the M-S model has the least difference of the mean values to the field data, the lowest RMSE value and the maximum R^2 value compared to the two other models.

The higher discrepancies between the results of the SH-model to the field data as compared to the M-S model indicates larger analytical displacement response which results from the decreased stiffness system of the SH-model compared to the M-S model. In contrast, the S-S model showed a higher percentage of deviance response to the field data compared to the two other models, which indicates that the interface point has a significant impact on the accuracy of the S-S model. Additional effort is required to find the optimum position of the interface points for the S-S model compared to the M-S approach to achieve the most accurate response. However, S-S model is still a valuable design development tool to estimate the response of the critical target components in a complex structural system. The M-S model also shows an outstanding capability

to evaluate the performance of all critical locations as well as the global behavior of the structure, in a single model. Consequently, multiple comparison tools in this study illustrated that the M-S model could be a potential alternative for single scale shell models (shell element) in the modeling of the large structures.

Table 4-4 Linear regression for validating the FE models compared to the field data

Model	Mean difference	RMSE	R ²
M-S model	0.085	0.779	0.996
SH-model	0.396	1.011	0.991
S-S model	0.472	1.099	0.987

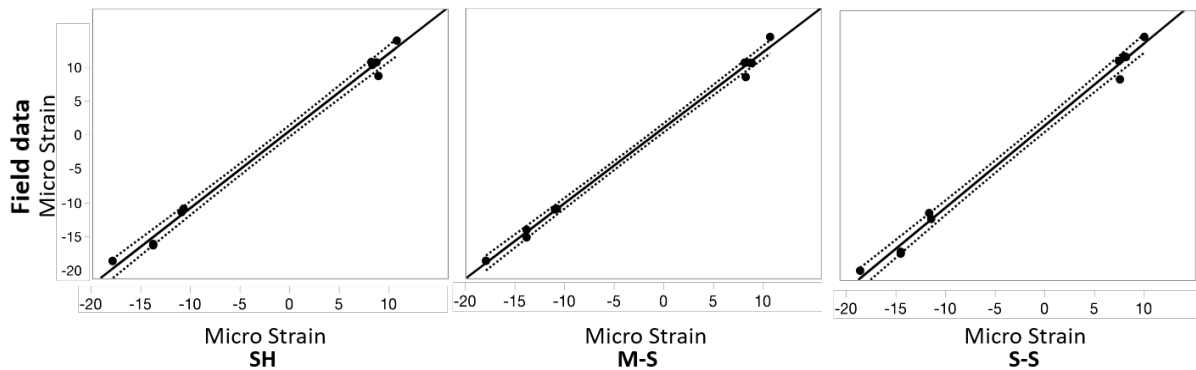


Figure 4-15 (a) Deviance strain response of SH, S-M and S-S from the field data with 95% confidence intervals

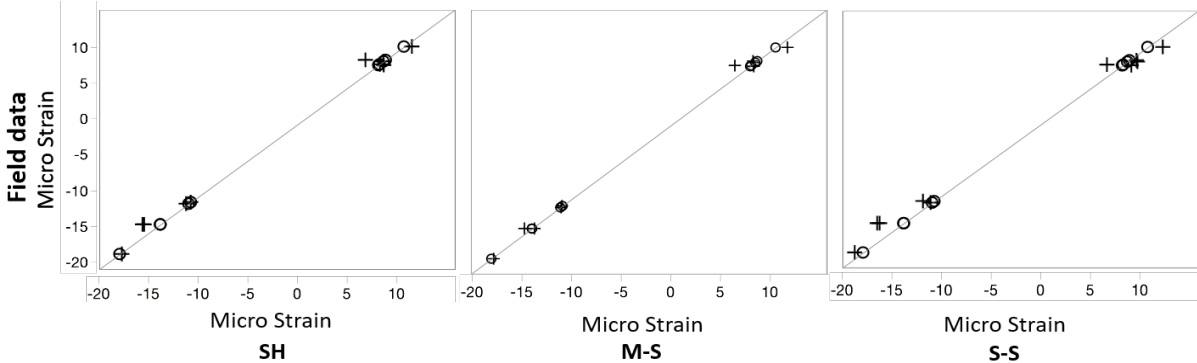


Figure 4-15 (b) Linear regression analysis to fit the strain response of SH, S-M and S-S (o) models to the filed data (+).

4.7 Conclusions

Multi-scale modeling provides the opportunity to consider the complex components of the bridges modeled with the finer-dimension elements in an efficient global FE model. This is crucial for complex bridge structures with the critical components such as truss connections, roller supports in bascule bridges or sheave girders for vertical lift bridges. This paper presents the development of an efficient multi- scale FE model to represent the global performance as well as the local detailed performance of the critical locations of the complex bridge structures using the developed MPC equations and determining the optimum interface point locations. The M-S model presented in this work using the developed MPC equations showed satisfactory agreement with the field-collected data through multiple model verification efforts. Careful consideration is required when creating a multi-scale model concerning the selection of the multiple element types, the constraint equations, and the interface points. These parameters are required to create a multi-scale model that is appropriate for the specific bridge structure and the intended assessment application.

In addition, the development of the M-S model was aided by the use of a full-scale SH-model, which can be cost-prohibitive for most design projects. However, the full-scale shell model that was created for this study may not be required for all applications, where engineering judgment can be used for the initial interface point location and MPC equations. These parameters can then be refined during the verification process with the field-collected structural response data. For design purposes, where the field-test data is not applicable for validation of the model, it is suggested to develop an initial global model with the coarser-dimension elements for comparison. The critical areas for the bridge designer should be replaced by the finer-dimension elements

during the design development to create the multi-scale model while the results of the initial model and the multi-scale model are comparable. The interface locations can be conservatively considered at a reasonable distance from the critical areas based on the designer's judgments. However, application of the method for the concrete structures having complex connections between the members requires more investigation for the development of the appropriate constraint equations.

Acknowledgments

This material is based upon work partially supported by the National Science Foundation under Grant No. 1430260, FHWA AID: DEMO Program and funding from the NHDOT Research Advisory Council. Any opinions, findings, and conclusions or recommendations expressed in this material are those of the author(s) and do not necessarily reflect the views of the National Science Foundation.

References

- 1) Liao, M., Okazaki, T., Ballarini, R., Schultz, A.E., Galambos, T.V. 2011. "Nonlinear Finite-Element Analysis of Critical Gusset Plates in the I-35W Bridge in Minnesota", *Journal of Structural Engineering* 137 (1), 59-68.
- 2) Santini-Bell, E., Lefebvre, P. J., Sanaye, M., Brenner, B., Sipple, J., and Peddle, J. 2013. "Objective Load Rating of a Steel-Girder Bridge Using Structural Modeling and Health Monitoring", *Journal of Structural Engineering*, 1771-1779.
- 3) Gao, Y. and Mosalam, K.M. 2018. "Deep Transfer Learning for Image-based Structural Damage Recognition", *Computer-Aided Civil and Infrastructure Engineering*, 33(9), 748-768.
- 4) Li, Z., Park, H.S., and Adeli, H., 2017. "New Method for Modal identification and Health Monitoring of Super high-rise Building Structures using Discretized Synchro squeezed Wavelet and Hilbert Transforms, *The Structural Design of Tall and Special Buildings*, 26(3), (DOI: 10.1002/tal.1312).
- 5) Li, Z. X., Chan, T. H., Yu, Y., and Sun, Z. H. 2009. "Concurrent Multi-Scale Modeling of Civil Infrastructures for Analyses on Structural Deterioration–Part I: Modeling Methodology and Strategy", *Journal of Finite Element Analysis* 45 (11), 782-794.
- 6) Fish, J. and Shek, K. 2000. "Multi Scale Analysis of Large Scale Nonlinear Structures and Materials," *International Journal of Computational Civil Structural Engineering*, 1(1), 79-90.
- 7) Surana, K.S. 1980, "Shape Functions for the Isoparametric Transition Elements for Cross-Sectional Properties and Stress Analysis of Beams", *International Journal for Numerical Methods in Engineering* 15 (9), 1403-1407.
- 8) Surana, K.S. 1980, "Transition finite elements for three-dimensional stress analysis", *Numerical methods in Engineering* 15 (7), 991-1020.
- 9) Gong, Y. 1988, "Local/global structural analysis by transition elements", *Computers and Structures*, 30 (4), 831-836.
- 10) Liao, C.L., Reddy, J.N. and Engelstad, S.P. 1988, "A solid-shell transition element for geometrically nonlinear analysis of laminated composite structures", *International Journal for Numerical Methods in Engineering* 26 (8), 1843-1854.
- 11) Gumur, T.C., Kauten, R.H. 1993, "Three-dimensional solid-to-beam transition elements for structural dynamic analysis", *International Journal for Numerical Methods in Engineering*, 36 (9), 1429-1444.
- 12) Guzelbey, I. H., and Kanber, B. (2000), A practical rule for the derivation of transition finite elements, *International Journal of Numerical Methods Engineering* 47 (5), 1029-1056.
- 13) Yue, J., Fafitis, A., Qian, J. (2010), On the kinematic coupling of 1D and 3D finite elements, *Interaction and Multiscale Mechanics* 3 (2), 192-211.
- 14) Carrera, E., Pagani, A., Petrolo, M. (2013), Use of Lagrange multipliers to combine 1D variable kinematic finite elements, *Computers and Structures* 129, 194-206.
- 15) Ainsworth, M. 2001, "Essential boundary conditions and multi-point constraints in finite element analysis", *Computer Methods in Applied Mechanics and Engineering* 190 (48), 6323-6339.
- 16) Erkmen, R.E. 2015, "Multiple-point constraint applications for the finite element analysis of shear deformable composite beams – Vibrational multiscale approach to enforce full composite action," *Computers and Structures* 149, 17-30.
- 17) McCune, R.W. 1998, *Mixed dimensional coupling and error estimation in finite element stress analysis*, Belfast, UK: PH.D. Thesis: The Queen's University of Belfast.
- 18) Monaghan, D.J., Doherty, I.W., McCourt, D. and Armstrong, C.G. 1998, Coupling 1D beams to 3D bodies, Sandai National lab. Dearborn, Michigan, USA: *Proceedings. 7th International Meshing Roundtable*, 285-293.

- 19) Li, Z.X., Zhou, T.Q., Chan, T.H.T., Yu, Y. 2007, Multi-scale finite element on dynamic response and local damage for long-span bridge, *Engineering Structures* 29, 1507-1524.
- 20) Zhu, Q., Xu, Y.L., Xiao, X. 2015, Multiscale Modeling and Model Updating of a Cable-Stayed Bridge. I: Modeling and Influence Line Analysis, *Journal of Bridge Engineering* 20 (10).
- 21) Wang, F. Y., Xu, Y.L. and Qu, W.L. 2014, Mixed-Dimensional Finite Element Coupling for Structural Multi-Scale Simulation, *Journal of Finite Element Analysis*, 92, 12-25.
- 22) Izzuddin, B.A., Jokhio, G.A. 2017, Mixed-Dimensional Coupling for Parallel Partitioned Nonlinear Finite-Element Analysis, *Journal of Computing in Civil Engineering*, 31 (3).
- 23) Minga, E., Macorini, L, Izzuddin, B.A. 2018, A 3D mesoscale damage-plasticity approach for masonry structures under cyclic loading. *Meccanica*, pp. 1591-1644.
- 24) Macorini, L and Izzuddin. B.A. 2014, Nonlinear Analysis of Unreinforced Masonry Walls under Blast Loading Using Mesoscale Partitioned Modeling, *Journal of Structural Engineering* 140(8), A4014002.
- 25) Monaghan, D.J. 2000, *Automatically Coupling Elements of Dissimilar Dimension in Finite Element Analysis*, Queen's University of Belfast Northern Ireland, UK., Ph.D. thesis.
- 26) Yu, Y. 2012, *Multi-Scale Modeling of Long-Span Bridges for Health Assessment in Structural Health Monitoring*, Hong Kong: PH.D. Thesis, Hong Kong Polytechnic University, Hong Kong.
- 27) Reissner, E. 1947, *On bending of elastic plates*, Quarterly of Applied Mathematics, 5, 55-68.
- 28) Shim, K.W., Monaghan, D.J. and Armstrong, C.G. 2002, "Mixed Dimensional Coupling in Finite Stress Analysis", *Engineering with Computers* 18 (3), 241-252.
- 29) Yu, Y., Chan, T.H.T., Sun, Z.H., Li, Z.X., 2012, "Mixed-dimensional Consistent Coupling by Multi-Point Constraint Equation for Efficient Multi-Scale Modeling", *Advances in Structural Engineering* 15 (5), 837-852.
- 30) Timoshenko, S.P. and Goodier, J.N. 1970, Theory of Elasticity. 3rd. New York: McGraw Hill Inc.
- 31) Reddy, J.N. 2006, *An introduction to finite element method*, 3rd Edition, McGraw-Hill.
- 32) NHDOT.2016, Memorial Bridge Project Innovations. July 31, <http://memorialbridgeproject.com/index.php/design-and-construction/innovations/>
- 33) Adams, T., Mashayekhizadeh, M. Santini-Bell, E., Wosnik, M., Baldwin, K., and Fu, T. 2017, Structural Response Monitoring of a Vertical Lift Truss Bridge, *96th Annual Meeting. Washington, D.C.: Transportation Research Board*.
- 34) Adeli, H., Saleh, A. 1999, *Control, optimization, and smart structures: high-performance bridges and buildings of the future*, John Wiley and Sons.
- 35) Mashayekhizadeh, M., Mehrkash, M., Shahsavari, V., Santini-Bell, E. 2018, "Multi-Scale Finite Element Model Development for Long-Term Condition Assessment of Vertical Lift Bridge", *Journal of Infrastructure systems, Structure Congress, ASCE, Fort Worth, TX*. <https://doi.org/10.1061/9780784481332.008>
- 36) Kelly, D.W., Gago, J.P. de SR, Zienkiewicz, O.C. Babushka, I. 1983, "A posteriori error analysis and adaptive processes in the finite element method: Part I-error analysis", *International Journal for Numerical Methods in Engineering* 19 (11), 1593-1619.
- 37) McCune, R.W. Armstrong, C.G., Robinson, D.J. 2000, Mixed Dimensional Coupling in Finite Element Models, *International Journal for Numerical Methods in Engineering* 49: 725-750.
- 38) Amezquita-Sanchez, J.P., Park, H.S., and Adeli, H. 2017, A Novel Methodology for Modal Parameters Identification of Large Smart Structures Using MUSIC, Empirical Wavelet Transform, and Hilbert Transform," *Engineering Structures*, 147, 148-159.
- 39) Yao, X.J., Yi, T.H., Qu, C., and Li, H.N. 2018, "Blind modal identification using limited sensors through modified sparse component analysis by time-frequency method", *Computer-Aided Civil and Infrastructure Engineering*, 33(9), 769-782.

- 40) Sanaye, M., Phelps, J. E., Sipple, J. D., Santini-Bell, E. M. and Brenner, B. R., 2012,
“Instrumentation, Nondestructive Testing, and FEM Updating for Bridge Evaluation using Strain
Measurements”, *Journal for Bridge Engineering*, ASCE, February 17(1), 130-138.

Chapter 5

5 FATIGUE ASSESSMENT OF THE GUSSET-LESS CONNECTION USING FIELD DATA AND NUMERICAL MODEL

Mashayekhi, M., Santini-Bell, E., Fatigue assessment of the gusset-less connection using field data and numerical model, *Bridge Structures* 15 (2019) 75–86, DOI: 10.3233/BRS-190157.

5.1 Abstract

Fatigue assessment of the novel structural components that are not explicitly addressed in the existing bridge design codes require the application of the local fatigue assessment methods. This study presents fatigue assessment of the novel gusset-less connection of the case-study vertical lift truss bridge, the Memorial Bridge, in Portsmouth, NH. The long-term structural health monitoring responses are collected from the instrumented gusset-less connection at the Memorial Bridge to determine the nominal fatigue response using the collected strain responses. In addition, a global multi-scale finite element model of the bridge is created to effectively model the structural components of the bridge. A local sub-structure finite element model of the connection is created to determine the stress concentration factors that are applied for the hot-spot fatigue assessment method. The acquired stress concentration factors under the static and dynamic load test are applied for hot-spot fatigue assessment of the gusset-less connection.

5.2 Introduction

Critical components of in-service steel bridges experiencing cyclic stresses may face shorter fatigue life. The failure of the structural components can occur due to the propagated fatigue crack that formed at the fatigue prone areas. The fatigue cracks are frequently initiated at the high-stressed welded components that include the structural discontinuity or imperfections in the weld. The regular evaluating the fatigue status of the critical structural components in steel bridges during the service life of the bridges, can help to reduce the probability of high cost of bridges' maintenance and replacements.

In fatigue assessment of large structures including the long-span steel bridges, providing the stress responses at the high-stressed welded areas is one of the crucial steps. The stress ranges are frequently measured through instrumenting the data acquisition systems at the objective structural components of bridges. However, the limitation of access for installing the data acquisition systems, at the welded areas of the bridge, can influence the measured fatigue response. Consequently, the computed fatigue responses, using the stresses at a reasonable distance to the weld toe, may not reflect the fatigue condition of the welded component.

Multiple fatigue assessment methods, in recent years, are developed to determine the remaining life of the welded structural components. The stresses-based fatigue methods vary based on the stresses that are achieved for fatigue analysis. In addition, for each fatigue assessment method, unique S-N curves are developed for the categorized welded structural components. Fatigue assessment of the modern-design components that are not documented in the existing bridge design codes can be addressed through the application of local fatigue assessment methods.

The local fatigue assessment methods, using local stress ranges at the welded areas, can consider the local stress concentration effects induced by weld geometry (1). The hot-spot stress method or notch stress methods are the local fatigue assessment methods that apply the stresses at the weld toe for fatigue analysis (2). The local fatigue assessment methods, primarily, rely on the development of numerical models to provide the explicit stresses at the stress concentrated areas close to the weld toe (3) (4). In recent years, extensive research efforts have been made to evolve the hot-spot stress method for fatigue assessment of the complex structural components using theoretical, experimental and numerical approaches (5).

The hot-spot stress method is primarily applied to address the fatigue assessment of the tubular welded connections (6). In recent years, many studies address the incorporation of the hot-spot stress methods for fatigue assessment of the welded components at the large-scale bridges in the local and global level (7). Ni et al. performed fatigue reliability assessment of the welded connections of a cable-stayed bridge using field collected data and hot-spot stress method (8). Aygul et al. compared the fatigue assessment of four different welded components of steel bridges using the nominal and hot-spot stress method (9). Wie et al. performed the fatigue assessment of the cope-hole details through the hot-spot methods using the experimental and numerical efforts (10). Alancer et al., recently, provided a global finite element (FE) model for fatigue assessment of a composite steel-concrete roadway bridge using the hot-spot stress method (11). In most of the available studies, the focus is made on the local performance of the welded components under the simplified loading conditions. The structural connections of steel bridges can have complex boundary and loading condition that is applied through multiple structural members connected to that the connection.

This study focuses on fatigue assessment of a newly designed gusset-less connection in a case-study bridge using the hotspot stress method. The case-study is the Memorial Bridge in Portsmouth, NH, a vertical lift truss bridge that carries the vehicular and naval traffics. The bridge has a long-term structural health monitoring (SHM) program that collects continues field data including the nominal stresses at the multiple locations of the gusset-less connection. In addition, a global FE model, that includes all the structural members of the bridge, is developed to complete the information required to understand the performance of the connection. The FE model, in this study, is also applied to determine the variability of the hotspot stresses and the nominal stresses at the welded area of the connection. The hotspot stresses at the weld toe of the gusset-less connection is achieved using the field collected nominal stresses and the stress concentration factors defined by the FE model.

5.3 Fatigue Assessment methods

The installed strain rosettes at the representative structural component of steel bridges provide the structural response as the strain time-history at the sparse locations of the connection. The field collected responses are in a reasonable distance to the weld toe, providing the nominal strain responses. Consequently, the acquired SHM data can be applied for fatigue assessment of the objective critical components using the nominal stress method. The structural hot-spot stress response of at the weld toe of the component is provided through a validated FE model, in this study. The numerical hot-spot stresses at the weld toe are applied for fatigue assessment of the gusset-less connection using the hot-spot stress method. The two applied approaches for fatigue assessment of the investigating connection, the nominal stress method and the hot-spot stress method, are explained in this section.

5.3.1 The nominal stress method

The nominal stresses at the welded structural components are determined in a distance to the weld toe, as shown in Figure 5-1. In the nominal stress method, the nominal stress as well as the appropriate S-N curve, developed for the category of the investigating component, is applied to measure the fatigue remaining life of the component. The bridge design code, AASHTO, has documented a variety of the welded structural components various structural component into multiple fatigue categories, A-E (12). However, for the complex welded components, that are not considered in the existing fatigue design codes, application of the S-N curves relies on engineering judgments and the assumptions.

The novel gusset-less connection is not cataloged in the standard fatigue design codes, including AASHTO. Therefore, based on the designer's assumption and the existing studies for the fillet welds, the category C is employed for fatigue assessment of the connection. The determined properties of Category C are applied to measure the fatigue damage index, using the Miner's rule that is expressed as Eq. (5-1). The required stress/cycles are provided through post-processing the field collected data, using the rainflow cycle algorithm (13).

$$\sum \frac{n_i}{N_i} \quad \text{Eq. (5.1)}$$

5.3.2 The hot-spot stress method

The hot-spot stress method does consider the local stress concentration due to the notch effect at the weld toe, while excluding the non-linear peak stress, as shown in Figure 5-1. The hot-spot stress can be determined by extrapolating the stress responses at the reference points (Figure 5-1). The distance of the reference points to the weld toe depends on the type of the weld and size of the mesh in numerical models. For the investigating fillet weld toe, the reference points at the

web of the connection, are located at the $0.4t$ and $1.0t$ (t is the thickness of the web) in a perpendicular distance to the weld toe, respectively, expressed in Eq. (5.2). The stress responses at the reference points can be achieved using the numerical model and the fine mesh sizes. In the experimental efforts, the hotspot stresses are achieved by placement of the data acquisition system at the reference points (13).

$$\sigma_{hs} = 1.67\sigma_{0.4t} - 0.67\sigma_{1.0t} \quad \text{Eq. (5.2)}$$

The ratio of the hot-spot stress range at the weld toe to the nominal stress is defined as the stress concentration factor (SCF) expressed in Eq. (5.3). The SCF, that is frequently determined using the numerical models, can be multiplied to the nominal stresses to achieve the hot-spot stress without the requirement to the reference points. The SCF is frequently applied for fatigue assessment of the structural components using the field collected nominal strain responses. Even if the variable amplitude traffic loads may result in multiple SCFs, a single SCF ratio is applied to the collected responses (14).

$$SCF = \frac{\Delta\sigma_{hs}}{\Delta\sigma_n} \quad \text{Eq. (5.3)}$$

The hot-spot stress method applies less S-N curves as compared to the nominal stress method. In IIW (international institute of welding), the fatigue classes (FAT class) and the associated S-N curves are expressed based on the type of the weld as well as the weld geometry (16). For the fillet welds, it is recommended to apply FAT 90 for the load carrying fillet welds and FAT 100 for the load carrying fillet welds (17). In this study, regarding the performance of the weld at the gusset-less connection, FAT 100 is applied for fatigue assessment at the curved fillet welds.

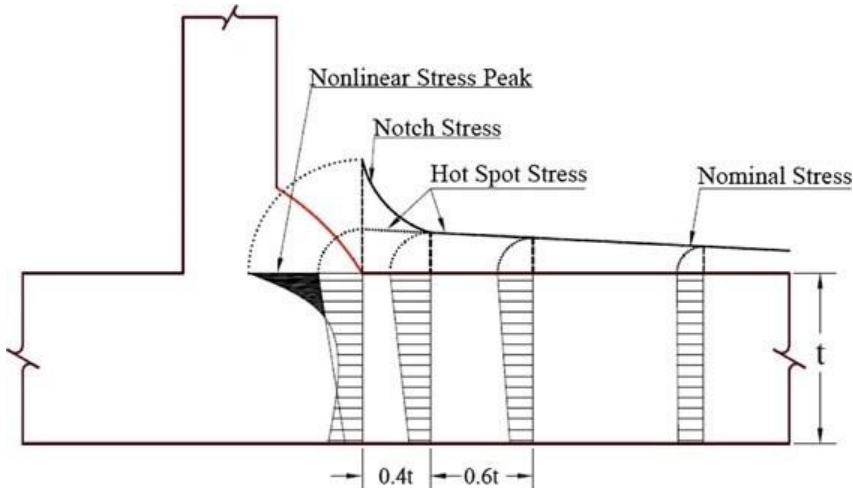


Figure 5-1 Hot-spot stress extrapolation at the weld toe (2)

In developing the appropriate numerical model for the hot-spot stress, an extensive study is performed by the researches to specify the requirements of an efficient FE model. The appropriate FE model for the hot-spot stress method requires a careful attention in providing the mesh insensitive models. In the previous studies, it is recommended to apply the fine mesh sizes (maximum of $0.4t$) and higher dimensional elements such as the three-dimensional solid elements, as shown in Figure 5-2. Also, the incorporation of the weld geometry in the FE model, is illustrated to have a significant impact in predicting the precise hotspot stresses at the weld toe (110). The weld geometry can be either modeled using the thick shell elements or solid elements, as shown in Figure 5-2. In this study, due to the considerable size of the weld and the geometry of the curved fillet weld, the 20-noded solid elements are applied to model the gusset-less connection and the fillet welds.

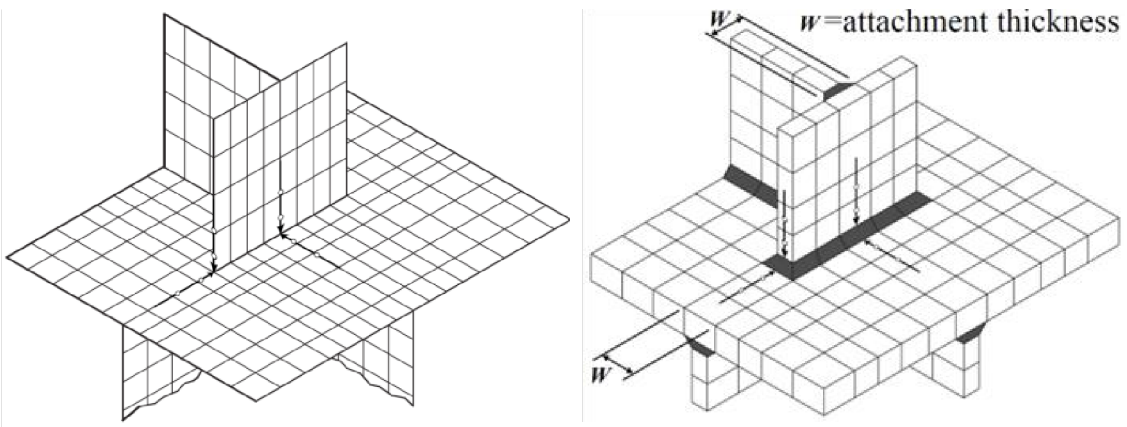


Figure 5-2 FE modeling of the welded component (a)shell element, (b) solid element with weld geometry (18)

5.4 The case study: The Memorial Bridge

5.4.1 The bridge specifications

The newly reconstructed Memorial bridge is a vertical lift truss bridge in Portsmouth, NH, inaugurated in 2013 (19). The bridge includes three identical spans, two fixed and one moving span at the middle which is lifted through the two lifting towers in each side of the span, as shown in Figure 5-3a. The bridge also includes a novel gusset-less connection situated at the tower, top and bottom chords of the truss bridge which directly joints the horizontal chords to the diagonal members (shown in Figure 5-3b). The connection consists of a complex-geometry web and cold-bent flanges which are joined through the 1.58cm curved fillet welds.

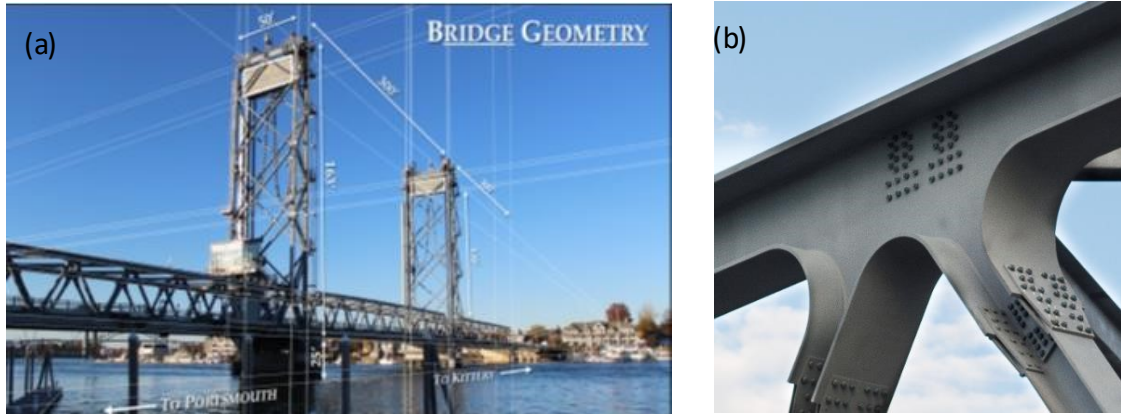


Figure 5-3 (a), The Memorial Bridge, Portsmouth, NH, (b), The gusset-less connection of the Memorial Bridge (20).

The Memorial Bridge has a long-term SHM program, following one of the “Living Bridge project” goals, to provide continues information on the global performance of the bridge as well as the local performance of the gusset-less connection (21). The acquired data are applied for the design verification and condition assessment of the bridge, under the induced excitations of the traffic loads and lift operation. The SHM system is installed at the south span and south tower of the bridge through a designed instrumentation plan to provide real-time data since March 2017. This instrumentation plan includes 16 strain rosettes, 2 uni-axial strain gages, 12 uni-axial accelerometers, 4 tiltmeters and a weather station installed at multiple locations of the bridge that collect data with the sample rate of 50 Hz (21). Shown in Figure 5-4 is the array of five strain rosettes that are installed at the top and bottom gusset-less connections of the bridge, aimed at providing enough information on the structural response of the connection. In this study, the long-term collected time-history strain responses of the strain rosettes, installed at the bottom connection, are applied for fatigue assessment.

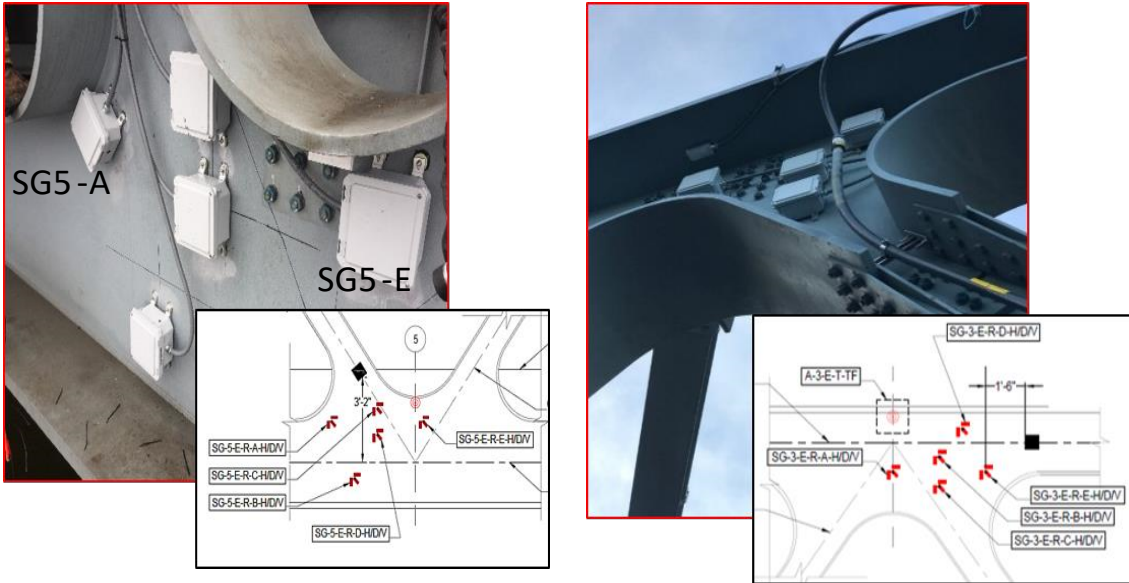


Figure 5-4 Instrumentation of the gusset-less connection at the bottom (left) and top chord (right)

5.4.2 The gusset-less connection

The innovative gusset-less connection is designed to improve the local performance of the connection by increasing the robustness of the component while decreasing the requirement for maintenance of the component. The gusset-less connection that is applied in a truss bridge is connected to multiple structural members in the planar and out-of-plane direction. In the planar direction, the bottom connection is continuously connected to the bottom chords. In addition, through bolted connection, the gusset-less connection is connected to the diagonal members. In the out-of-plane direction, the gusset-less connection is connected to the transvers floor beam, connecting the two trusses at the east and west side of the bridge. There are also, skewed floor beam, connecting the floor beam to the web of the gusset-less connection through the bolted joints. Under the variable amplitude traffic load, the connecting members to the gusset-less connection apply a complex loading condition to the connection that changes with the traffic conditions. Therefore, apart from the complex geometry of the gusset-less connection, it is essential to

investigate the influence of the variable loading condition on fatigue performance of the connection. The changes in the direction and amplitude of the stress ranges can influence the location of the crack initiation and the direction of the fatigue crack propagation. Application of the global FE model, in this study helps to understand the variability of the loading and conditions under the dynamic traffic loads. Using the global FE model, the dynamic truck loads are simulated and the stresses at the gusset-less connection are achieved as the time-history responses.

5.5 The numerical model of bridge

5.5.1 The global model of the long-span bridges

A global FE model that incorporates all the structural members, aids to understand the details of stress distribution at the welded area of the gusset-less connection. In addition, the numerical model helps to determine the location of the maximum hot-spot stress that is prone to fatigue crack initiation. However, the global FE model that includes all of the structural components significantly increases the computation time which adversely impacts the efficiency of the model. In this study, a global time-efficient multi-scale FE model is applied to determine the structural responses at the welded locations, under the traffic loads.

5.5.2 The FE model of the case-study bridge

In this study, the multi-scale approach which incorporates multiple dimensional elements in a single global model is applied to develop a three-dimensional global model which is shown in Figure 5-5. The model is developed in LUSAS, a commercial FE software package, applied for the large-scale models. The developed model considers the gusset-less connection as the three-dimensional members, modeled with the thick shell elements, while the remainder of the structural

members are modeled with the two-dimensional beam elements. The coupling of the opposing dimensional elements is performed using the multi-point constraint equations, addressed in (17).

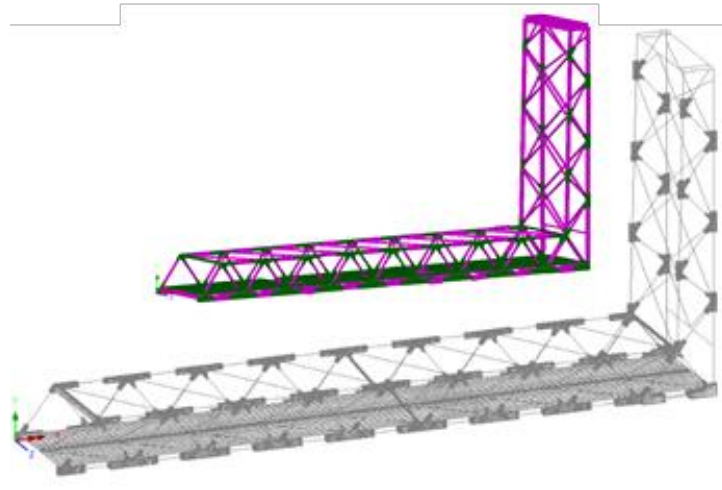


Figure 5-5 Multi-scale global model of the Memorial Bridge in LUSAS

However, to determine the hot-spot stress response at the weld toe, due to the complex geometry of the curved welds, application of the shell element to predict the precise hot-spot stresses is less convenient. The recommended prerequisites of fine mesh sizes, as well as the higher dimensional element, can considerably increase the computation time that opposes with the time-efficiency goal of the model. Therefore, a sub-structure of the gusset-less connection, which is modeled correspond to the requirements for the hot-spot stress method, is created, as shown in Figure 5-6. The sub-structure model includes the 20-nodded hexahedral solid elements for the welded areas, and 10-nodded tetrahedral elements for the rest of the connection. The boundary conditions of the substructure model are defined by the displacement results of the global model at the equivalent locations. In Table 5-1, the properties of the global multi-scale model and the associated sub-structure in terms of the type and the number of elements is expressed.

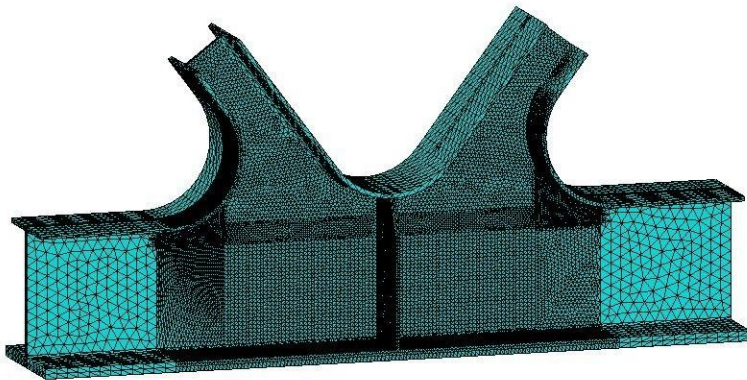


Figure 5-6. The sub-structure model of gusset-less connection at the Memorial Bridge in LUSAS

Table 5-1 Properties of the sub-structure and multi-scale finite element models

Model properties	Sub-structure	Multiscale global model
Applied elements	Three-dimensional quadrilateral solid element	Linear quadrilateral thick shell Three-dimensional thick beam
Number of elements	Solid elements: 210726	Shell elements:158993 Beam elements:5160
Computational time: static analysis	2 minutes	0.81minutes

5.5.3 Verification of the developed FE models

To validate the accuracy of the model, applied for the further fatigue assessment goal, it is essential to verify the developed models, properly. In this study, the verification of the developed FE model is performed through a designed load test with measured truck size and weight. The selected truck is a two-axle dump truck, weighting 255 MPa (103 MPa and 151 MPa axle loads). A total of twelve tests, including the dynamic and the pseudo-static load tests (with two stops) are performed at the northbound and southbound lanes of the bridge. The numerical results are achieved by applying the truck loads as the four-point loads that are applied to the deck of the model. The model verification is performed by comparing the field measured to the numerically

provided strain responses at the location of the strain rosettes of the gusset-less connections. Since the focus of the current study, is the performance assessment of the bottom gusset-less connection, only the verification results for this connection are provided.

In Figure 5-7, the strain results of the strain rosettes during the load test are compared in a bar chart to the numerical response of the global model as well as the local responses of the sub-structure model. The strain response, expressed in the bar charts, report the second stop of pseudo static load test in the northbound, where the induced strain responses at the strain rosettes have the highest value. It can be observed that the results of the sub-structure model are slightly higher than the multi-scale global model.

The higher strain response of the sub-structure model can be due to the application of the solid elements that provides a lower stiffness as compared to the shell and beam elements. In addition, in the location of the strain rosette D, the field strain response is higher than the numerical results, which can be due to the difference between the applied load to the model and the field conditions. The acquired results indicate the verification of the global and the sub-structure FE models in predicting the desired stress responses, applied in this study.

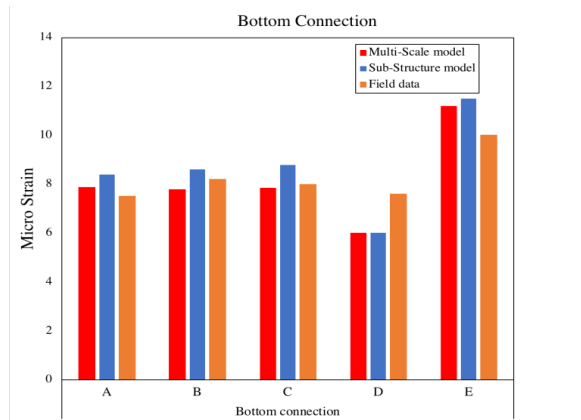


Figure 5-7 Comparison between the numerical result and field data at the load test for model verification

A more detailed comparison is provided between the strain contours of the models to understand the difference between the application of the global and local model as well as the shell and solid elements, respectively. As shown in Figure 5-8, it can be observed that the models can represent the hot-spot locations at the curved weld toe. The higher stress concentrations, induced at the substructure model, can be due to the short length of the floor beam modeled in the substructure model. Since the truck load is directly applied to the floor beam, large bending moment is applied to the web of the connection. The illustrated difference between the results of the substructure to the field data and the multi-scale model notifies for modifications of the substructure model. Before the application of the model for the fatigue assessment purpose, the boundary conditions of the sub-structure model are calibrated to acquire the desired response. In the next section, the application of the models for fatigue assessment is explained.

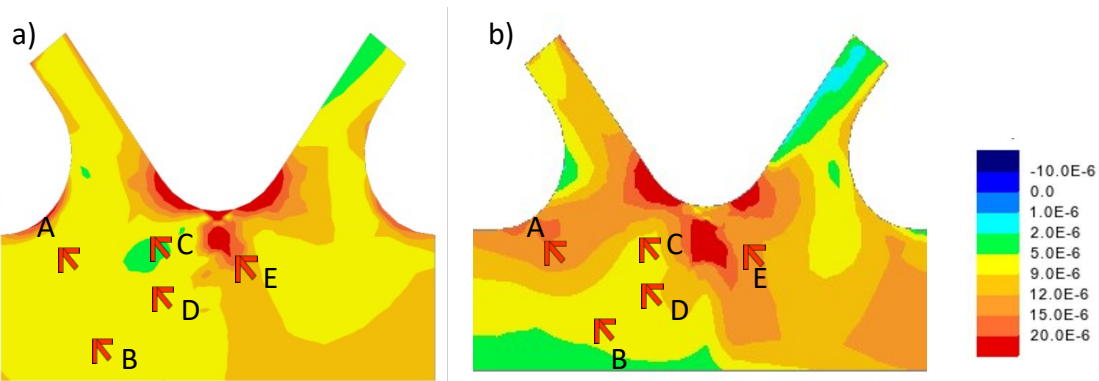


Figure 5-8 Strain contours of the gusset-less connection for the a) multi-scale model and b) the sub-structure model

5.6 Fatigue assessment of the gusset-less connection

5.6.1 Using the field collected SHM data

For fatigue assessment of the gusset-less connection, one-year period of data is collected and post-processed. The long-term period of data collection ensures that the frequent experienced

stress ranges at the bridge are considered for fatigue assessment. As shown in the instrumentation plan of the bottom connection in Figure 5-2a, two strain gages are close to the curved welds, SG5A and SG5-E. In Figure 5-9, the examples of the time-history stress response of the two strain rosettes are shown. In this study, SG5-A, which is located close to the curved weld of the gusset-less connection, is selected to investigate the fatigue performance of the gusset-less connection. In Table 5-2, the results, including the maximum recorded stress range, the average of the measured fatigue response, are provided for the four different seasons at the year of data collection. The less observed variability in the recorded stress ranges for the four different seasons, results in the negligible difference in the measured averaged fatigue responses.

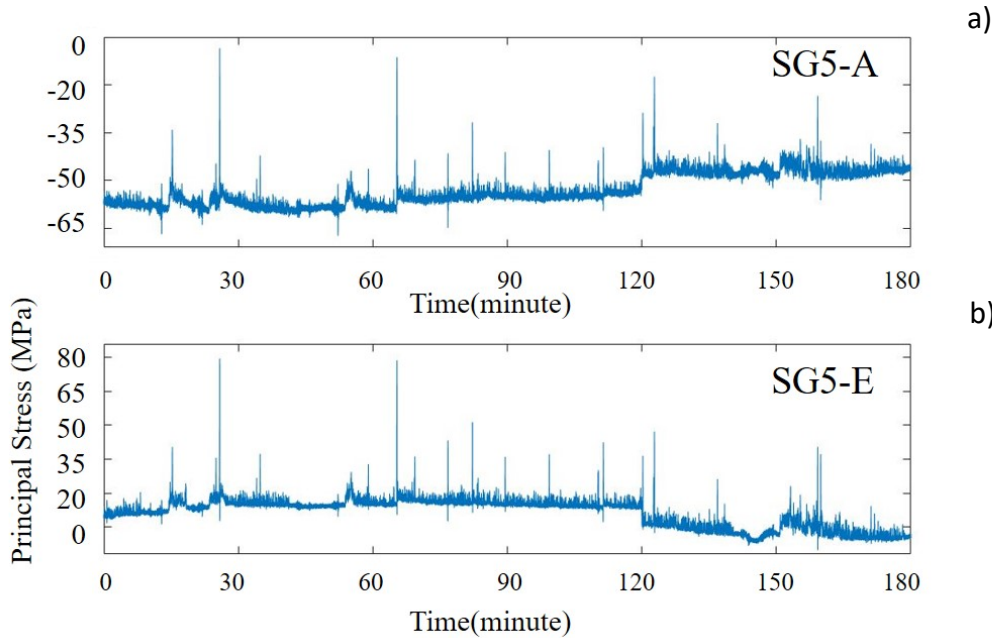


Figure 5-9 Examples of time history responses (a) SG5-A, (b) SG5-E

Table 5-2 . Recoded stress ranges and the measured fatigue response over a year

Month of data collection	Maximum recorded stress range (Mpa)	Average of applied stress range (Mpa)	Fatigue response
Spring	78.8	46.1	1.04E-06
Summer	81.3	53.7	1.18E-06
Fall	80.7	52.2	1.07E-06
Winter	77.6	51.6	9.60E-07

5.6.2 The hot-spot stress at the gusset-less connection

Instrumentation of the structural components of steel bridges at the weld toe, to determine the hot-spot stresses may not be feasible. In this study, the hotspot stresses are achieved through the application of a well-defined SCF multiplied by the field collected data. The numerical model is applied to determine the SCF. The variability of the SCFs due to the complex geometry of the weld and the variability of the loading conditions, applied to the connection, is investigated in this study.

5.6.2.1 The static loading

For the longitudinally welded connections, less variability of the hotspot stresses and the resulting SCF along the weld toe can be observed. For the curved weld of the current study, the complex geometry of the weld can induce disparity between the hot-spot stress responses along the weld toe. Also, the geometry can influence on the rate of dissipation of stress response with the distance to the weld toe is required to be studied. In this section, six different paths that are perpendicular to the weld toe and have the specified locations of the reference points, are selected to study the variation of the measured hot-spot stresses along the weld toe, as shown in Figure 5-10.

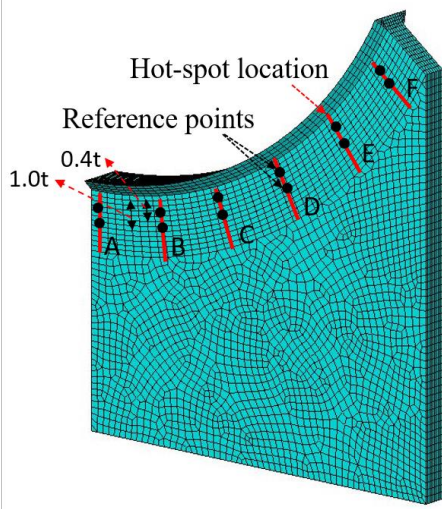


Figure 5-10 The selected paths along the curved weld toe for hot-spot stress measurements

The decreasing trend of the strain response versus the distance to the weld toe for the six investigating paths are provided for two different load cases, shown in Figure 5-11. The load cases are the second stop of the truck at the northbound and the southbound, respectively. Considerable agreement between the trends of the paths for the two loading conditions can be observed. However, the rate of stress reduction between the different paths along the weld toe is not identical. In addition, the path F, has a different strain variation as compared to the other paths for the two different loading cases. The path F, that is closer to the diagonal as compared to the other paths, displays a different trend as compared to the other paths. It is investigated that this path can be more influenced by the transferred loads from the diagonal member than the bottom chord.

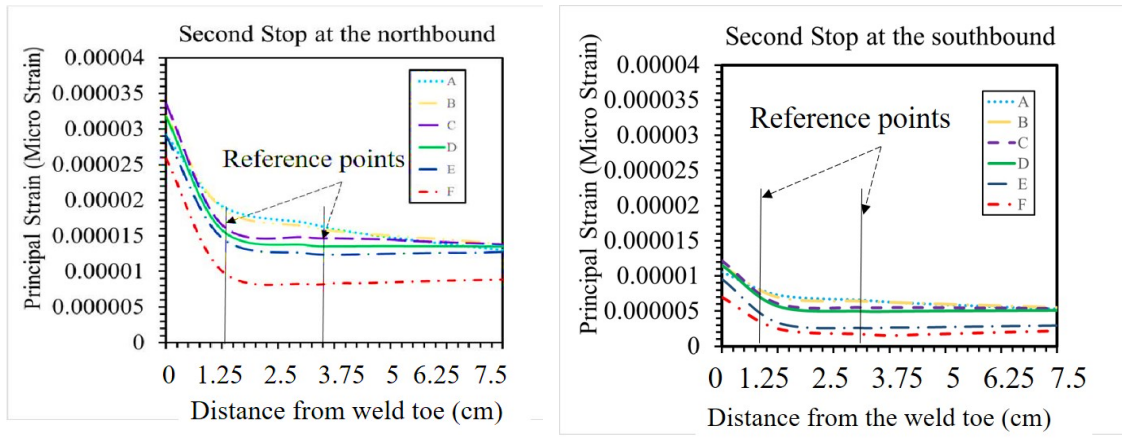


Figure 5-11 Strain variation with the distance from the weld toe under the static truck load at the northbound (left) and southbound (right)

The acquired results in Figure 5-11 for the northbound and the southbound truck loads are applied to determine the SCFs for the investigating paths. In Figure 5-12, for each path, the SCF ratios are measured for the two loading conditions, expressed as north and south. It can be demonstrated that the larger induced stresses by the northbound truck loading, proportionally results in higher SCFs, as compared to the southbound loading condition. In addition, for the path B, the maximum SCF is acquired. The SCF responses for the paths C, D, and E, are similar, as previously indicated in Figure 5-11. Consequently, for fatigue assessment of the connection, maximum, minimum or the average SCFs can be selected to be applied to the field collected nominal responses of the investigating strain rosette.

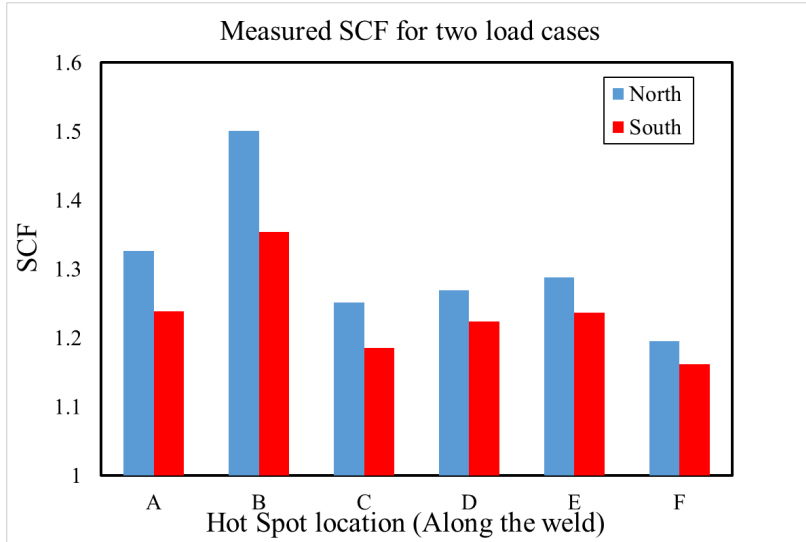


Figure 5-12 SCF under the static truck load at the northbound and southbound

5.6.2.2 The dynamic loading

It is observed that for the variable amplitude traffic loads and the induced strain responses, the SCF can change regarding the loading conditions. In this section, the variations of the SCFs along the weld toe is investigated under the dynamic moving load. For the dynamic loading, the SCFs are measured as the ratio of the hot-spot strain range to the nominal strain ranges for each path. The stress ranges are achieved through the numerical time-history response of the model at the desired locations. The time-history results of the global model to the substructure is transferred as multiple static loads, through a small step procedure. In Figure 5-13, the SCF results for the dynamic truck load travelling at the northbound and the south bound are shown. Compared to Figure 5-12, it is illustrated that the variations of the results along the weld toe follows a similar trend for the northbound and southbound with a negligible difference. Consequently, the SCF results, achieved from dynamic loading, are multiplied to the nominal stresses for fatigue assessment purpose.

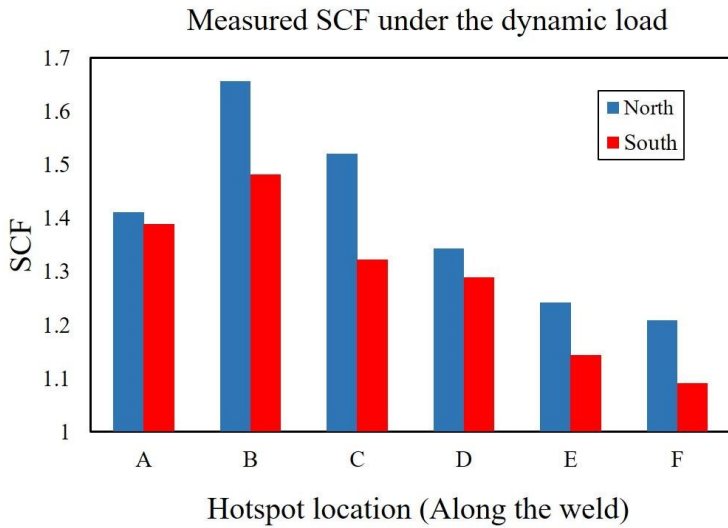


Figure 5-13 SCF under the dynamic truck load at the northbound and southbound

5.6.3 Fatigue response of the gusset-less connection using the SCFs

To measure the nominal and hot-spot fatigue response at the six investigating paths, the nominal and hot-spot stress ranges must be determined, respectively. For the six investigating paths, the acquired numerical hot-spot and nominal stress ranges under truck-moving load at the northbound and southbound of the bridge expressed in Table 5-3. In addition, for the six investigating paths, the SCFs are measured for the two loading conditions. It can be observed that for the two considering loading conditions, the SCF results follow the same trend along the weld toe. The measured SCFs for the northbound are about ten percent higher than the SCFs responses for the southbound truck loads.

Table 5-3 Hot-spot and nominal stress variations for six paths along the weld toe

Traffic load	A (MPa)	B (MPa)	C (MPa)	D (MPa)	E (MPa)	F (MPa)
Nominal Stress range north	2.7	2.3	2.5	2.8	3.1	3.1
Nominal Stress range south	1.6	1.5	1.7	1.7	1.9	2.0
Hot-spot Stress range north	3.8	3.8	3.8	3.8	3.8	3.8
Hot-spot Stress range south	2.0	2.0	0.33	0.33	0.33	0.33
SCF (north)	1.41	1.66	1.52	1.34	1.24	1.21
SCF (south)	1.39	1.48	1.32	1.29	1.14	1.09

It can be concluded that the achieved SCF responses are more dependent on the geometry of the curved weld. For the curved welds, the trend of the SCFs along the weld toe can be dependent on the radius of the curve. Consequently, for hot-spot fatigue assessment using the field collected data, the appropriate SCF for the location of installed strain rosette has to be determined. The SCF can be determined through a perpendicular path, starting from the position of the strain rosette to the weld toe to measure the associated hot-spot stress.

In addition, due to the variability of the SCFs with the changes in the traffic patterns, more comprehensive responses can be achieved by measuring multiple SCF responses under multiple simulated traffic conditions that are experienced at the bridge. The resulting SCFs can be averaged to apply as a single SCF for the variable amplitude field collected responses. The resulting acquired hot-spot fatigue responses through the averaged SCF can be conservative. Alternatively, a range of SCFs for the location of interest can be defined. Consequently, a range of hot-spot fatigue responses can be provided for the bridge manager to make the decisions about the maintenance program of the bridge. Defining an upper level and lower level fatigue responses can provide a broad view on the fatigue status of the investigating component. As a consequence, the bridge

manager can make a better decision for the inspection program of the bridge and prevent the excessive cost of unnecessary inspections.

In Table 5-4, the maximum, minimum and the average values of SCFs for the investigating strain rosette in this study (SG5-A) are determined. The expressed nominal stress response in the table is the average of the field collected principal stress responses for a limited period. The hot-spot stresses are measured by multiplying the nominal stress to the three different SCFs. The acquired fatigue responses are subsequently expressed as the maximum, average and minimum values. The observed difference in the fatigue responses demonstrates the importance of reporting a range measured fatigue responses. For the near threshold stress ranges, a slight change in the SCF can result in the prediction of either infinite fatigue life or limited fatigue life. Consequently, it is recommended in fatigue assessment of welded components of steel bridges using field data and hot-spot stress method, define a range of possible SCFs.

Table 5-4 Application of multiple SCFs for fatigue assessment using field collected data

Nominal stress range (MPa)	SCF	Hot-spot stress range (MPa)	Nominal Fatigue response	Hot-spot fatigue response
58	Maximum:	1.41	81	2.75E-7
	Minimum:	1.14	66	0.98E-7
	Average:	1.27	71	1.45E-7
				2.02E-7

5.7 Conclusion

Novel-designed structural components of steel bridges that are not explicitly included in the documented details of the available fatigue design codes require a comprehensive protocol for the fatigue assessment. The protocol requires a thorough understanding of the local performance of the component under the global loading and boundary conditions of the structural components at the bridge. In this study, fatigue assessment of the novel gusset-less connection at the case study,

Memorial Bridge is investigated. The local performance of the connection under the global loading are provided using the field collected SHM data at the connection as well as an efficient global FE model. In addition, a more detailed information on the local performance of connection is provided through the local sub-structure model of the connection. It is demonstrated that, the numerical global model has a significant impact in determining the SCFs with regard to the global loading conditions. Consequently, in fatigue assessment of the welded structural components of bridges that have a complex loading conditions, it is recommended to determine the SCFs based on the global numerical model. In addition, in fatigue assessment of complex structural components, using the field collected data, it is essential to determine the SCF for the specific location of the data acquisition system. However, the result of this study illustrates the variability of the SCF responses with the changes in loading condition. Application of multiple SCFs acquired through multiple loading conditions can be timely inefficient. It is recommended to determine the dominant loading conditions and the induced stress ranges at the target data acquisition system of the bridge. Consequently, the measured hot-spot fatigue responses are reported as the maximum and minimum fatigue response showing the conservative and non-conservative conditions, respectively. As the future work it is suggested to apply the mathematical model to quantify the SCF responses for multiple loading condition.

References

- 1) Hobbacher, A.F. Recommendations for fatigue design of welded joints and components, IIW document IIW-2259-15/ex XIII-2460-13/XV-1440-13. International Institute of Welding, Springer, 2015.
- 2) Niemi, E., Fricke, W., Maddox, S.J. *Fatigue analysis of welded components: Designer's guide to the structural hot-spot stress approach*. Cambridge, UK.: Woodhead Publishing, 2006.
- 3) Petershagen, H. Fricke, W. and Massel, T. *Application of the local approach to the fatigue strength assessment of welded structures in ship*. IIW Doc. XIII-1409-91. International Institute of Welding, 1991.
- 4) Doerk, O., Fricke, W., Weissenborn, C. Comparison of different calculation methods for structural stresses at welded joints. *International Journal of Fatigue* 25, no. 5 (2003): 359-369.
- 5) Maddox, S.J. Hot-spot stress design curves for fatigue assessment of welded structures. *International Journal of Offshore and Polar Engineering* 12, no. 2 (2002): 131-141.
- 6) Lotsberg, I. Recommended methodology for analysis of structural stress for fatigue assessment of plated structures. Houston, USA: Proceedings of OMAE specialty symposium on integrity of FPSO system, 2004.
- 7) Chan, T.H.T, Li, Z. X., Ko, J.M. Fatigue analysis and life prediction of bridges with structural health monitoring data—Part II: Application. *International Journal of Fatigue* 23, no. 1 (2001): 55-64.
- 8) Ni, Y.Q., Ye, X.W., Ko, J.M. Monitoring-Based Fatigue Reliability Assessment of Steel Bridges:
- 9) Aygül, M., Bokesjö, M., Heshmati, M., Al-Emrani, M. A comparative study of different fatigue failure assessments of welded bridge details. *International Journal of Fatigue* 49 (2013): 62-72.
- 10) Wei, X., Xiao, L., Pei, S. Fatigue assessment and stress analysis of cope-hole details in welded joints of steel truss bridge. *International Journal of Fatigue* 100 (2017): 136-147.
- 11) Alancer, G., de Jesus, A.M.P., Calcade, R.A.B., da Silva, J.G.S., Fatigue life evaluation of a composite steel-concrete roadway bridge through the hot-spot stress method considering progressive deterioration. *Engineering Structures* 166 (2018): 46-61.
- 12) American Association of State Highway and Transportation Officials, AASHTO. *LRFD Bridge design specifications*. 5. Washington, DC, 2012.
- 13) Downing S.D., Socie D.F., Simple rainflow counting algorithms. *International Journal of Fatigue* 4, no. 1 (1982): 31-40.
- 14) Radaj, D. *Design and analysis of fatigue resistant welded structures*. Cambridge, UK: Abington Publishing, 1990.
- 15) Niemi, E., Tanskanen, P., *Hot-Spot Stress Determination for Welded Edge Gussets*. The International Institute of Welding - IIW Doc. XIII-1781-99, 1999.
- 16) Dong, P. A structural stress definition and numerical implementation for fatigue analysis of welded joints. *International Journal of Fatigue* 23, no. 10 (2001): 865-876.
- 17) Frickes, W. Recommended Hot Spot Analysis Procedure for Structural Details of FPSOs And Ships Based on Round-Robin FE Analyses. *The Eleventh International Offshore and Polar Engineering Conference*. Stavanger, Norway: The International Society of Offshore and Polar Engineers, 2001.
- 18) Savaidis, G., and Vormwald, M., Hot-spot stress evaluation of fatigue in welded structural connections supported by finite element analysis. *International journal of fatigue* 22, no. 2 (2000): 85-91.

- 19) NHDOT. *Memorial Bridge Project Innovations*. New Hampshire Department of Transportation, 2016.
- 20) Nash, T.P. An Objective Protocol for Movable Bridge Operation in High-Wind Event Based on Hybrid Analysis by European and American Design Code, Durham: M.Sc. thesis, Univ. of New Hampshire, NH, 2016.
- 21) Adams, T., Mashayekhizadeh, M. Santini-Bell, E., Wosnik, M., Baldwin, K., and Fu, T. Structural Response Monitoring of a Vertical Lift Truss Bridge. *96th Annual Meeting*. Washington, D.C: Transportation Research Board, 2017.
- 22) Mashayekhizadeh, M., Santini-Bell, E. and Adams, T. Instrumentation and Structural Health Monitoring of a Vertical Lift Bridge. Jacksonville, Fl: Proceedings of 27th ASNT Research Symposium, 2017.
- 23) Mashayekhi, M., Santini-Bell, E. 2018. Three-dimensional multiscale finite element models for in-service performance assessment of bridges. *Computer-aided civil and infrastructure engineering*. doi: <https://doi.org/10.1111/mice.12424>.

Chapter 6

6 FATIGUE ASSESSMENT OF A COMPLEX WELDED STRUCTURAL CONNECTION STEEL VERTICAL LIFT BRIDGE USING A THREE-DIMENSIONAL MULTI-SCALE FINITE ELEMENT MODEL

*Under review: Maryam Mashayekhi and Erin Santini- Bell

6.1 Abstract:

Some novel complex structural components of steel bridges are not explicitly addressed in the existing fatigue design codes and require an alternative local fatigue assessment method. This paper proposes a fatigue assessment protocol for these complex critical components of steel bridges, using the hotspot stress method. A computationally efficient finite element model of a large-scale bridge is created to provide the local structural response of the complex components, under the simulated dynamic traffic loads. A multi-scale model is implemented to accommodate the higher dimension elements, which are recommended for fatigue assessment via hotspot stress method. The multi-scale model is created for the case study, the Memorial Bridge in Portsmouth, NH, which is a vertical lift steel truss bridge with a novel gusset-less curve-welded connection. A truck load test is used to validate the multi-scale model by comparing the numerical results to the field collected data through the structural health monitoring system of the bridge. The result shows that the multi-scale model can determine the critical hotspot stresses, to study the fatigue performance of the bridge's critical components.

Keywords: multi-scale model, hotspot stress, gusset-less connection, traffic simulation,

6.2 Introduction:

A routine fatigue assessment protocol of steel bridges can support the decision-making, related to resource allocation for retrofit or replacement of the structural component. Through the fatigue protocol results, the frequency and focus of the bridge's inspection procedure can be established. The accuracy of the fatigue life expectancy depends on the precision of the measured or predicted stress ranges at the fracture-critical structural steel components. In fatigue assessment of steel bridges, field collected strains are preferred, which mirror the stress concentrations due to the traffic loads. However, in a geometrically complex structural component, sensor limitations may impede capturing the critical fatigue responses. For fatigue assessment of complex welded components, local fatigue methods are specifically recommended (1).

Local fatigue assessment methods of welded components, including the hotspot stress method, measure the fatigue responses based on the computed hotspot stresses at the weld toe. The hotspot stresses are frequently determined through finite element (FE) models. Thus, extensive efforts have been made to clarify the specifications for FE model preparations and to obtain precise fatigue responses (2). Incorporation of numerical methods and application of a validated structural FE model can supplement the field collected strain responses with predicted local strain measurements in fracture-critical regions, such as the weld toe. However, the reasonably accurate responses require a fine mesh sizes and high-dimensional elements, both of which, increase the computation cost.

As a consequence, the stipulations of the hotspot stress method are frequently applied to a local FE model of the concerning structural component and under simplified loading and boundary

conditions. Therefore, the resulting fatigue response, using the numerical hotspot stresses, may not accurately reflect the fatigue status of the components in a complex structure. In the global model of a bridge, the boundary conditions are defined based on the predicted global performance of the structures, and its collaboration with the connecting members. Furthermore, the resulting stresses can be determined for variable traffic loading conditions, which consider the truck weight and its dynamic impact.

FE models of bridges have been developed in recent years in order to make the fatigue assessment of welded structural components of bridges more efficient and accurate. Li et al. are one of the pioneers in applying sub-structure local models of the structural components to implement the hotspot stress method for fatigue assessment of steel bridge' components (3). The higher dimensional elements of the local sub-structure model could improve the application of local fatigue assessment methods for large-scale steel bridges (4). Moreover, through a global FE model of the bridge, multiple traffic loads can be simulated as dynamic loads applied to the deck of the bridge (5). The model-predicted traffic-induced stress response can result in a more realistic fatigue response as compared to single amplitude stress ranges (6), (7), (8). In recent years, the idea of developing a multi-scale model which incorporates different dimensions of elements in a single model, is growing. Yan developed a multi-scale global FE model for a cable-stayed bridge to study the fatigue assessment under a single traffic load (9). Alancar developed a global FE model to consider the progressive pavement deterioration in fatigue assessment of composite roadway bridges, using the hotspot stress method (10). In other works, heavy truck dynamic loads were applied to FE model for the fatigue assessment of old riveted road bridges and bridge suspenders (11) and (12).

In this study, the fatigue assessment of complex structural components of steel bridges is investigated, through the hotspot stress method. An efficient global FE model is created for a case-study bridge. The model includes multiple dimensions of elements that are selected based on the structural performance of the components to optimize the degrees-of-freedoms (DOFs) and the computation time of the analysis. The multi-point constraint equations (MPC) method is applied to a couple of different dimensions of elements at the interfaces to provide a compatible stress response on the structural members. The optimum selection of the dimensions and the location of the interface is also addressed in this study. The model is verified through the quasi-static and dynamic truckload tests at the bridge. In addition, the dominant traffic scenarios, experienced at the case-study bridge, are simulated through the verified FE model to obtain the corresponding hotspot stress responses at the weld toe for fatigue assessment.

6.3 Background

6.3.1 Hotspot stress method

The classical fatigue assessment of the welded structural components relies on the application of the nominal stresses and the appropriate S-N curves, which are specified for different categories of structural components (13). The nominal stress method, however, does not consider the geometrical effects of the structural component, which makes the method less attractive for the fatigue assessment of the complex structural elements (14). Geometrical characteristics can have a significant impact on the amplitude and location of stress concentrations in fatigue assessment of a complex welded component. In addition, the defined categories in the existing design codes may not uniquely consider the fatigue strength of the welded components.

The structural hotspot stress method considers the geometrical effects of the welded components, including the dimensional and stress concentrating effects. However, the method ignores the local nonlinear stresses, induced by the notch effect at the weld toe (15). The notch effect is included in the experimentally developed hotspot S-N curves (16). The hotspot or structural stress method was primarily developed for the fatigue assessment of the tubular joints in offshore structures (17), (18), (19). In recent years, application of the method is also extended to plate-type structures (20). The hotspot stress is measured at the toe of welds through a linear or nonlinear extrapolation of the stress responses at the reference points (2). Based on the weld type, different extrapolation points (also known as reference points) have been proposed in the existing literature (21). The reference points, as a factor of the plate thickness, are placed in a perpendicular distance to the weld toe Figure 6-1. The hotspot stress relationships employed in this study is expressed in Eq. (6-1).

$$\sigma_{hs} = 1.67\sigma_{0.4t} - 0.67\sigma_{1.0t} \quad \text{Eq. (6.1)}$$

The hotspot stress is frequently determined through developing a well-detailed FE model. To accurately compute the hotspot stress at the weld toes, the model must be created based on the stipulated specifications, including the geometry of the component and mesh configurations, type, and size (22). The provisions for measuring hotspot stresses of the curved welds have been considered in several studies, which are specifically applied in tubular joints, hollow sections, and welded components of ships, (18), (23). Dong et al. extensively studied the requirements for the mesh size and element-type sensitivity for the continuous welds, such as curved fillet welds (24), (25). Dong proposed the hotspot stress procedure, which is based on the work equations of the nodal force of the elements along the weld toe, through a linear equation system. In this study, the

recommendations for modeling by Dong (26), are implemented to model the curved fillet weld, for the case-study component of this paper.

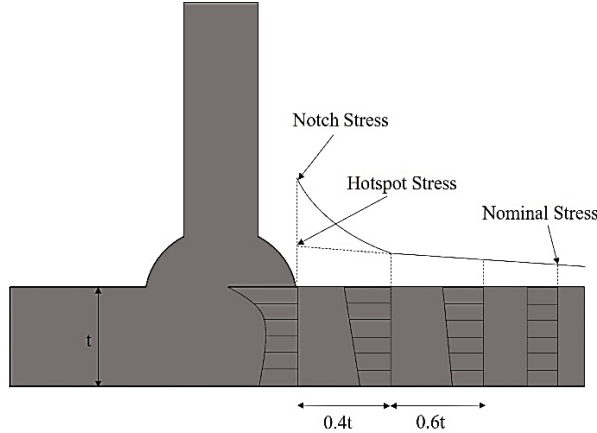


Figure 6-1 Hotspot stress extrapolation at the weld toe

6.1 The Case study: The Memorial Bridge

6.1.1 The bridge characteristics

The Memorial Bridge, connects Portsmouth, NH, to Kittery, ME, as shown in Figure 6-2a., and is the case-study bridge for this paper. The Memorial Bridge is a vertical lift truss bridge, which includes a novel gusset-less connection. The gusset-less connection, shown in Figure 6-2b, consists of a complex web geometry and cold-bent flanges, which are connected through a curved fillet weld having 1.562 cm thickness (27). The innovative design of the connection motivated this research to perform a detailed fatigue condition assessment. In addition, the complex performance of the connection, under the global loading and boundary conditions of the truss bridge, makes the case-study a suitable example for the goals of this research.

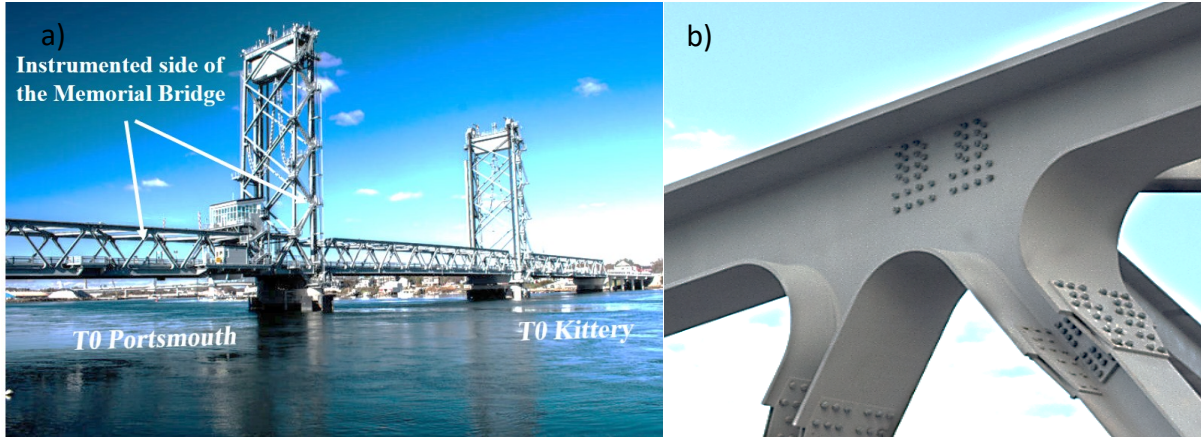


Figure 6-2 (a) The Memorial Bridge, Portsmouth, NH, and (b) The gusset-less connection of the Memorial Bridge.

The Memorial Bridge is equipped with multiple structural sensors type, distributed throughout the Portsmouth-side of the Memorial Bridge. The monitoring program of the bridge seeks to collect the information that is required for model verification, condition assessment, and operational decision-making support of the bridge structure. The structural health monitoring (SHM) program of the Memorial Bridge, operational as of March 2017, provides a continuous real-time data at the critical locations of the bridge (28). The focus on this paper is the strain rosette clusters distributed on the gusset-less connections, which are permanently installed for a long-term SHM program. As shown in Figure 6-3, the objective gusset-less connection includes an array of five strain rosettes to capture the strain variations in the vicinity of the fillet welds (nominal strains). The collected strain responses, via these strain rosettes, are applied for the fatigue assessment of the component, using the nominal stress method for comparison with the hotspot stress method.

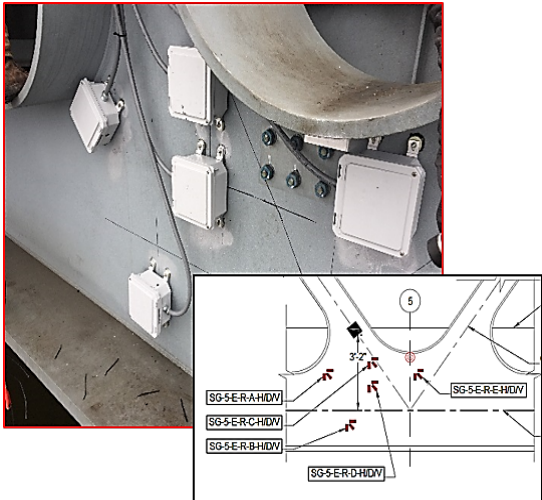


Figure 6-3 Instrumentation of the bottom gusset-less connection.

6.1.2 Load Test at the Memorial Bridge

A truck load test was conducted at the Memorial Bridge for model verification and to conduct a sensitivity analysis of the sensor. The objective of the load test was the evaluation of the FE model-predicted structural responses, subjected to the traffic loads. For this load test, a NHDOT dump truck, with a measured weight, is applied to load the bridge, as shown in Figure. 6-4a. and 4b. As reported by NHDOT, this class of vehicle has a higher contribution in the daily traffic program of the bridge, in comparison with the other vehicle classes.

The load test includes three different traffic scenarios, each following a specific goal, expressed in Table 6-1. The traffic scenarios were performed in both lanes of the bridge. Each traffic scenario is repeated three times, and the collected responses are averaged for model verification purposes. In addition, before the load test starts, the sensors were calibrated.

1. Load case 1 is a quasi-static load test with two stops in each lane. The second stop of the quasi-static load test is located at midspan, where the rear axle of the truck is placed above the instrumented gusset-less connection, shown in Figure. 6-4a.

2. Load case 2 is a dynamic load test, which the truck crosses along the northbound and southbound of the bridge. This test aims to improve the validity of the FE model in simulating the traffic load, using the dynamic moving load.
3. Load case 3, is a dynamic load test and represents a complex traffic pattern, which consists of multiple vehicles (including the load test truck), crossing on both lanes of the bridge. This load test is defined to evaluate the accuracy of the FE model in simulating the complex traffic scenarios.

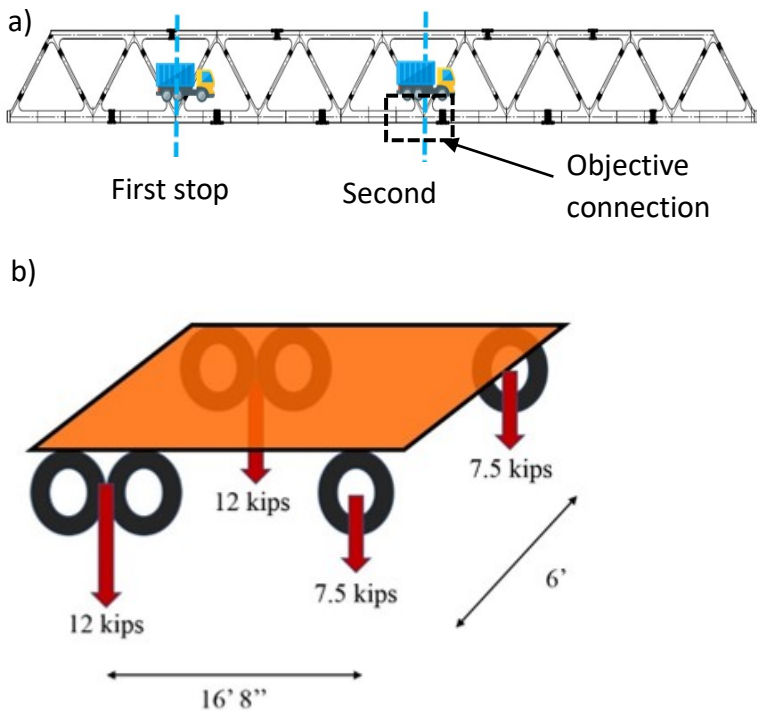


Figure. 6-4 a) Truck stops at the quasi-static load test, b) the size and weight of the load test truck.

Table 6-1 Truck Load test specifications at the Memorial Bridge.

Load test	Load test description	Traffic condition	Speed	Objective
			(KM/h)	
1	Quasi static/two stops	Single truck	10	Model verification
2	Dynamic	Single truck	48	Model verification
3	Dynamic	Multiple vehicles plus truck	48	Traffic simulation/fatigue assessment

The three load tests are applied in this study for model validation and simulation of the traffic scenarios, discussed in the following.

6.2 Finite Element Models of the Memorial Bridge

The main objective of this paper is the fatigue assessment of the structural components of complex steel bridges, through the hotspot stress method and the development of an efficient global FE model of the case-study bridge. In this study, the multi-scaling method, which can couple multiple dimensions of elements, is applied to create a single global model. The higher-dimension elements are applied to meet the requirements for the hotspot stress method at the critical components. The lower-dimension elements are selected for the long members in order to reduce the computational time. Three models were developed in this section, 1) a global single-scale model, modeled with shell elements, 2) a local sub-structure model of the gusset-less connection made of solid elements and 3) a global multi-scale model. The first two models are applied to evaluate the efficacy of the multi-scale model, in terms of accuracy and computational cost.

6.2.1 The shell element model

In the shell element (SH) model, all of the structural members are modeled with shell elements, as shown in Figure 6-5. The implemented shell elements are the eight-noded thick shell elements with six DOFs at each node. The size of the shell elements varies based on the performance of the structural components (29). Application of the shell elements for the structural members can result in a uniform stress distribution between the connected members, for a global FE model. However, the model requires high modeling and computation costs, which makes it impractical in FE modeling of long-span bridges. In this study, the SH model is developed for comparison with the multi-scale model structural response. In addition, the model is a tool to understand the structural performance of the members to efficiently select the dimension and interface locations of elements in the multi-scale model.

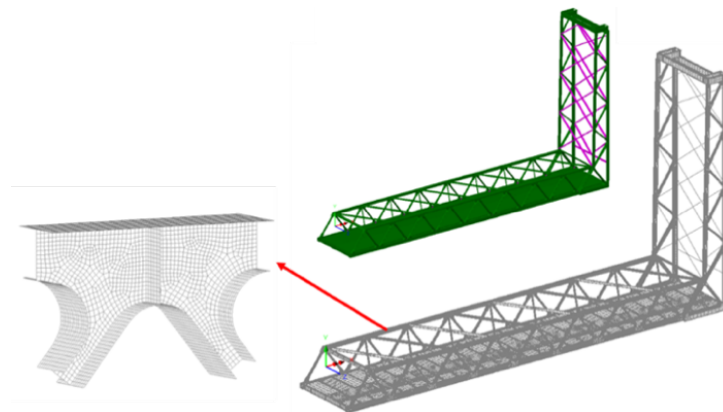


Figure 6-5 The SH global model of the Memorial Bridge created in LUSAS.

6.2.2 The sub-structure model

The sub-structure (S-S) model is a local model of the gusset-less connections, which is modeled by three-dimensional solid elements, as shown in Figure 6-6. The weld geometry is also

considered in the model, as recommended for computing the hotspot stresses at the weld toe. The welded area of the connection is meshed based on the provisions for the hotspot stress method. The S-S model is identical to the three-dimensional solid part of the multi-scale model, which is discussed in the next section. The beam elements are connected to the gusset-less connection, to apply the boundary conditions in a reasonable distance to the curved welds. The distance is required to reduce the possible stress concentrations due to the direct application of the loads or boundary conditions to the member. The boundary conditions are applied to the nodes, as shown in Fig. 6-6, which are the obtained displacement results from the SH model, at the same locations. This model is developed to compare the efficacy of the multi-scale model to the S-S model in obtaining the hotspot stresses.

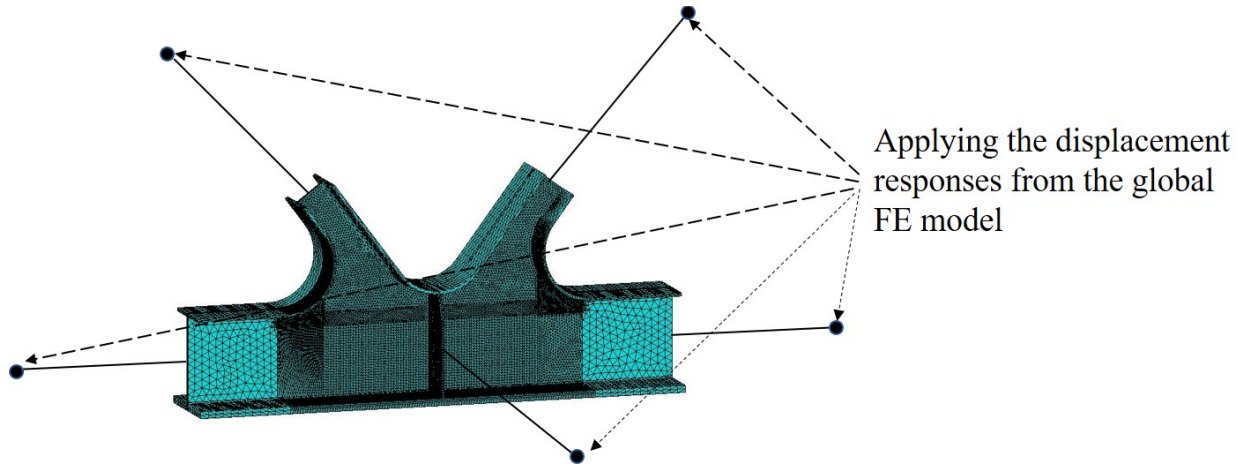


Figure 6-6 The SS global model of the Memorial Bridge created in LUSAS.

6.2.3 The multi-scale model

The multi-scale (M-S) model, shown in Figure 6-7, is a global model that incorporates three different dimensional elements to model the structural members. The dimension of the elements is selected based on the structural performance of members, and the expected accuracy

of the numerical response. In addition to the type of elements, the size of the meshes is determined by considering the structural responses of the SH model. The model considers the three-dimensional thick beam elements for the long structural members, including floor beams, braces, diagonals, and parts of the top and bottom chords. The gusset-less connections of the case-study bridge are modeled with the linear thick shell elements. The gusset-less connection, which is located in the middle of the truss, in the bottom chord, is selected for the hotspot fatigue assessment purpose (Figure 6-7). This connection is modeled, using three-dimensional solid elements. The welds geometry, which is advised for predicting the accurate hotspot stress at the weld toe, is also modeled through the solid elements in this connection.

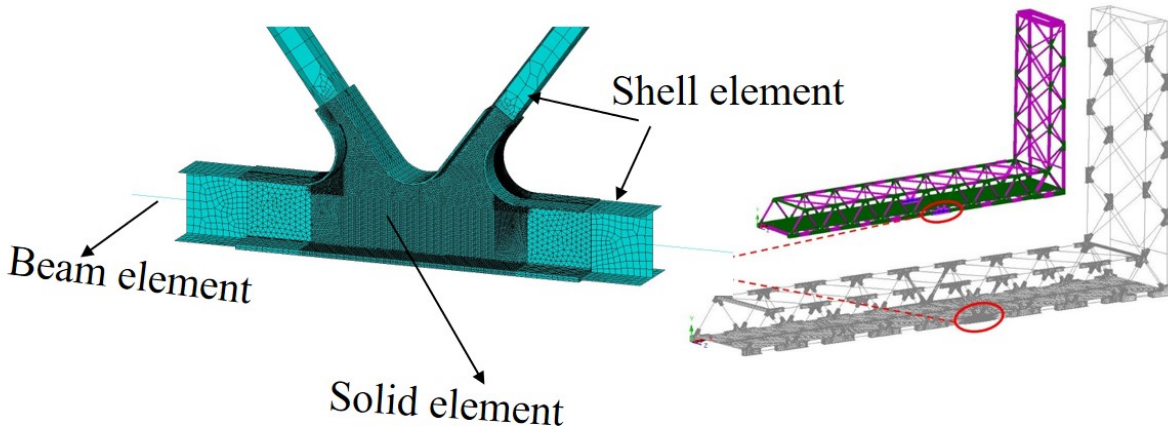


Figure 6-7 The MS global model of the Memorial Bridge created in LUSAS.

6.2.3.1 Coupling multiple dimensional elements

In the multi-scale modeling, it is crucial to appropriately couple elements of different dimensions at the interface point, in order to provide a uniform stress distribution and continuous displacement in the structural members. In the in-plane direction, the bottom chords gusset-less connection is connected to the diagonal members. In the out-to-plane direction, it is connected to the transverse floor beams and skewed floor beams. The coupling between different dimensions

of elements is provided by using Multi-point constraint (MPC) equations, developed by Mccune (30), (31). The details for the development of the coupling relationships between different scales are expressed for multiple cross-sections in the in-plane and out-of-plane directions (32). In the M-S model, the coupling is provided at the interface of the beam to shell element, shell to solid elements and beam to solid elements, in the in-plane and out-of-plane directions.

6.2.3.1.1 Coupling beam to shell elements

As shown in Figure 6-7, all of the gusset-less connections (except the objective connection) are modeled with the shell element, which are located in the bottom chord, the top chord, and the tower were modeled. The longitudinal members were modeled by beam elements, which are connected to these gusset-less connections. The coupling of the beam to shell elements is performed in the in-plane and out-of-plane directions, as detailed in (32).

6.2.3.1.2 Coupling solid to beam elements

The objective gusset-less connection is modeled with solid elements, which is required to be coupled to the connecting members, modeled by beam elements. The coupling of the beam to solid elements in the planar direction is addressed in (33). In the planar direction, the bottom chord, modeled with beam elements, are required to be coupled to the connection, modeled with solid elements. However, the initial investigations of the structural responses confirm that the direct coupling of the beam to solid elements at the bottom chord may not sufficiently provide the transformation of the displacements for the nodal DOFs of the weld geometry. Therefore, the direct coupling of the beam to solid elements is avoided for the cross-sections that include the weld geometry at the interface. Alternatively, a part of the bottom cord is modeled with shell element to be coupled to the beam element which is connected to the gusset-less connection. The coupling of the beam to shell elements and shell to solid elements is created in the model, respectively. In

addition, in the out-of-plane direction, the transverse floor beams and skewed floor beams, are modeled with beam elements. Therefore, these members are required to directly be coupled to the solid elements of the gusset-less connection, expressed in Eq. (6.2).

$$F_x u = \sum_{i=1}^{N_{element}} \int_A \sigma_x [N_i] dA \{U_i\} = [B] \{U\}$$

$$F_x u = \sum_{i=1}^{N_{element}} \left\{ \sum_{j=1}^4 \sum_{k=1}^4 \sigma_x(k, j) w_j \cdot w_k |J| [N_i] \{U_i\} \right\} = [B] \{U\} \quad \text{Eq. (6. 2)}$$

6.2.3.1.3 Coupling solid to shell elements

The objective gusset-less connection that is modeled with solid elements, was coupled to the shell elements of the bottom chord members, in the planar direction. The coupling of the shell to solid element is performed using Eq. (6.3).

$$\sum_{i=1}^{N_{element}} t_i \int_0^l \sigma_{x_{sh}} [N_i] dy \{u_i\} =$$

$$\sum_{i=1}^{N_{element}} \left\{ \sum_{j=1}^4 \sum_{k=1}^4 \sigma_{x_S}(k, j) w_j \cdot w_k |J| [N_i] \{U_i\} \right\} = [B] \{U\} \quad \text{Eq. (6. 3)}$$

In addition, the location of the interface between the solid and shell elements must be determined. Due to the possible stress concentration, around the weld geometry, it is recommended to locate the interface in an appropriate distance to the curved welds. The location of the interface can play a dominant role in the number of DOFs. Therefore, in the global model of bridges, the stiffness of the structure can be influenced by the interface location. In this study, the interface location is defined such that the number of DOFs and the computation time can be minimal.

6.2.3.1.4 Coupling of the solid to shell elements of the weld geometry

In the literature, the coupling between different dimensions of elements has been implemented between the two identical cross-sections (30). Solid elements of the weld geometry

require to be coupled to the equivalent shell elements, properly. Therefore, the weld geometry was also modeled, using shell elements at the interface, analogous to the cross-section of the weld, as shown in Figure 6-8. Considering the weld geometry in the shell element can ensure a continuous stress distribution at the welded area. Coupling of the solid elements to the shell elements of the weld geometry is required to provide a uniform stress distribution at the interface. Turlier expressed the details of modeling the weld geometry, using the shell elements (34).

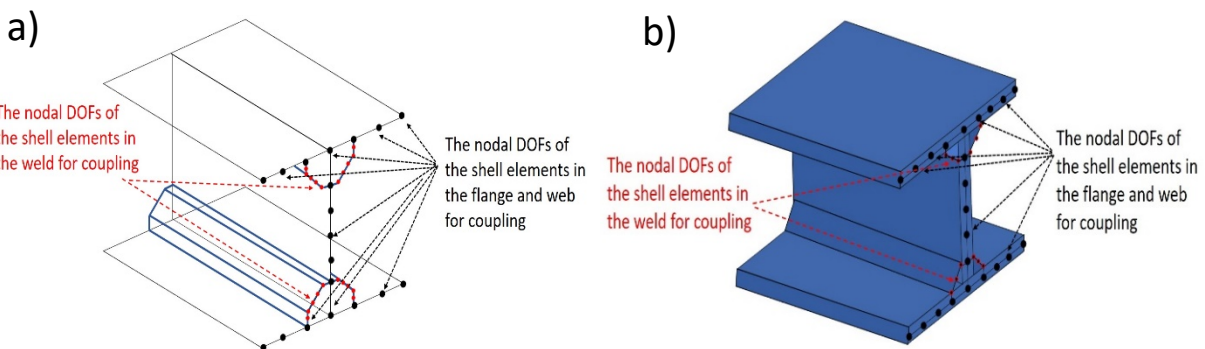


Figure 6-8 Coupling the nodal DOFs in a) shell elements b) solid elements.

The nodal DOFs of the weld geometry should be appropriately coupled to the nodal DOFs of the shell elements at the weld face. As shown in Figure 6-9, the weld is modeled parallel to the perimeter of the weld geometry in the solid element at the shell element part of the interface. The nodal DOFs of the solid elements, located at the perimeter of the weld, are directly coupled to the equivalent nodal DOFs of the shell elements. The nodal DOFs, located within the cross-section of the weld, are also required to be coupled to the nodal DOFs of the shell element. However, the shell element does not include the nodal DOF corresponding to the interior nodal DOFs of the solid element (Figure 6-9). Therefore, the coupling at the interface is performed to the existing nodal DOFs of the shell element. The MPC equations, in Eq. (6.4), are applied at the interface to

transfer the displacements of the weld. The equation is obtained by equating the amount of work performed by the nodal DOFs of the solid elements and nodal DOFs of the shell element.

$$\sum_{i=1}^{N_{element}} \int_0^l \sigma_{x_{sh}} [N_i] dy \{u_i\} = \sum_{n=1}^{N_{element}} \int_0^l \sigma_{x_S} [N_n] dy \{U_n\} +$$

$$\sum_{n=1}^{N_{element}} \left\{ \sum_{j=1}^4 \sum_{k=1}^4 \sigma_{x_S}(k,j) w_j \cdot w_k |J| [N_n] \{U_n\} \right\} = [B] \{U\} \quad \text{Eq. (6.4)}$$

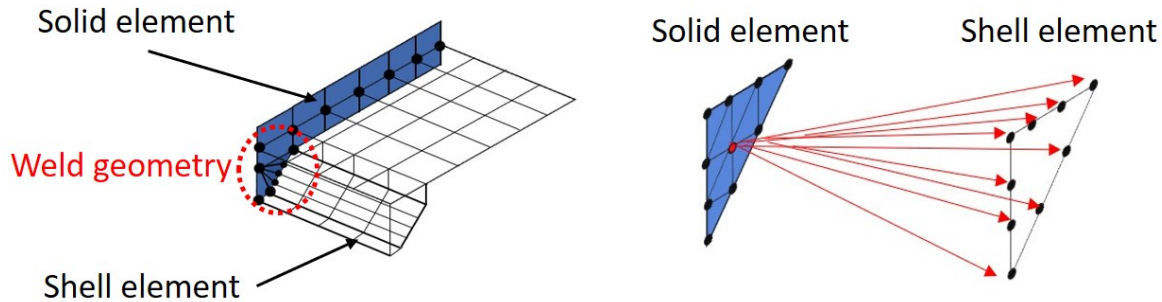


Figure. 6-9 Coupling the DOFs of the weld geometry modeled with the shell and solid elements.

6.2.3.1.5 Mesh configuration

The size and type of elements are determined based on the size and response of the structural components under a specific load. However, identical sizes of elements are applied to similar members. The solid elements, 20-noded hexahedral elements, and 10-noded tetrahedral elements were considered in the model. In accordance to the provisions, addressed in the available literature for the hotspot stress method, the adjacent elements to the curved weld were the 20-noded hexahedral solid elements (35). The mesh size at the weld toe is selected to be as fine as 0.2t for the careful measurement of the hotspot stresses. The remainder of the gusset-less connection was modeled via 10-noded tetrahedral solid elements, varying in size from 0.5t to 1.0t, as illustrated in Figure 6-10. The number of elements of the models is presented in Table 6-2.

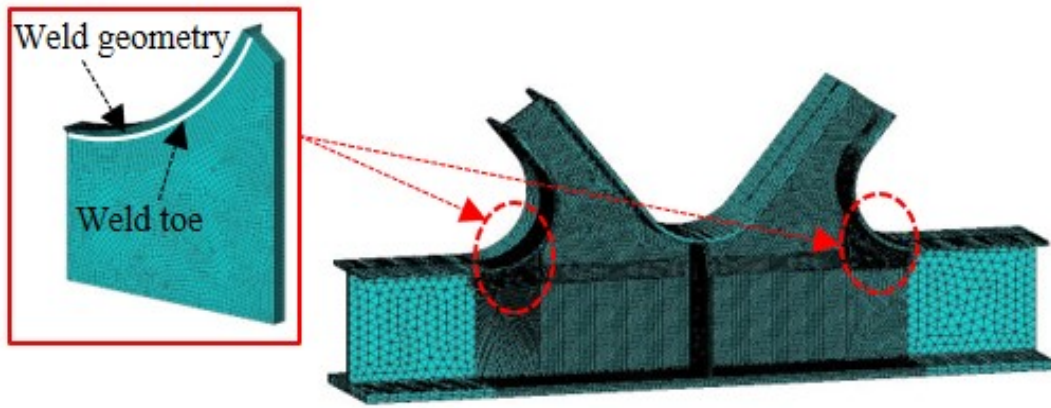


Figure 6-10. Mesh configuration at the solid element part of the M-S model.

Table 6-2 Element properties for the three developed models in LUSAS.

Model properties	SH model	SS model	M-S model
Applied elements	Thick shell element	Solid element	Linear quadrilateral thick shell 3D linear thick beam
Number of elements	297,418	210,726	Shell elements: 158,993 Beam elements: 5160 Solid elements: 88,504,920

6.2.4 Verification of the FE models using the load test results

The set of FE models are validated with respect to the collected structural strain response from the quasi-static and dynamic load tests. The model verification, using the natural modes are addressed in the previous research (32). In this section, the comparison between the numerical strain responses and the field-collected strain responses is conducted for model verification. In Figure 6-11, the comparison is performed between the field-collected strain response and numerical strain responses of the developed models at the identical locations of the bottom

connection. The strain results belong to the second stop of the quasi-static load test (northbound), which are applied for model verification.

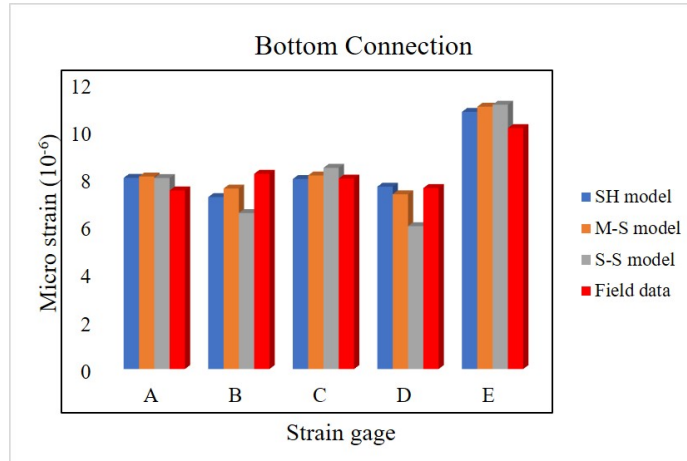


Figure 6-11. Comparison of the numerical response of the FE models with the field data at the second stop of the Loadcase1 (northbound).

The validation of the developed models for further condition assessments is accepted through the agreement between the numerical and field responses. The comparison demonstrates a satisfactory agreement of the M-S model's responses to the field-collected data. The S-S model, however, shows a higher percentage of a difference to the field data, as compared to the two other models. The observed difference can be due to the direct application of the loads to the local S-S model.

In Figure 6-12, the contours of the principal strains at the gusset-less connection are compared to evaluate the proficiency of the developed models in expressing the hotspot stresses at the weld toe (36). In the SH model (Figure 6-12.a), a more uniform stress variation can be observed, as compared to the two other models (Figure 6-12.b and Figure 6-12.c). However, the model has a restricted performance in determining the hotspot location and through-the-thickness stress variations, given that the weld geometry is not included in the SH model. Thus, the SH

model is not considered for fatigue assessment scope of this study. The S-S model, and M-S model that both include the weld geometry, demonstrate a better performance in representing the hotspots strains at the weld toes, shown in Figure 6-12b and Figure 6-12c. The S-S model does include some stress concentration effects, as a result of the out-of-plane bending moment and shear forces, applied to the model. The high-strain concentrated responses, around the curved welds of the S-S model can be misinterpreted as the hotspot stress, and therefore, is not recommended, for fatigue assessment.

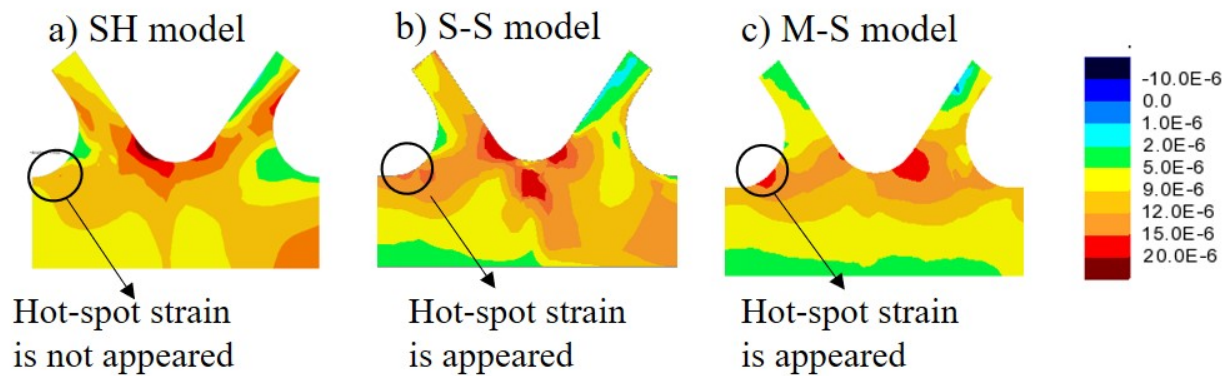


Figure 6-12 Comparing the principal strain contours of a) SH model, b) S-S model and M-S model in LUSAS, at the second stop of the Loadcase1 (northbound).

In addition, the proficiency of the developed M-S model in predicting the hotspot stress locations at the weld toe certifies the applicability of the model for the fatigue assessment goal of the study. In the following sections, the predicted responses from the M-S model are solely used for the fatigue assessment of the objective gusset-less connection.

6.3 Numerical hotspot stresses of the gusset-less connection

The complex geometry of the gusset-less connection and the curved fillet welds may cause the variability of hotspot stresses along the weld toe. In this section, the verified M-S model is

utilized to determine the hotspot stresses along the curved weld toe of the connection. The pseudo-static load test (Loadcase1) is implemented to investigate the variability of the hotspot stresses along the weld toe, and with the distance to the weld, under a unique loading condition. In addition, the dynamic load test (Loadcase2) is applied to study the variability of the hotspot stresses with the change in loading. As shown in Figure 6-13, six paths that are perpendicular to the weld toe, are defined to evaluate the hotspot and nominal stress variations along the weld toe. For each path, the hotspot response at the weld toe is measured through the stresses at the reference points. The nominal stress is also measured in the distance to the weld toe for the selected paths (yellow dots).

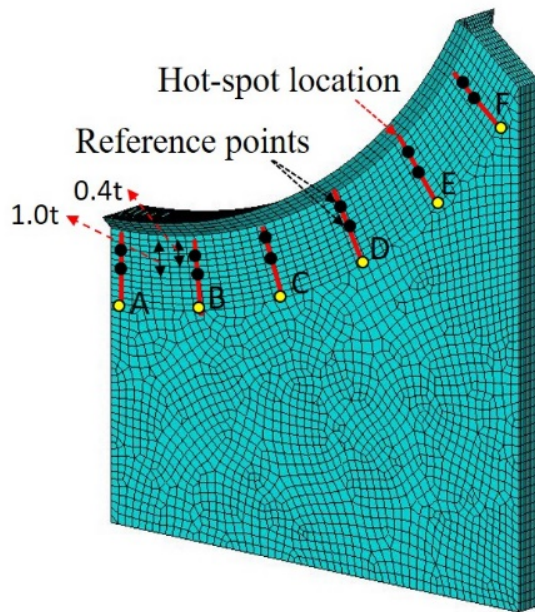


Figure 6-13. The selected paths to measure the hotspot and nominal stresses along the weld toe.

6.3.1 Variation of the hotspot stresses under static loads

In this section, the static loads are the second stop of the quasi-static load test, at the northbound and southbound lanes of the bridge (shown in Figure. 6-4.). In Figure 6-14, the trend of principal strain responses with the circumferential distance to the weld toe is displayed for the

six defined paths. It is demonstrated that the strain dissipation trend has a variable property, which depends on the position of the path along the weld toe. For each path, identical trends of the strain responses are illustrated for the two loading conditions. More loading conditions are required to clarify the geometry impacts on the resulting hotspot and nominal responses.

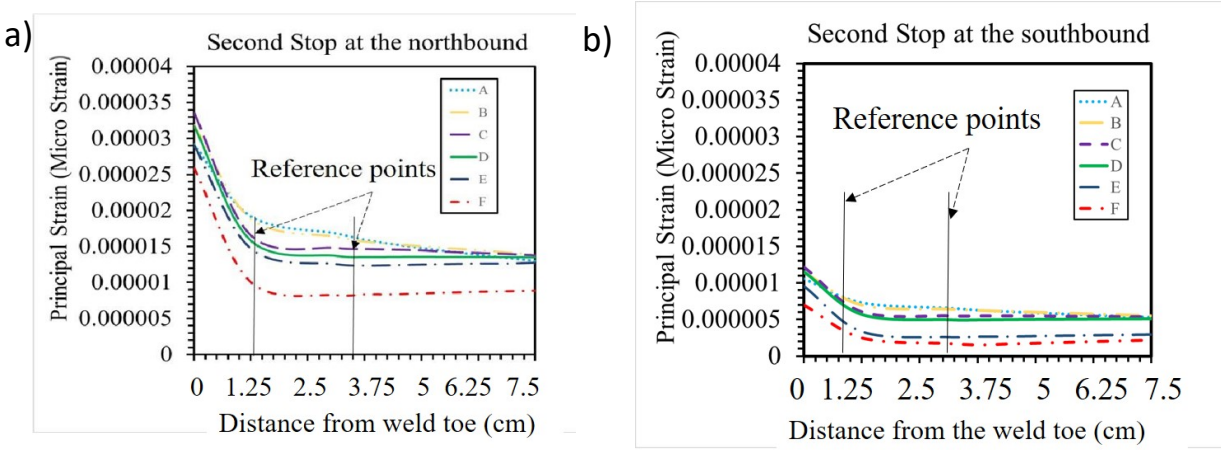


Figure 6-14. Variation of the numerical principal strain response with the distance to the weld toe for the six selected paths under the static truck load at a) a northbound b) a southbound.

6.3.2 Variation of the hotspot stresses under dynamic loads

6.3.2.1 Simulating the dynamic traffic loads using the M-S model

In this section, Loadcase2 is applied to verify the numerical time-history responses of the M-S model. In Figure 6-15, the numerical strain time-history response is compared to the field strain response of the located strain rosette at the bottom connection (SG5-A). It is illustrated that the numerical response of the M-S model can appropriately predict the peaks, resulting in a compatible stress range to the field-collected response. The observed difference can be due to the vehicle-deck interaction that the M-S model does not consider. However, the observed difference in the time-history responses may cause a negligible effect on the stress ranges, which are applied in the fatigue assessment procedure.

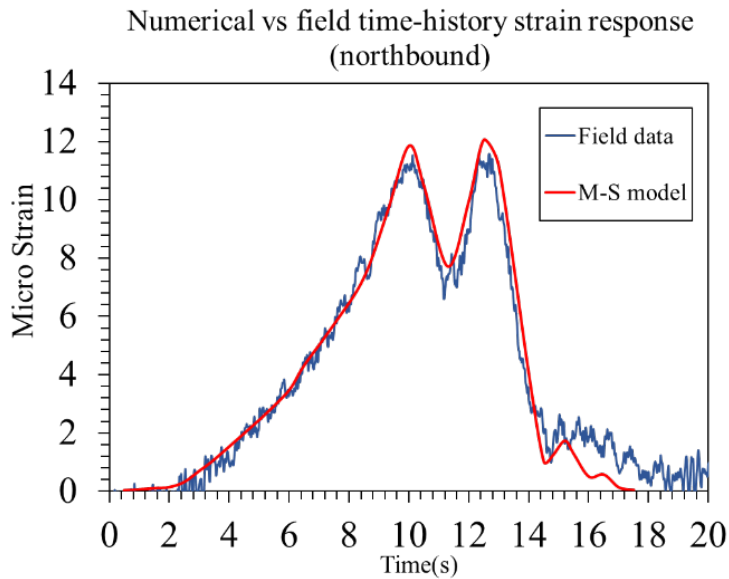


Figure 6-15. Comparing the field collected strain response and the numerical time-history response of model in LUSAS, under the dynamic truck load, Loadcase2.

6.3.2.2 Hotspot strain time-history responses using the M-S model

In this section, the M-S model is applied to study the trend of the hotspot strain variations along the weld toe under the dynamic load. The dynamic load test, Loadcase2, is considered as the dynamic load. The hotspot and nominal strain time-history results of the investigating paths for the northbound and southbound truckload, are shown in Figure 6-16. The numerical time history responses of the hotspot and nominal strain for the six selected paths under the dynamic truck load at the northbound (a and b), southbound (c and d).

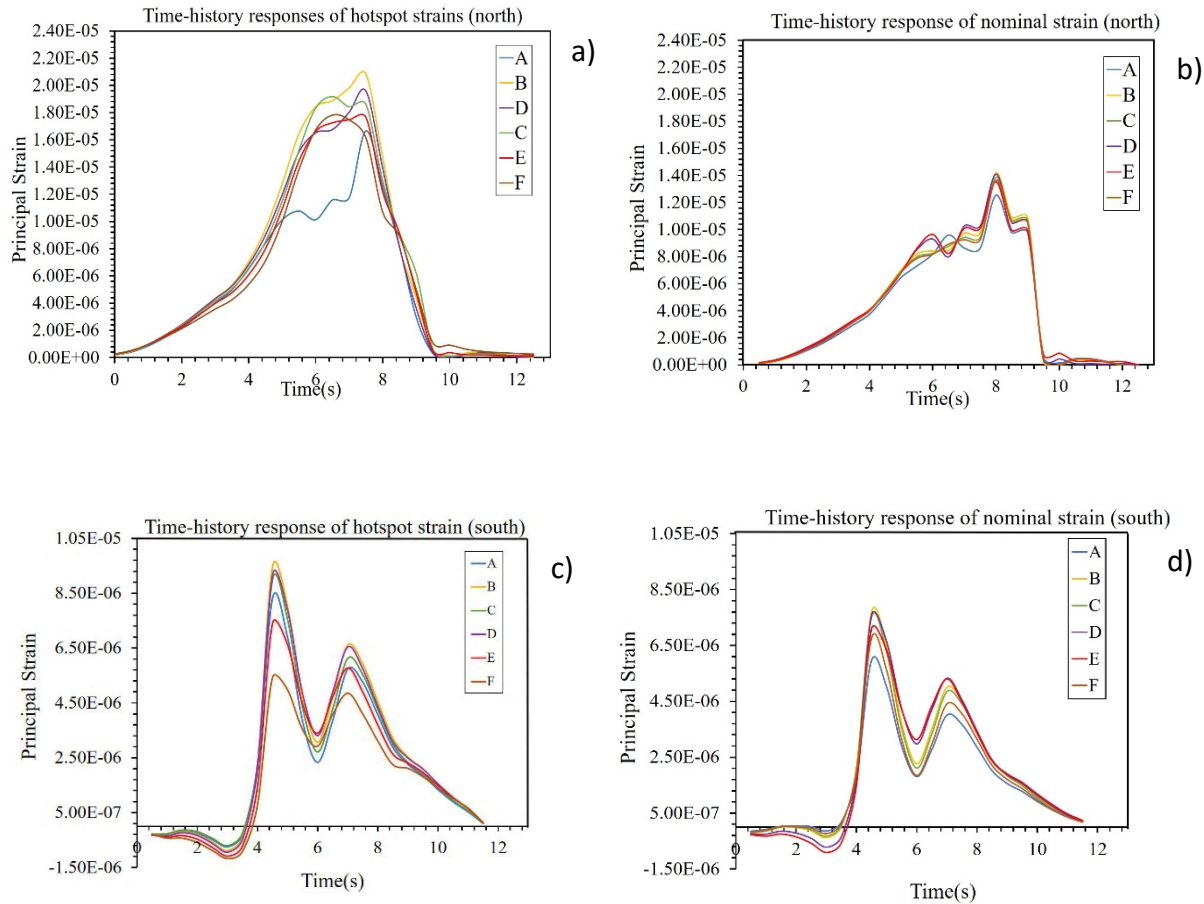


Figure 6-16 The numerical time history responses of the hotspot and nominal strain for the six selected paths under the dynamic truck load at the northbound (a and b), southbound (c and d).

It can be demonstrated that the change in the loading condition, may not impact the location of the maximum hotspot strain stress at the weld toe. In addition, in each loading, the time-history responses of the six investigating paths follow a similar trend. However, the trend of the measured hotspot and nominal time-history responses are not identical. Consequently, using an efficient global FE model may provide more realistic hotspot stresses, which can be applied for fatigue assessment.

6.4 Fatigue assessment using nominal and hotspot stresses

6.4.1 The traffic scenarios defined through the M-S model

Due to the computational costs, it is feasible to consider a few simplified traffic scenarios, if they are carefully selected. Complex traffic scenarios, including multiple vehicles, shall be decomposed into simple traffic scenarios, which generate a single stress cycle. In this section, some traffic scenarios, which were observed through the video camera records, are applied as a demonstration. Using Loadcase3, it is concluded that the complex traffic scenarios include a massive truck as well as multiple lightweight vehicles. Such complex traffic scenarios can be conveniently simulated in the model via a single truck.

There are also traffic scenarios that induce a negligible stress response at the connection and, can be conveniently removed from the simulation. In addition, the less frequent stress ranges (below 1% of the traffic volume) can be excluded from the simulation. NHDOT has provided the information about the traffic volume and proportion of different classes of vehicles at the Memorial Bridge. It is observed that the overloaded trucks (causing a significant strain response), are rarely reported in the current traffic program of the bridge. Therefore, using the field collected data, an infinite fatigue life is obtained according to the AASHTO stipulations for determining fatigue remaining life (13).

In this section, using the validated M-S model, a total of eight traffic scenarios are defined for simulation, expressed in Table 6-3. The traffic scenarios are implemented in the northbound (NB), southbound (SB), and both lanes (NS). The traffic scenarios 1-3 include the load test dump truck. The traffic scenarios 4-8, consist of the load test truck with the increased weight (36.5 ton) and number of trucks. The latter scenarios are defined to demonstrate the variability of the stress

responses along the weld toe under the possible heavy traffic conditions. The nominal and hotspot stress results of the defined scenarios are utilized for fatigue assessment.

6.4.2 Predicted fatigue remaining Life

In Table 6-3, the defined eight traffic scenarios are implemented in the M-S model. For each scenario, the nominal and hotspot stresses are measured, and the resulting remaining fatigue life is calculated at the maximum location along the weld toe (Path B).

Table 6-3.The nominal and hotspot stress and measured fatigue responses of simulated traffic scenarios.

Traffic scenarios (#trucks North, #truck South)	Nominal stress range (MPa)	Hotspot stress range (MPa)	Nominal fatigue damage index (10^{-4})	Hotspot fatigue damage index (10^{-4})
1 (1, NB)	8.27	10.55	0.06	0.32
2 (1, SB)	6.02	8.81	0.02	0.19
3 (1, NS)	12.41	20.84	0.19	2.47
4 (2, NB)	25.52	34.68	1.66	11.38
5 (2, SB)	19.74	26.98	0.77	5.36
6 (1NB,2 SB)	33.85	46.19	3.88	26.88
7 (2 NB,1 SB)	39.53	54.13	6.18	43.26
8 (2, NS)	45.91	63.22	9.68	68.91

It is observed that in the low-stress ranges, the difference between the nominal and hotspot stress ranges are less significant. In the traffic scenario 8, where the maximum stress responses are increased, a substantial difference can be observed between the nominal stress and hotspot stress responses. Therefore, the influence of the fillet weld geometry on the resulting hotspot and nominal strain responses is demonstrated.

In addition, using the traffic scenario 8, the hotspot and nominal stress ranges, and the measured fatigue lives are computed for the six-investigating paths along the weld toe, as expressed in Table 6-4. A minor difference is illustrated between the nominal remaining life results along the weld toe, as compared to the hotspot stress remaining lives. In higher hotspot stress ranges, a minor difference between the stress responses along the weld toe can cause a significant difference in the remaining life of the component. Therefore, for the fatigue assessment of complex structural component, it is recommended to determine the maximum hotspot stress at the weld toe. In addition, the ratio of the hotspot stress to the nominal stress may not be identical for different paths, along the weld toe. Thus, it is recommended to exclusively determine the stress concentration factor for the target path while using the field-collected nominal stress data. The obtained results emphasize the efficacy of the M-S model in predicting the hotspot stresses at the key structural elements of steel bridges.

Table 6-4. Stress range and fatigue remaining life response at the six selected paths under the traffic scenario 8

Path	Nominal Stress (MPa)	Hotspot Stress (MPa)	Nominal fatigue damage index (10^{-4})	Hotspot fatigue damage index (10^{-4})
A	36.76	53.50	4.97	41.76
B	45.91	63.22	9.68	68.91
C	45.71	62.05	9.55	65.16
D	45.68	60.81	9.53	61.33
E	42.54	57.50	7.70	51.85
F	39.01	56.60	5.94	49.45

6.5 Conclusion and Recommended Future Work

In this paper, an efficient methodology was proposed to study the fatigue performance of complex welded components of steel bridges, using the hotspot stress method. An M-S global model of the Memorial Bridge was created and validated with field data. The novel gusset-less connection in the Memorial Bridge was selected as the case-study for fatigue performance assessment. The validated FE model is utilized to obtain the hotspot stress ranges under some simulated traffic loads. The main conclusions withdrawn from the current work can be summarized as follows:

- Application of the proposed global M-S model facilitates the study of the influence of the geometry of the component and the loading conditions on the induced hotspot stress ranges at the complex welded structural components.
- In the complex welded component, the hotspot stresses vary along the weld toe, while less variability is observed in the nominal stresses. A well-developed FE model can precisely clarify the amplitude and location of maximum hotspot stress along the weld toe. In addition, the model determines the difference between the amplitude of the hotspot stress and the nominal stresses. The resulting numerical stresses are practical to evaluate the fatigue status of the objective component, based on the maximum hotspot stress at the weld toe.
- In addition, the application of the comprehensive model can be an efficient tool in designing a practical instrumentation plan for novel complex structural components. The data acquisition system can be installed in the critical paths to achieve the maximum hotspot and nominal stresses along the weld toe.

- More sophisticated models and assessment tools are warranted for performance prediction by simulating the traffic scenarios, experienced by the bridge. The global M-S model can illustrate the hotspot stresses under the simulated traffic conditions. Moreover, the rarely experienced traffic scenarios can be simulated, to evaluate the structural responses under the unexpected conditions, which may occur during the designated service life of the bridge.

Advanced modeling technology exists to predict the structural performance of bridges. In this study, hotspot stress methodology was applied to for a healthy bridge to predict the remaining fatigue life under an extreme traffic excitation and pattern. The M-S model presented can be modified to mimic the structural discontinuities of bridges, such as imperfections in the weld or the fatigue cracks in the global model, which is suggested for future studies. The fatigue responses of this study can be implemented in the maintenance and replacement programming of bridges.

Acknowledgment

This material is based upon work partially supported by the National Science Foundation under Grant No. 1430260, FHWA AID: DEMO Program and funding from the NHDOT Research Advisory Council. Any opinions, findings, and conclusions or recommendations expressed in this material are those of the author(s) and do not necessarily reflect the views of the National Science Foundation. The research team is also grateful to HNTB Corporation, in particular Ted Zoli and Christopher Engel, for sharing design information on the Memorial Bridge.

References

- 1) Dong, P. 2001,"A structural stress definition and numerical implementation for fatigue analysis of welded joints". *International Journal of Fatigue*;23(10): 865-876.
- 2) Niemi, E., Fricke,W., Maddox, S.J. 2006,"Fatigue analysis of welded components: Designer's guide to the structural hot-spot stress approach". Cambridge, UK.: Woodhead Publishing,.
- 3) Li., Z.X. Zhoua., T.Q. Chan, T.H.T, Yu. Y. 2007, "Multi-scale numerical analysis on dynamic response and local damage in long-span bridges" *Engineering Structures*;29: 1507-1524.
- 4) Ni, Y.Q., Ye, X. W., Ko, J. M. 2012, "Monitoring-Based Fatigue Reliability Assessment of Steel Bridges: Analytical Model and Application" *Journal of Structural Engineering*;110 (12): 1563-1573.
- 5) Chen Z.W., Xia,Y.L., Xia, Y., Li ,Q., Wong., K.Y. 2011, "Fatigue analysis of long-span suspension bridges under multiple loading:Case study" *Engineering Structures*;33: 3246-3256.
- 6) Chiewanichakorn, M., Aref, a.J., & Alampali, S. 2007, "Dynamic and fatigue response of a truss bridge with fiber reinforced polymer deck" *International Journal of Fatigue*;29: 1475-1489.
- 7) de Jong, F.B.P. 2007, "Renovation techniques for fatigue cracked orthotropic steel bridge decks" Edited by Delft University of Technology. TU Delft,.
- 8) Fu, Z., Wang, Y. Ji, B. & Liu, T. 2018, "Assessment approach for multiaxial fatigue damage of deck and U-rib weld in steel bridge decks" *Construction and Building Materials*; 20: 276-285.
- 9) Yan, F. Chen, W., Lin, Z. 2016, "Prediction of fatigue life of welded details in cable-stayed orthotropic steel deck bridges" *Engineering Structures*;127: 344-358.
- 10) Alencar, G., M.P.de Jesus,. A., A.B.Calçada, R., Guilherme S. daSilva, J. 2018, "Fatigue life evaluation of a composite steel-concrete roadway bridge through the hot-spot stress method considering progressive pavement deterioration" *Engineering Structures*;166(1): 46-61.
- 11) Kużawa, M., Kamiński, T., Bień, J. 2018, "Fatigue assessment procedure for old riveted road bridges". *Archives of Civil and Mechanical Engineering*; 18(4): 1259-1274.
- 12) Chen, B., Li,X., Xie,X., Zhong,Z., & Lu., P. 2015, "Fatigue Performance Assessment of Composite Arch Bridge Suspenders Based on Actual Vehicle Loads" *Shock and Vibration*, 2015: 1-13.
- 13) AASHTO. 2012, LRFD bridge design specifications. 5. Washington, DC,.
- 14) Hobbacher, A. 2013, IIW Recommendations for fatigue design of welded joints and components. IIW Doc. XIII-2460-13.
- 15) Niemi, E. 1995, Stress determination for fatigue analyses of welded components. Cambridge: Abington Publishing.
- 16) Fricke, W., Kahl, A. 2005, "Comparison of different structural stress approaches for fatigue assessment of welded ship structures" *Marine Structures*;18 (7-8): 473-488.
- 17) De Back, J. The design aspects and fatigue behaviour of tubular. 1987, *Proceedings of the Third International ECSC Offshore Conference on Steel in Marine Structures*. Amsterdam: Noordhoek C, de Back J, editors.;. 205-240.
- 18) Fricke, W. 2001, "Recommended hot spot analysis procedure for structural details of FPSO's and ships based on round-robin FE analyses" *International Journal of Polar Engineering*;12(1): 1-8.
- 19) Maddox, S.L. 2002, "Hot-spot stress design curves for fatigue assessment of welded structures" *International Journal of Polar Structures*;12(2): 134-141.
- 20) Lotsberg, I. 2004, Recommended methodology for analysis of structural stress for fatigue assessment of plated structures. Houston, USA: *Proceedings of OMAE specialty symposium on integrity of FPSO system*.
- 21) Doerk, O., Fricke,W., Weissenborn, C. 2003, "Comparison of different calculation methods for structural stresses at welded joints", *International Journal of Fatigue*;25(5): 359-369.

- 22) Radaj, D., Sonsino, C.M., Fricke, W. 2006, Fatigue assessment of welded joints by local approaches. 2nd. Cambridge: Woodhead Publishing and Boca Raton Fl.
- 23) Connolly, M. P., Helier, A. K., and Sutomo, J. 1990, A parametric study of the ratio of bending to membrane stress in tubular Y- and T-joints. *International Journal of Fatigue*;12(1): 3-11.
- 24) Dong, P. and Hong, J. K. A., 2002, Structural Stress Based Master S-N Curve, 55th International Institute of Welding (IIW). Doc. XIII-1930-02/XV-1119-02, Copenhagen, Denmark: IIW.
- 25) Dong, P., Hong, J. K., and Cao, Z. 2003, Stress and Stress Intensities at Notches: Anomalous Short Crack Growth. *Intenrational Journal of Fatigue*;25: 811-825.
- 26) Dong, P. 2005, A Robust Structural Stress Method for Fatigue Analysis of Offshore/Marine Structures. *Journal of Offshore Mechanics and Arctic Engineering* (ASME);127: 68-74.
- 27) Adams, T., Mashayekhizadeh, M., Santini-Bell, E., Wosnik, M., Baldwin, K., Fu, T. 2017, Structural Response Monitoring of a Vertical Lift Truss Bridge. 96th Annual Meeting Compendium of Papers ,*Transportation Research Board*. Washington D.C.
- 28) Mashayekhizadeh, M., Santini-Bell, E. and Adams, T. 2017, "Instrumentation and Structural Health Monitoring of a Vertical Lift Bridge". Jacksonville, Fl: *Processings of 27th ASNT Research Symposium*.
- 29) Mashayekhizadeh, M., Mehrkash,M., Shahsavari, V., Santini-Bell, E. 2018, "Multi-Scale Finite Element Model Development for Long-Term" . Fort Worth, TX: Structure Congress, ASCE.
- 30) McCune, R.W. Mixed Dimentional Coupling and Error Estimation in Finite Element Stress Analysis. Belfest,UK: PHD Thesis, Queen's University, 1998.
- 31) Shim, K.W., Monaghan, D.J. and Armstrong, C.G. 2002, "Mixed Dimentional Coupling in Finite Stress Analysis" *Engineering with Computers*;18(3): 241-252.
- 32) Mashayekhi, M., Santini-Bell, E. 2018, "Three-dimensional multiscale finite element models for in-service performance assessment of bridges" Computer-aided civil and infrastructure engineering;34(5):385-401.
- 33) Monaghan, D.J., Doherty, I.W., McCourt, D. and Armstrong, C.G. 1998, Coupling 1D beams to 3D bodies. *Proceedings of the 7th International Meshing Roundtable*, Sandia National Laboratories, Dearborn, MI, ;285–293.
- 34) Turlier, D., Facchinetti, M.L., Wolf, S., Raoult, I., Delattre, B., Magnin, A. and Grimonprez, N. 2018, Seam weld shell element model for thin walled structure FE fatigue design. 12th International Fatigue Congress (FATIGUE 2018). MATEC Web of Conferences.
- 35) Dong P, Hong JK, Cao Z. 2001, A mesh-insensitivity structural stress procedure for fatigue evaluation of welded structures. IIW doc.XIII-1902-01/XV-1089-01. International Institute of Welding.
- 36) Mashayekhi, M, Santini-Bell. 2019, Fatigue assessment of the gusset-less connection using field data and numerical model. *Bridge Structures*,15(1-2):75-86.

Chapter 7

7 FATIGUE CRACK PREDICTION IN COMPLEX WELDED COMPONENTS OF IN-SERVICE STEEL BRIDGES USING STRUCTURAL HEALTH MONITORING DATA AND NEURAL NETWORK METHOD

*In preparation

7.1 Abstract

Fatigue crack detection in complex welded structural components of steel bridges can be a complicated task due to the less-known performance of the component. This study aims to predict the fatigue crack occurrence via a Neural Network model, which is trained with the fatigue responses of an objective structural component. The fatigue responses are measured through the field-collected data over a discrete period of data collection for the structural component. The proposed neural network model is used for a case-study vertical lift truss bridge, the Memorial Bridge, located in Portsmouth, NH. A 12-month of data collection period, from the long term SHM program of the bridge, is used to investigate variability of the traffic pattern and impact on the correlation between the measured fatigue responses at the instrumented areas of the component. Through a validated global finite element model of the bridge, multiple physical damage cases are simulated to compute the damage-induced stresses variations at the unhealthy condition of the component. The healthy and damaged induced fatigue responses are data input the NN model to predict a fatigue crack through the changes that occurred in the correlation between the fatigue

responses at different instrumented locations. It is demonstrated an efficient mathematical model can predict a possible fatigue crack when the long-term collected data are carefully post-processed to input the model.

7.2 Introduction

Structural health monitoring (SHM) program of civil infrastructure play a significant role in mitigating the unexpected structural failures through providing continuous health status reports (1). Long-term SHM programs can also provide the information needed during the service life of steel bridges to continuously estimate the fatigue strength of fatigue prone critical components of steel structures (2) (3). One of the significant elements in condition evaluation system of steel bridges is fatigue health assessment of welded components. An estimated lifetime of finite fatigue due to an initiated crack reported to the bridge manager may help in the early stages of seizing cracks.

Given the induced fatigue cracks at welded areas, the crack detection task depends on the changes in crack-induced stress range, reported at the cracked area of the component. SHM programs frequently report nominal stresses in the distance to the welded area, which might not be effective in estimating crack-induced fatigue life. The emerged fatigue cracks might not considerably influence the trend of collected responses due to the insufficient instrumented sensors. Therefore, additional information shall be provided to determine the crack-induced changes in structural responses of the investigating component. A database can be created to determine the significant characteristics of the structural responses through a careful signal-processing of the collected SHM data. The database will provide sufficient information to obtain a unique pattern, which is signature to the structural elements. The pattern can be continuously

upgraded to track the damage-induced changes in the structural component during the service life of the component.

In the available studies, damage detection in long-span bridges is frequently executed by focusing on the global response of the bridges, using vibration responses from field data or numerical models (4) (5) (6). However, strain responses of strain gages are less applied, as they locally report the responses at the instrumented areas of structural components (7). Phares et al. applied the strain response for damage detection of steel bridge to developing the relationship between near the fault strain response to the global behavior of the bridge (8). Reiff et al. applied the strain data to establish a bridge signature for damage detection, using the girder distribution factors (GDFs) (9). Hong et al. developed a long-gauge strain-based damage assessment method to detect damage in bridges under moving vehicular loads. The method verified using an indoor experiment and an on-site real bridge test (10). Weinstein et al., applied the strain responses of a bridge to training a Neural Network (NN) for damage detection (11). Chen et al. recently applied the long-gauge fiber Bragg grating to identify the damage location, using numerical responses of a finite element model of a long-span bridge (12). Neves et al. developed a model-free NN model using vibration responses for damage detection of a railway bridge (13).

In this study, a protocol is proposed to inform fatigue cracks in welded complex structural components of steel bridges, using long-term SHM data. The SHM data is being used to calculate fatigue responses at the instrumented locations of a welded component. The correlation between measured fatigue responses is being predicted, using mathematical methods to demonstrate the healthy conditions of the structure. In addition, SHM data is integrated with numerical responses of a validated FE model to train an NN model and obtain a well-detailed crack detection pattern. A crack shall be predicted when the correlations of the fatigue responses are corrupted.

The protocol is implemented to a case-study bridge, the Memorial Bridge in Portsmouth, NH, that has a long-term SHM program via permanently installed sensors. The bridge also includes a complex structural component, the gusset-less connection, which is selected for the fatigue crack detection goal of this study. Besides SHM data, the FE model of the bridge is calibrated to acquire knowledge about the crack-induced structural responses of the component. Multiple fatigue cracks varying in size and location, are simulated through the FE model. Stepwise crack propagation is also implemented to the FE model to determine the minimum size of the crack, which can be detected via the proposed NN model. It is demonstrated that the proposed NN model can efficiently report the presence of fatigue cracks via the collected strain responses.

7.2 Proposed fatigue crack detection protocol

In this section, the proposed fatigue crack detection protocol is briefly explained (shown in Figure 7-1). A stepwise procedure of the protocol is as follows:

1. Determine a period of data collection to measure fatigue responses, which includes adequate cycles of recorded stress ranges.
2. Using the recorded stress cycles, compute fatigue damage responses for each selecting period.
3. Predict the correlation between the measured fatigue responses of the sensors,
4. Implement the obtained relationship in Step 3 to validate the FE model.
5. Simulate fatigue crack samples via the validated FE model to obtain sufficient crack-induced structural responses and the associated fatigue responses.
6. Input the healthy and crack-induced fatigue responses to train an NN model for crack prediction.

7. Evaluate the accuracy of the developed network.

A one-year data interval is utilized in this study to identify the major sources of variations, which may impact the pattern of the measured fatigue responses.

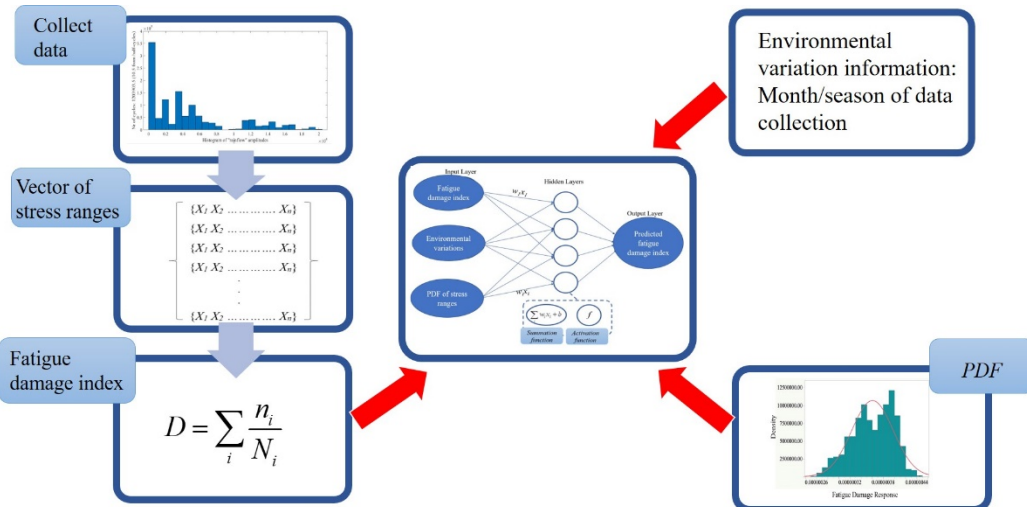


Figure 7-1 The procedure to develop a NN model for fatigue crack detection

7.3 Methodology

7.3.1 Using long-term SHM data for fatigue assessment

To compute the fatigue strength of a structural component, the resulting stress cycles at the component must be applied. Due to changes in bridge's traffic loads, the induced stress ranges at the structural components of bridges have a variable property. Application of SHM data for fatigue assessment, benefits from considering the variable range of amplitude stress in fatigue responses. The time-history strain responses of strain gages are frequently applied for fatigue assessment. As the linear elastic relationship is valid, the collected strain responses are converted into stress responses. Furthermore, the cycles of stress ranges are extracted from the time-history stress responses, using the Rainflow cycle algorithm (14).

It is recommended to use the Miner's rule to compute the fatigue responses through the variable amplitude of stress range stress. Miner's rule superposes the cycles of variable stress ranges to compute the fatigue damage index (15). Fatigue damage index expressed in Eq (7.1), is a ratio, varying from 0 to 1 that reflects the fatigue damage level of the investigating component.

$$D = \sum_i \frac{n_i}{N} \quad \text{Eq. (7.1)}$$

where N denotes the number of collected stress cycles and N represents the number of remaining cycles to failure. N can be determined through the appropriate S-N curves for an investigating component, recommended by AASHTO (16).

7.3.1.1 Data collection period for fatigue assessment

The fatigue strength of in-service bridge's structural components can be estimated over discrete periods of data collection, using the long-term SHM data. An exclusive data collection period helps to study the trend of the measured fatigue damage index in a long-term service life of a bridge. The period is required to include the frequent stress ranges, experienced by the structural components of the bridge. The choice of the optimum data collection interval depends on the traffic pattern, as well as the structure's performance. The fatigue damage index may also have a variable trend due to the seasonal impacts, when the traffic pattern of the bridge is considerably associated with the seasonal variations. In addition, before computing the fatigue damage index, the existing outlier due to the random noise or malfunction of the sensor must be removed from the collected SHM data.

7.3.2 Using numerical data for fatigue assessment

Fatigue assessment of welded structural components using SHM data is restricted to the instrumented locations of the structural component. Welded structural component, prone to fatigue cracks are often less accessible areas for instrumentation. Consequently, the crack-induced stress concentration may not be detected through the fatigue damage index, measured which is measured through the long-term SHM data. Alternatively, it is possible to implement a model-based fatigue assessment method to obtain the numerical stress responses at the desired locations through a validated FE model. A validated FE model can mirror the structural responses of the objective component, if the model is appropriately created and calibrated corresponding to the field's responses. The models also required to consider any inspection results concerning the structural defects. To compute the fatigue damage index, the required stress cycles can be counted for the equivalent stress ranges, through the SHM data.

The model-based fatigue assessment method also benefits from anticipating the remaining fatigue life and structural performance of the component, due to an induced fatigue crack, when a fatigue crack is simulated to the model. The crack propagation leading to fracture of a concerning component, and the structural responses variations are other advantages of model-based fatigue assessment method. However, if the bridge does not include any detected damage, using the cycle counts of the bridge for the crack-induced stress ranges is required to be implemented with caution. In addition, it is necessary to calculate the remaining cycles to failure, if the simulated fatigue cracks cause higher stress ranges than the experienced stresses at the bridge. The location and type of the crack is also required to be selected based on the structural analysis results.

7.3.3 The Neural Network Method

Neural Network (NN) is a mathematical tool to predict the behavior of a system, through a learning algorithm of the connections between the neurons. The connection is provided by weight functions, which include the required information to solve the problem. The weights are then defined and allocated to the connections through a training process. A typical NN model consists of input, output and hidden layers, developing a multi-layer neural network. A Multilayer Perceptron (MLP) is a back-propagation algorithm, that trains the networks to correspond the nodes of the input layer to the output layer (17). In addition to the training process, estimating the error is required to evaluate the accuracy of the output (validation and test). During the training process, the MLP network modifies the weight and biases, resulting in a new output, through multiple attempts until the optimal responses (minimized error) are achieved. In Figure 7-2, the schematic architecture for MLP network is shown. The error of the NN model is frequently measured, using the root mean square error (RMSE) or epoch value (18).

MLP models are extensively applied for damage detection purposes in conditional assessment of structural components. Long-term SHM data have the advantage of providing sufficient samples of the structural responses to train MLP model for predicting the structural condition goals. For damage detection purposes, however, samples of healthy and damaged structural components are necessary to input the network. Therefore, the trained model can accurately differentiate the healthy versus damage induced responses, when the features of each conditions are precisely extracted.

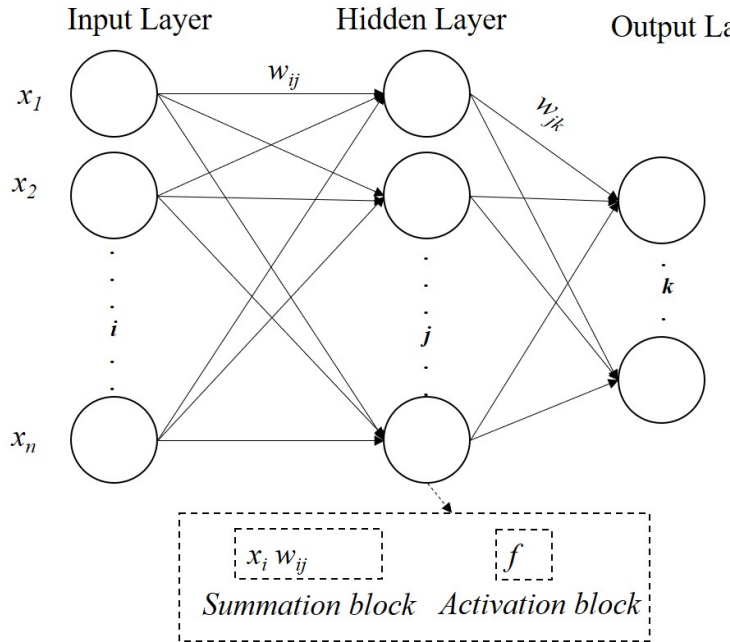


Figure 7-2 Schematic Multi-layer Perceptron Neural Network Architecture

7.4 The case study, the Memorial Bridge

7.4.1 Details, design and construction

The case study in this research is the recently reconstructed Memorial Bridge, a steel vertical-lift truss bridge in Portsmouth, NH, that connects two states of NH and ME shown in Figure 7-3(a) (19). The bridge which was inaugurated in August 2013. The bridge includes a novel gusset-less connection which has a specific complex web geometry and cold-formed bent flanges shown in Figure 7-3 (b). The bent flanges are connected to the web through a curved fillet weld, which make the connection a suitable example for the scope of this study (20).

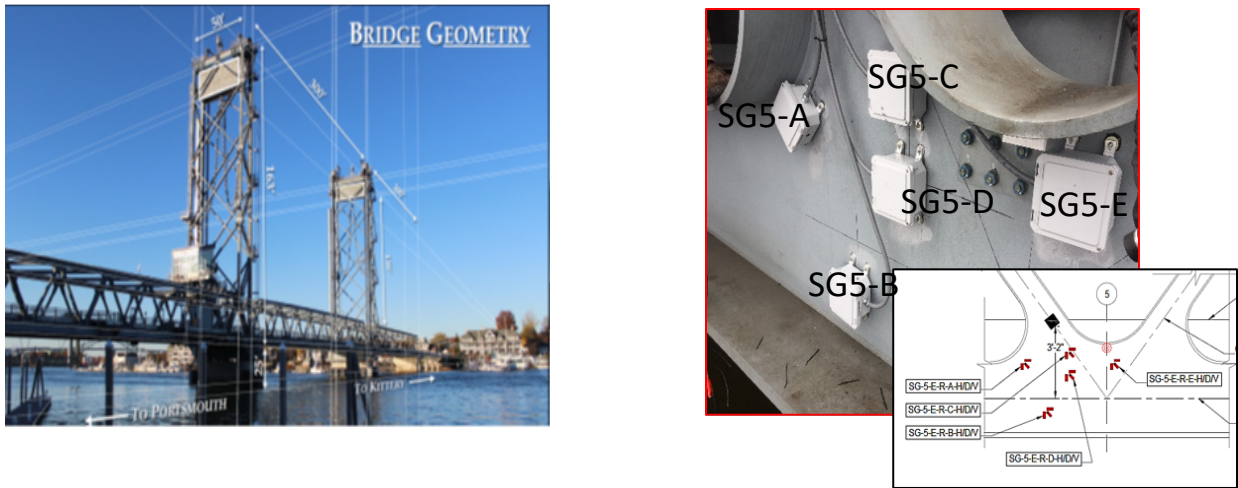


Figure 7-3 (a) The Memorial Bridge, Portsmouth, NH, (b) The gusset-less connection of the Memorial Bridge

7.4.2 Long-term SHM program of the bridge

A long-term SHM program was designed and has been started to operate since March 2017 to provide a continuous real-time data at the critical locations of the bridge. The sensors are instrumented at the south span and south tower of the bridge. This SHM instrumentation plan includes 16 strain rosettes, 2 uni-axial strain gages, 12 uni-axial accelerometers, 4 tiltmeters installed at multiple locations of the bridge to provide 24/7 data (21).

Fatigue assessment of the gusset-less connection is one of the essential tasks in the maintenance programs of the bridge because of the complex performance of the gusset-less connection. An array of five strain rosettes is installed at multiple locations of the top chord and bottom chord gusset-less connection bridge to precisely understand the local performance of the connection (Shown in Figure 7-3b). The current inspection results did not report any detected damage. Therefore, no information is available about the damage-induced stress responses. The less-experienced strain distribution and fatigue performance of the gusset-less connection motivates the proposed protocol be applied for this component.

7.5 Fatigue assessment of the case study bridge

7.5.1 Define a unique period of data collection

In this section, the SHM data of the five installed strain rosettes at the bottom connection are implemented to measure the fatigue damage index. Based on the performance of the gusset-less connection and the designer's assumption, fatigue category B is implemented to the nominal collected strain responses. By postprocessing the recorded time-history responses of the strain rosettes, the stress ranges and associated cycles are obtained, via Rainflow cycle algorithm. Using the stress range/cycles of a period of data collection, fatigue damage index is exclusively measured for each strain rosettes.

Consistent intervals must be chosen to investigate the pattern of fatigue damage index during the service life of bridges. For each period, the stress ranges are applied to estimate the fatigue damage index. In this section, an exclusive duration is defined to compare the fatigue responses of different periods based on the recorded cycles. The duration of period is defined based on the cycles of high-amplitude strain ranges (above 20 micro strain). The higher amplitude strain ranges are frequently induced under the heavy truck passages. Therefore, the duration of periods is specified as the truck events.

In Figure 7-4, the trend of fatigue damage index with incremental truck events is depicted for four different periods. Four periods were started in the four different seasons of a year. As the number of truck events reaches to a specific level, the sufficiency point, each graph's trend begins to plateau. It is also illustrated that the sufficiency points for the selected periods may not be identical. However, a period of about 600 truck events, seems to be a reasonable interval to be selected as the exclusive period of data collection.

In this study, the one-year data collection period consisting of 600 truck events is divided into multiple periods. For each period the fatigue damage index is calculated. As a consequence, the resulting responses, each having equal cycles counts, become only dependent on the amplitude of collected stress ranges (22). The resulting fatigue responses also reflect the changes in the stress responses due to the traffic pattern changes, seasonal impacts, ambient noise, and measurement errors.

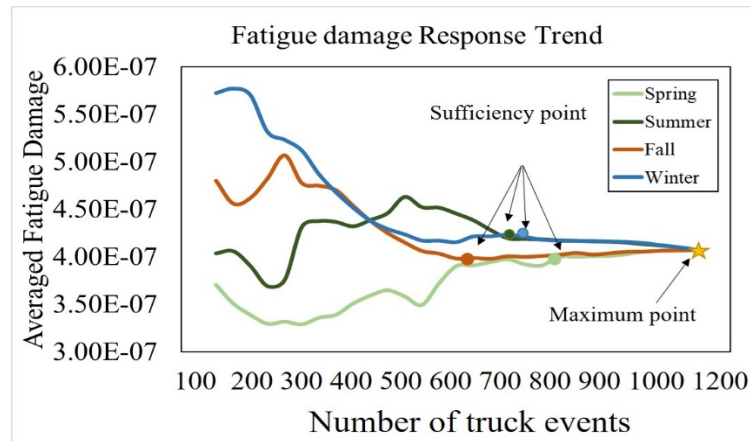


Figure 7-4 Trend of averaged fatigue damage index versus truck event cycles for four periods

7.5.1.1 Evaluating the trend of measured fatigue responses

In Figure 7-5, the monthly collected fatigue response is shown in a 12-month period of data collection for strain gage SG-A. It can be observed that the fatigue damage index has a variable mean value in different seasons, while within each season the responses are compatible. Therefore, using a consistent period can result in a more predictable trend, showing fatigue damage index variations, in long-term SHM programs. As a result, the damage-induced changes can be detected more efficiently through the estimated trend of fatigue damage index.

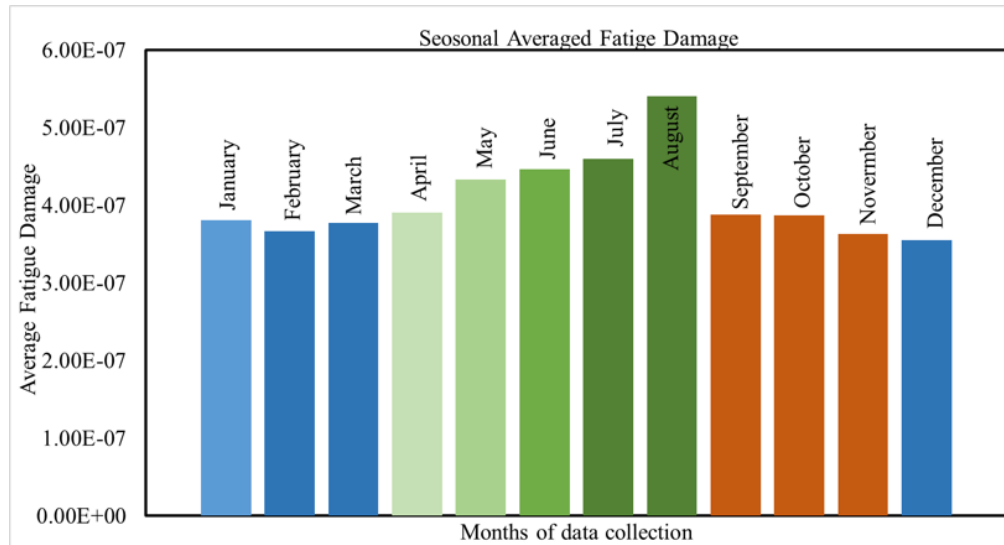


Figure 7-5 Monthly averaged fatigue damage index for 12-month period of data collection at SG-A

7.5.2 Correlation of measured fatigue damage indexes

The structural performance of a complex structural component in large-scale bridges requires a thorough understanding of the stress distribution at stress-concentrated locations of the component. Using SHM data, the structural responses can be studied under the global loading and boundary conditions of the component. The efficiency of SHM data in reporting variation in the structural responses depends substantially on the instrumentation plan and the number of sensors along the component.

In this section, the measured fatigue damage index of the five strain rosettes are implemented to find the correlation between the responses in the healthy conditions of the component. Predicting the accurate correlation between the responses is dependent on the complexity of the data. Given the close distance between the strain rosettes, the relationship between the responses can be predicted through regression methods (23). Creating a mathematical method for correlation prediction often is dependent on the complexity of the data, in terms of quantity and variation (24). In this section, a unique mathematical model is developed for each

strain gage location, that can predict the correlation of the fatigue damage index responses with the remainder fatigue responses of other strain gages. Consequently, five models are created of the five strain gages, via regression method and using 105 fatigue damage index responses which are obtained through 105 SHM data sets (25). NN can also be used when the number of inputs is considerable.

In Figure 7-6, the results of predicting the correlation between the fatigue responses are shown for each strain gage. It can be observed that the accuracy of each model is dependent on the location of the strain gage and the collected data. The complex geometry of the gusset-less component can be one of the major sources of variability, between the recorded strain responses and the resulting fatigue responses. The accuracy of the predicted responses is evaluated through R^2 value. The predicted fatigue responses at SG-B shows the lowest R^2 and, therefore, the least correlation to the other fatigue responses. SG-C and SH-D shows relatively similar accuracy. SG-A and SG-E illustrated higher R^2 results for correlation prediction, as compared to the other strain rosette responses.

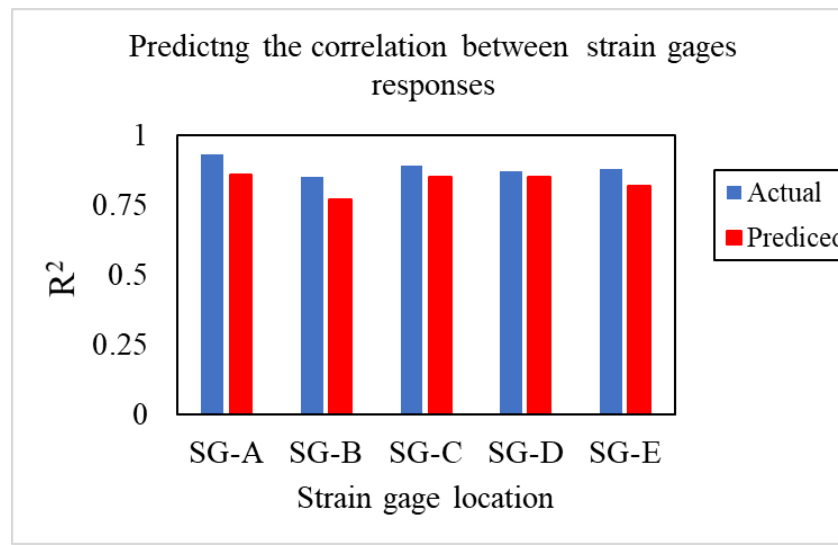


Figure 7-6 Results of predicting the correlation between the measured fatigue damage index of five strain rosettes

The predicted models demonstrate the correlations between the fatigue responses at the healthy condition of the gusset-less connection. This predicted correlation will be considered as a criterion for acceptance or rejection of fatigue responses in the subsequent NN model. When sufficient samples of field-collected fatigue responses are available, the correlation between the responses will be directly obtained through the NN model. The suggested protocol aims for early detection of a damage using the predicted correlation between the fatigue responses. It is, therefore, important to obtain information about the changes caused by fatigue cracks in the predicted correlation. Since the concerning gusset-less connection does not include any reported crack, the fatigue cracks are simulated via an FE model of the bridge. The predicted correlation is utilized to validate the FE model. Through the validated FE model, the crack-induced stress responses and resulting fatigue damage indexes can be obtained.

7.5.3 Simulate fatigue cracks via FE model

7.5.3.1 The FE model properties

A global FE model of the Memorial Bridge is used in this section for fatigue crack simulation purposes. As shown in Figure 7-7, the model includes the instrumented part of the bridge (south span and south tower). The created model considered the structural members of the bridge, which are modeled with 4-noded thick shell elements (26). The model is created in LUSAS, that is a FE software package appropriate for modeling the bridges. The model is verified through a designed load test, as detailed in the previous studies (27). The validated numerical time-history strain responses of the model will be applied for fatigue assessment goals of this study.

7.5.3.2 The FE model calibration

The validation of the FE model is required to be provided prior to launch for crack simulation. The validated model represents the current healthy condition of the bridge. In this section, the predicted correlation between the measured fatigue responses in section 7.5.2, is utilized to calibrate the model. The mesh layout and mesh sizes of the model are adjusted, corresponding to the predicted correlation between the responses of five strain rosettes. The comparison between the numerical versus the predicted stress range results is shown in Figure 7-7. The acceptable agreement between the results demonstrates the calibration of the model for the subsequent crack simulation goals.

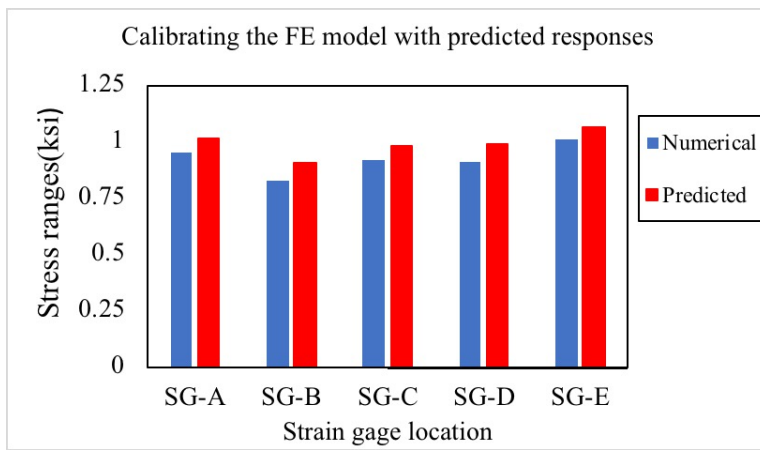


Figure 7-7 Calibrating the numerical responses of FE model corresponding to the predicted fatigue responses

7.5.3.3 Simulating fatigue crack via calibrated FE model

The fatigue cracks are often initiated at the high-stressed welded locations. Imperfections and the structural discontinuity at the welds can significantly increase the local stress concentrations and hence, the potential for crack initiation. In this study, fatigue crack is simulated at high-stressed location of the connection, at the weld toes of the gusset-less connection. Most of the available literature considers a possible damage as the reduction of stiffness, thickness or

change in material properties in the FE models (11). In complex structural components, less information is available on the changes in structural properties that are induced due to a possible crack or other damage types. Therefore, a more accurate method is essential to simulate damage via FE models. In this section, fatigue cracks are physically simulated via three-dimensional shell elements (28). In addition, small sizes of fatigue cracks are selected for simulation since the current study seeks to detect the possible cracks at the early stages.

The available literature has multiple recommendations for initial crack sizes (29). In this study, a minimum of size of 0.1 inch is selected for crack initiation due to the considerable size of the thickness (1.25 inch). The initiated crack is then extended to 5-inch crack size with 0.2-inch step, to study the stress response variation due to crack propagation. Three locations of the connection are selected for crack simulation, as shown in Figure 7-11. The cracks are simulated at the stressed concentrated locations along the weld toes of the gusset-less connection. Two of the cracks are implemented in a close distance to the instrumented strain rosettes. The third crack is simulated at the interior stiffener of the gusset-less connection. Also, the crack direction is determined based on the principal stresses at the crack tip. The mesh sizes around the cracked area are variable, which range from 0.1 inches to 1 inch. Additionally, the extended range of crack sizes aid to provide sufficient numerical stress responses (and measured fatigue damage index) to train the NN model.

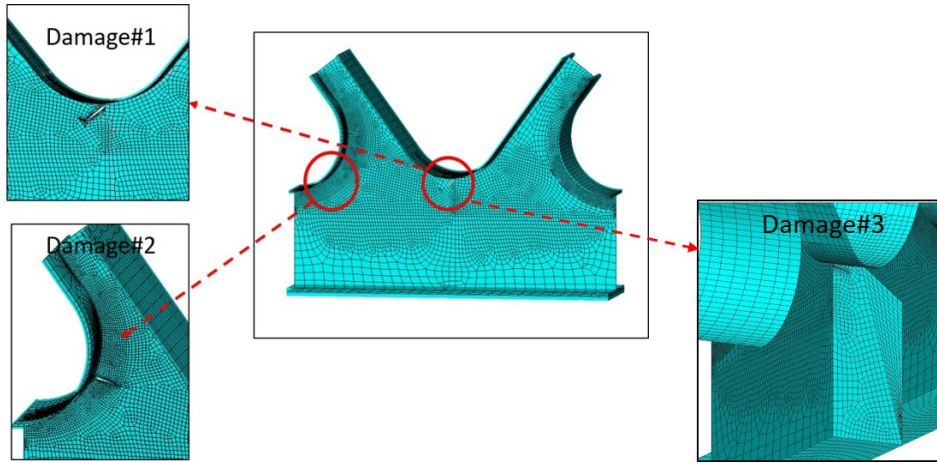


Figure 7-8 The simulated fatigue cracks at the gusset-less connection through FE model in LUSAS

7.5.3.4 Numerical crack-induced results of FE model

Every crack case is modeled in a unique FE model, while several FE models with different crack sizes are created for each crack case. Different traffic scenarios are provided for the numerical structural responses of the FE models. Figure 7-9 displays the stress contour results of the gusset-less connection for the three crack cases. The figure shows the maximum size of the crack and a static truck load (37 kips). It can be observed that the cracks cause a local stress concentration around the cracked area. However, the stress distributions are not identical for different crack cases.

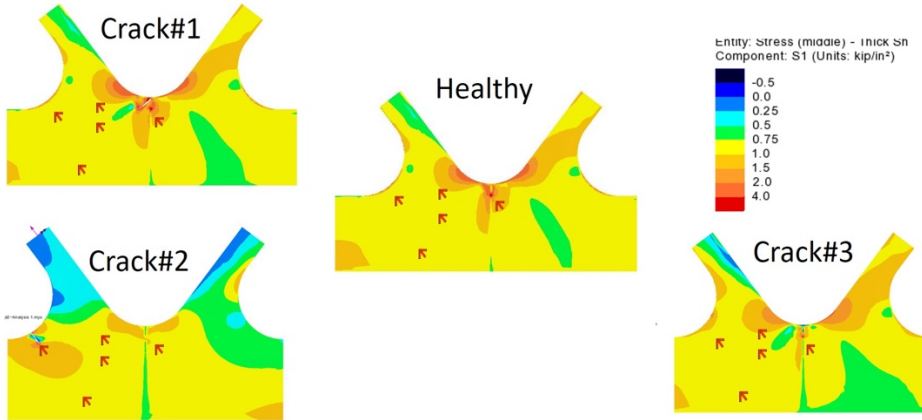


Figure 7-9 The stress contours of the gusset-less connection healthy and three crack cases

The traffic loads are implemented to the models via the dynamic moving loads. Therefore, in each FE model, multiple traffic scenarios are implemented, which consist of single or multiple truck at both lanes of the bridge. Eight traffic scenarios are simulated via the models to obtain time-history stress responses. In Figure 7-10, an example of time-history principal stress responses is shown for the three cracks cases, under the load test truck passage. It can be observed that, depending on the locations of the damage and the strain rosettes, the time-history results can differ from the healthy responses.

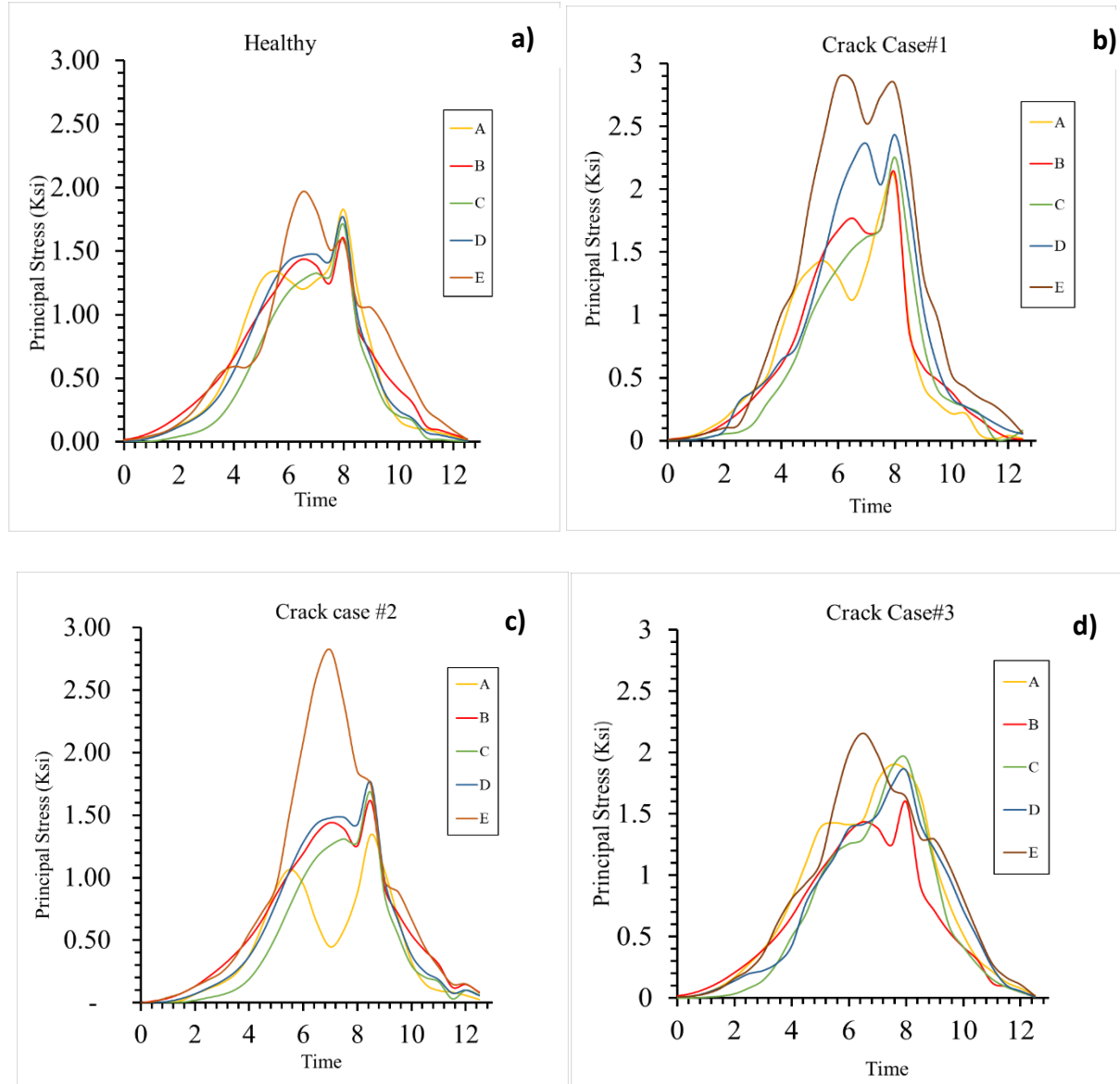


Figure 7-10 Numerical time-history principal stress responses under the dynamic moving loads for a) healthy, b) crack case#1, c) crack case#2, d) crack case#3.

The resulting numerical time-history stress responses are utilized to obtain the stress ranges, which is vital for fatigue estimation. Also, the required cycle quantities are obtained from the bridge SHM data collected in the field. For different crack cases and crack size, the healthy and crack-induced fatigue responses create a database to train a NN model for damage prediction.

In Figure 7-11, the variation of the measured fatigue damage indexes are shown considering different crack sizes of the three crack cases, at the five strain rosette locations.

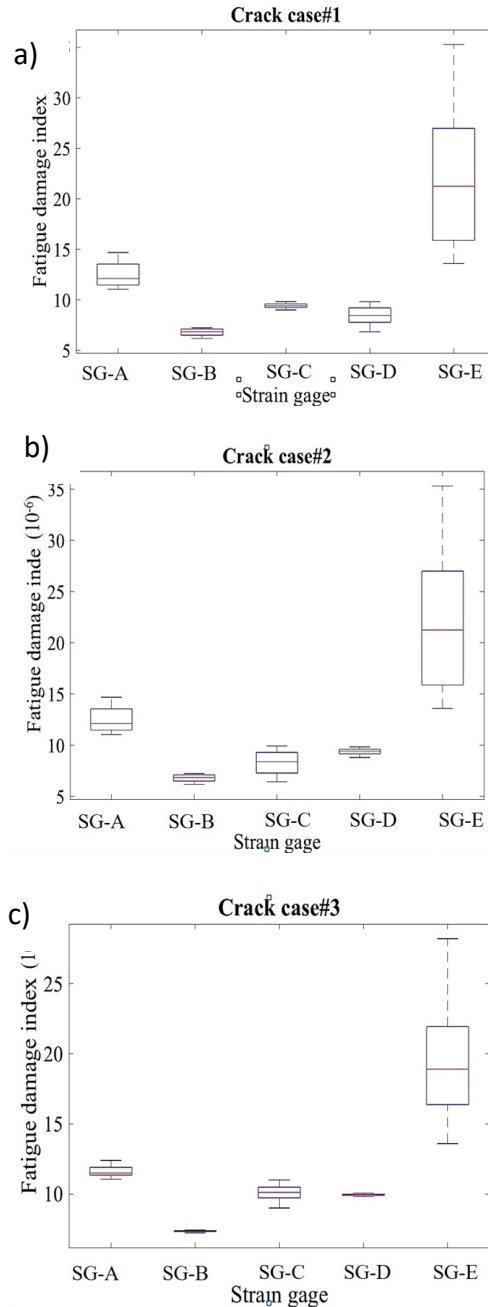


Figure 7-11 Variability of the measured fatigue damage indexes with multiple crack sizes for a) crack case#1, b) crack case#2, c) crack case#3

7.5.4 Train NN model for fatigue crack detection

7.5.4.1 Input data to NN model

In this section, the NN model is developed for crack predictions goal of the protocol. The fatigue damage index calculated for healthy and crack cases in section 5.3 are implemented to train the NN model. Sufficient numerical samples of the healthy and crack-induced fatigue damage indexes are required to input NN model for fatigue crack detection. Using different sizes of crack for each crack case can provides variable samples of crack induced fatigue responses. 1200 samples of the cracked-induced fatigue damage indexes are created to train the NN model.

However, samples for healthy fatigue responses via the FE model are limited, as they are created through only eight traffic scenarios. Accordingly, using the existing healthy fatigue responses, additional samples of the healthy fatigue damage indexes are generated to input the NN model. The healthy fatigue damage index samples are produced, using the Bootstrap method which considers the mean value of the input fatigue responses. The details of using Bootstrap method for sample production are selected based on the available studies (11). Healthy fatigue damage index samples from the numerical data are implemented to the Bootstrap method to generate 1200 samples of healthy fatigue damage index responses.

The healthy and cracked fatigue damage indexes, as well as the additional information about the crack type, and sizes are input to the NN model. Training the NN model is performed through the input data, using the Neural Network Toolbox in MATLAB (30). Three samples of fatigue damage indexes are labeled into three different categories. The categorizations are performed through dataset for each damage index. These categories include healthy, healthy-cracked, and cracked showing the included cycles of stress ranges in each data set. In the category

of Healthy, the fatigue damage index samples are computed from the data set which consists of healthy stress ranges. Therefore, a total of 1200 health samples are input to the model.

Two different categories are defined for the crack-induced fatigue responses. Healthy/cracked class is a transition state, when in a data set, part of stress ranges is healthy, and the remainder are cracked-induced stress ranges. The ranges of crack size in this category, vary from minimum to 2.5 inches, which include 600 fatigue damage index samples. Depending on the proportion of healthy to cracked stress ranges, the inputs are defined. The cracked category considers the data sets that consists of the cracked induced stress ranges. This category includes the cracked induced stress ranges where the crack sizes varies between 2.5 and 5 inches (600 samples). In Table 7-1, the percentage of the healthy and damaged samples of fatigue damage indexes are illustrated in training, validation and test part of the network. All of the fatigue damage index samples are randomly divided into the three sets training, validation and test set of the NN model.

Table 7-1 Number of samples for the NN models

Health conditions	Crack induced	Training	Validation	Test
of the component	stress cycles			
Healthy	0%	900	180	120
Healthy/cracked	25%	788	157	105
	50%	675	135	90
	75%	562	112	75
Cracked	100%	450	90	60

7.5.4.2 Development of NN models

A total of five networks for the five considering strain gages are developed. In each network, the predicted correlation of the fatigue damage indexes (Section 7.5.2) is considered as a determining feature for damage prediction. In Table 7-2, the details of the NN models are explained. The details of the NN model are not identical for the networks, depending on the variation of the fatigue damage index trend. Through each network, the correlation between the fatigue damage indexes is computed and is compared with the initial predicted correlation between the healthy fatigue responses. The samples of healthy and cracked conditions will train the networks to differentiate between the correlations of the healthy and cracked fatigue damage indexed, respectively. A possible damage will be predicted, when a fatigue damage index follows the correlation between the cracked induced fatigue damage indexes at the five strain rosette locations.

Table 7-2 Summary of the NN model properties

NN parameter	SG-A & SG-E	SG-D & SG-B	SG-C
Number of neurons	14	8	10
Type of back propagation		Levenberg-Marquardt	
Activation function		Sigmoid function	
Learning rate		0.01	
Training mode		Batch mode	

A summary of the NN models for the five strain gages is presented in Table 7-3. The mean square error (MSE) versus and C.O.Vs are evaluated against the predicted models. It is shown that the accuracy of the NN models in damage prediction is not identical. The observed disparity in the accuracy of the models may be due to the damage location and the distance to the strain rosettes.

The NN models for SG-E and SG-A with the lowest MSE results shows a better convergence, respectively, as compared to the remainder strain gage models. Therefore, the created networks are recommended to be considered simultaneously, for an efficient damage detection.

Table 7-3 Variation of prediction performance for the five strain rosettes

Strain gage	Training	validation	Test	COV
	MSE	MSE	MSE	%
SG-A	0.0063	0.0091	0.0089	12.2
SG-B	0.0150	0.0184	0.0273	24.5
SG-C	0.0091	0.0103	0.0106	16.3
SG-D	0.0172	0.0206	0.0194	21.7
SG-E	0.0012	0.0037	0.0025	6.8

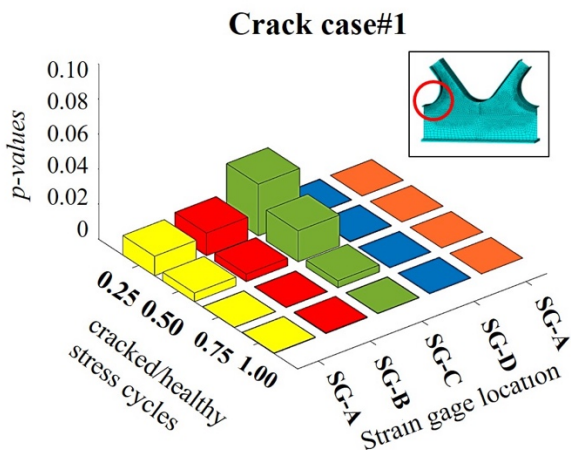
7.5.5 Damage detection via the NN models

According to the initially predicted correlation at healthy condition, a possible damage is detected through the deviated correlation of the fatigue damage indexes. The damage is be detected through either one or more trained networks. The comparison is provided by a *t-test* (31). The null hypothesis, H_0 , is defined when the correlation between the fatigue responses remains unchanged. The *p-value* results range from 0 to 1, revealing from completely expected to unexpected results, respectively. Any calculated *p-value* is evaluated with the “significant level” parameter, α . The *p-values* below α denotes the H_0 is rejected, while for the p-value above α , H_0 cannot be rejected. In this study, the α is considered as 0.001.

In Figure 7-12 the *p-values* are shown for the five strain rosettes and the three investigating crack cases. It is demonstrated that the NN models may successfully predict the cracks, when the

selected period of data collection entirely consists of the cracked-induced stress cycles. However, the NN model may not accurately predict the damage presences, when the proportion of cycles are less than 50 presents. Therefore, in addition to the crack-induced stress ranges, early damage detection is dependent on the amplitude as well as the number of cycles for crack-induced stress ranges, which are applied to measure the fatigue damage index.

In addition, it was investigated that the accuracy of the predicted model will increase when the fatigue damage index samples for lower proportion of cracked cycles are removed from the inputs. The success in damage detection is shown to be significantly dependent on the crack location, and the size. For the crack case 3, the detection at early stages may not be feasible (below 2-inch crack size). Consequently, the cracks that are initiated in a reasonable distance to the instrumented system might not be captured at early stages.



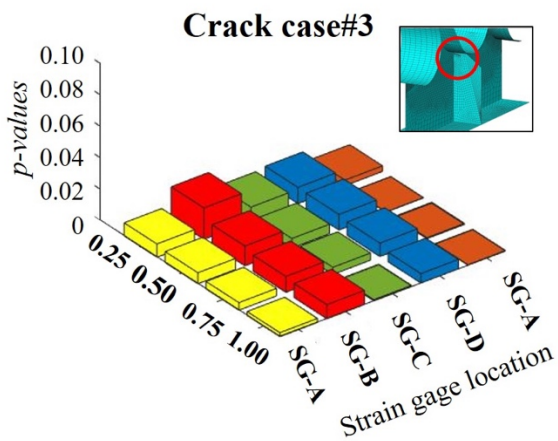
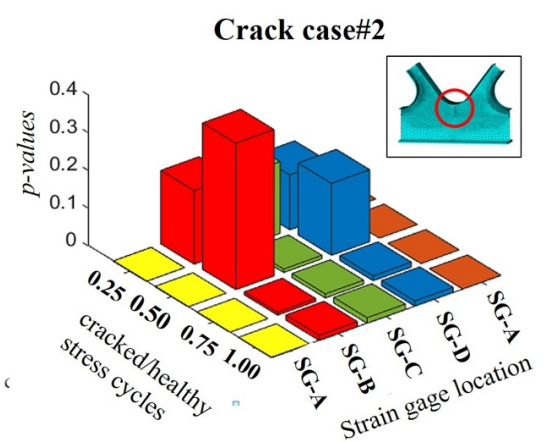


Figure 7-12 Crack size versus p-values for five sensors and damage case 1, 2,3.

Additionally, in this study, the minimum size of damage which can be captured through the NN model is also evaluated. In Figure 7-13, the minimum size for detected crack in each damage case is compared between the five installed sensors. It can be observed that some strain rosettes (SG-B and SG-D) may not predict the induced crack at the curved welds, due to the reasonable distance. The results confirm that even excessive number of data acquisition system might not warrant early damage detection, if they are not installed at the appropriate position.

Consequently, it can be demonstrated that the success of early stage damage detection relies on the instrumentation plan and the quantity of the sensors. As a consequence, the proposed mathematical model a tool which can be applied to design an efficient instrumentation plan for the complex structural components. Moreover, in the structural components with insufficient installed sensors, it is recommended to use temporarily installed sensor to obtain the initial correlation between the structural responses at different locations of the component. Additional information can be obtained through a well-detailed validated global FE model to supplement the insufficient SHM data. However, the measured fatigue responses through the numerical model is required to be consistent with the SHM-data measured responses.

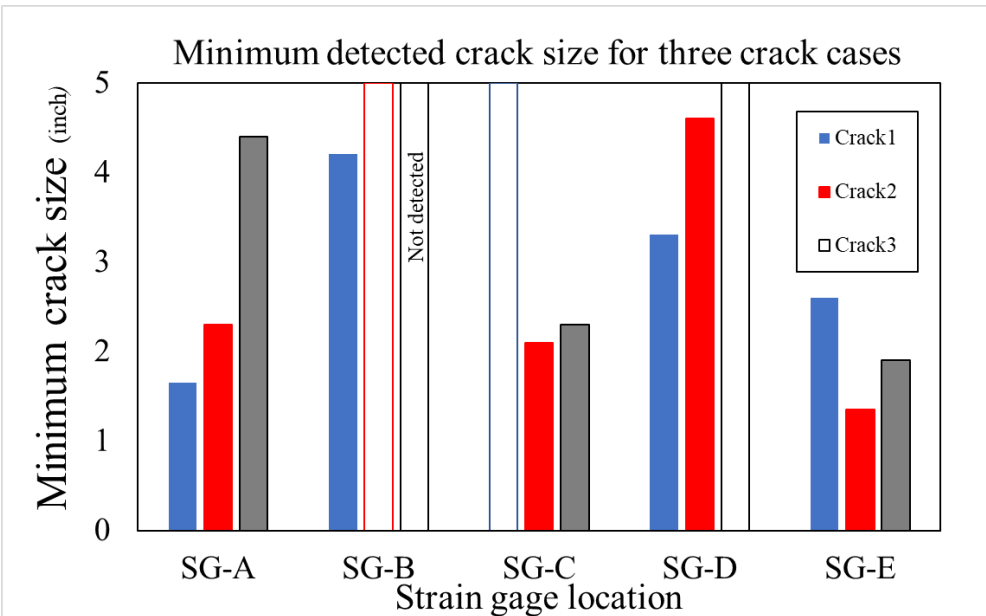


Figure 7-13 Minimum detected crack size through the NN models of the five strain rosettes for three crack cases

7.6 Conclusion

In this study, the prediction of fatigue crack is concerned with complex welded complements of steel bridges is. Using SHM data, fatigue damage index is measured at the instrumented locations

of the investigating component. Long-term estimation of fatigue damage index considers the changes in the recorded cycles of stress ranges due to the fatigue crack progress. Therefore, the proposed NN model, in this study can be utilized as an efficient tool to predict fatigue cracks at early stages. The NN model in this study is proposed to be developed during the healthy conditions of bridges. However, the proposed NN model can also be implemented to investigate the fatigue damage index changes with crack propagation for the structural component with detected crack. However, it is demonstrated that the crack detection through the SHM data can be substantially dependent on the instrumentation plan, the number and location of the sensors. Therefore, inefficient instrumentation may not result in a practical network to proactively detect fatigue cracks at early stages.

Alternatively, short term instrumentation can be implemented to obtain the required responses at the desired location. In this case, using a validated FE model will be beneficial to determine the critical locations for instrumentation, which can capture any possible cracked-induced stress response. In this study, a validated FE model is also utilized to supplement the required cracked-induced data for developing the NN model. Caution is required when using FE model for damage simulation. The crack location and extension are required to be based on the existing experiences of reported cracks in similar components. Simulating the cracks at the less plausible locations of the component, may lead to an inaccurate NN model for actual damage detection. It is also recommended that the FE model be updated during the service life of the bridge, according to the inspection results.

References

- 1) Downing S.D., Socie D.F., 1982. "Simple rainflow counting algorithms." (*International Journal of Fatigue*) 4 (1).
- 2) Miner, M.A. 1945. "Cumulative damage in fatigue." (*Journal of Applied Mechanics*) 12: 159-164.
- 3) AASHTO. 2012. *LRFD bridge design specifications*. 5. Washington, DC.
- 4) Adeli, H. 2001. "Neural networks in civil engineering." *Computer-Aided Civil and Infrastructure Engineering* 16 (2): 126-142. doi: <https://doi.org/10.1111/0885-9507.00219>.
- 5) Zhao, J., J. Ivan, and J. DeWolf. 1998. "Structural damage detection using artificial neural networks." *Journal of Infrastructure Systems* 4 (3): 93-101.
- 6) NHDOT (New Hampshire Department of Transportation). (Jul. 31, 2016). "Memorial Bridge Project Innovations."
- 7) Adams, T., Mashayekhizadeh, M. Santini-Bell, E. , Wosnik, M., Baldwin, K., and Fu, T. 2017. "Structural Response Monitoring of a Vertical Lift Truss Bridge." Washington, D.C.: Conference Proceedings of Transportation Research Borad, 96th Annual Meeting
- 8) Mashayekhizadeh, M., Santini-Bell, E. and Adams, T. 2017. "Instrumentation and Structural Health Monitoring of a Vertical Lift Bridge." Jacksonville, Fl: Processings of 27th ASNT Research Symposuim.
- 9) Saberi, M.R., Rahai, A.R., Sanaye, M., Vogel, R.M. 2016. "Bridge Fatigue Service-Life Estimation Using Operational Strain Measurements." *Journal of Bridge Engineering* 21 (5): 04016005-1-11.
- 10) Shahidi, S.G., Nigro, M.B., Pakzad, S.N., Pan, Y. 2015. "Structural damage detection and localisation using multivariate regression models and two-sample control statistics." *Structure and Infrastructure Engineering,Maintenance, Management, Life-Cycle Design and Performance* 11 (10): 1277-1293. doi:10.1080/15732479.2014.949277.
- 11) Gul, M., & Catbas, F. 2011. "Damage assessment with ambient vibration data using a novel time series analysis methodology." *Journal of Structural Engineering* 137 (12): 1518–1526.
- 12) Sohn, H., Farrar, C.R., Hunter, N.F., & Worden, K. 2001. "Structural health monitoring using statistical pattern recognition techniques." (*Journal of Dynamic Systems, Measurement and Control: Special Issue on Identification of Mechanical Systems*) 123 (4): 706-711. doi:<https://doi.org/10.1115/1.1410933>.
- 13) Mashayekhizadeh, M., Mehrkash,M., Shahsavari, V., Santini-Bell, E. 2018. "Multi-Scale Finite Element Model Development for Long-Term Condition Assessment of Vertical Lift Bridge." Fort Worth: Structure Congress,ASCE.
- 14) Mashayekhi, M., Santini-Bell, E. 2018. "Three-dimensional multiscale finite element models for in-service performance assessment of bridges." *Computer-aided civil and infrastructure engineering*. doi:<https://doi.org/10.1111/mice.12424>.
- 15) Weinstein, J. C., Sanaye, M., Brenner, B.R. 2018. "Bridge Damage Identification Using Artificial Neural Networks." *Journal of Bridge Engineering* 23 (11). doi:10.1061/(ASCE)BE.1943-5592.0001302.
- 16) Ayhan, A.O. 2011. "Simulation of three-dimensional fatigue crack propagation using enriched finite elements." (*Computers & Structures*) 89 (9): 801-812.
- 17) Aygül, M. 2013. *Fatigue evaluation of welded details – using the finite element method, Doctoral thesis*. Gothenburg, Sweden : CHALMERS UNIVERSITY OF TECHNOLOGY.
- 18) MathWorks. 2017a. *Create, train, and simulate shallow and deep learning*. <https://www.mathworks.com/products/neural-network.html>.
- 19) Montgomery, R.H., & Loftis, J.C. 2012. "Applicability of the t-test for detecting trends in water quality variables." (*American Water Resources Association*) 23: 653–662.

- 20) Bell, E.S. 2008. "Bridge Condition Assessment Framework Integrating Structural Health Monitoring and Intelligent Transportation Technology." Washington, D.C.: Transportation Research Board.
- 21) Zhou, Y.E. 2006. "Assessment of Bridge Remaining Fatigue Life through Field Strain Measurement Life through Field Strain Measurement." *Journal of Bridge Engineering* 11 (6).
- 22) Sampaio, R.P.C., Maia, N.M.M., Silve, J.M.M. 1999. "Damage detection using the frequency-response-function curvature method." *Journal of Sound and Vibration* 226 (5): 1029-1042.
- 23) Koh, B.H, Dyke, S.J. 2007. "Structural health monitoring for flexible bridge structures using correlation and sensitivity of modal data." *Computers & Structures* 85 (3-4): 117-130.
- 24) Anastasopoulos, D. De Smedt,M., Vandewalle, L., De Roeck, G., Reynders, E. 2018. "Damage identification using modal strains identified from operational fiber-optic Bragg grating data ." *Structural Health Monitoring* 17 (6): 1441-1459.
- 25) Zhang, J., Guo,S.L., Wu, Z.S., Zhang, Q.Q. 2015. "Structural identification and damage detection through long-gauge strain measurements." *Engineering Structures* 99: 173-183.
- 26) Phares, B., Lu, P., Wipf, T., Greimann, L., Seo, J. 2013. "Evolution of a Bridge Damage-Detection Algorithm ." *Transportation Reasearch Record: Journal of the Transportation Resaerch Borad* 2331 (1): 71-80.
- 27) Reiff, A., M. Sanaye, and R. Vogel. 2016. "Statistical bridge damage detection using girder distribution factors." *Engineering Structures* 109: 139-151.
- 28) Hong, W. Cao, Y. Wu, Z. 2016. "Strain-based damage-assessment method for bridges under moving vehicular loads using long-gauge strain sensing." *Journal of Bridge Engineering* 21 (10)
- 29) Chen, S.Z., Wu, G., Feng, D.C. 2019. "Damage detection of highway bridges based on long-gauge strain response under stochastic traffic flow." *Mechanical Systems and Signal Processing* 127: 551-572. doi:<https://doi.org/10.1016/j.ymssp.2019.03.022>.
- 30) Hu, X., Wang, B., & Ji, H. 2013. "A wireless sensor network-based structural health monitoring system for highway bridges." (Computer-Aided Civil and Infrastructure Engineering) 28: 193-209.
- 31) Neves, A.C., Gonza'lez, I., Leander, J., Karoumi, R. 2017. "Structural health monitoring of bridges: a model-free ANN-based approach to damage detection." (Journal of Civil Structural Health Monitoring) 7: 689-702.

Chapter 8

8 FATIGUE CRACK PROPAGATION PERFORMANCE ASSESSMENT OF COMPLEX STRUCTURAL COMPONENTS OF STEEL BRIDGES USING A MULTI-SCALE FINITE ELEMENT MODEL

*In preparation

8.1 Abstract

Complex welded structural components in steel bridges are subjected to cyclic stresses, rendering the component vulnerable to fatigue damage. In large span bridges, a complex loading condition is transferred to the welded joints through the structural members that are connected to the component in the plane and out-of-plane direction. Therefore, the investigating structural component may have a complicated fatigue performance concerning the crack initiation and propagation is not addressed using the available design codes. In addition, local performance assessment of these components may not result in practical outcomes, using experimental or numerical methods. In this study, the fatigue performance of a case-study structural component is investigated. In this study, the fatigue performance of welded complex structural components of large-scale bridges is investigated using a global multi-scale finite element (FE) method. The case-study bridge is the Memorial Bridge in Portsmouth, NH, a vertical lift truss bridge that includes a complex-designed gusset-less connection located in the top chord, bottom chord, and the tower. The multi-scale model is created to consider multiple dimensions of elements in a single global

model. Higher-dimensional elements are utilized to simulate three-dimensional crack propagation at the objective gusset-less connection under the dynamic traffic loads. The structural performance of the connection is investigated to determine the candidate locations for crack initiation. The remaining fatigue life of the gusset-less connection under crack propagation procedure is estimated using linear elastic fracture mechanics method (LEFM). It is demonstrated that through a validated multi-scale model, the fatigue performance of welded components in large-scale steel bridges can be evaluated. In addition, the obtained degrading results in fatigue strength due to crack propagation can be implemented in the bridge's maintenance program.

8.2 Introduction

Welded structural components in steel bridges sustain variable amplitude stresses due to cyclic traffic loads, during the service life of the bridge. The resulting concentrated stress ranges may cause fatigue crack initiation at the stress concentrated locations of the weld area. Continuity in cyclic stresses may trigger the crack propagation process, announcing a finite fatigue life of the cracked component. The characteristics of crack propagation might not be identical for the welded component, depending on multiple factors that include material and structural properties of the components. Available fatigue design codes have been attempted to characterize and quantify crack propagation details of multiple welded structural components based on the weld type, welding history, and the induced structural discontinuity at the weld. The existing codes frequently consider conventional weld geometries that exist in the recognized welded structural details. Geometric properties of welds may cause stress concentrations and, therefore, impact on crack propagation properties concerning the crack's direction, extension, and closure.

Complex welded structural components are designed and implemented in different structure types to achieve better performance with minimized maintenance costs during the designated service life of the structure. The details for some of the welded components might not be documented in the available design codes, which causes a less-known fatigue crack performance (1). Geometric characteristics of the welds, loading, and boundary conditions of the components are the distinctive features that identify an exclusive crack propagation performance in complex welded components. The welded structural components in large-span bridges also suffer from stress variations, which continuously change due to the variable amplitude traffic loads. Therefore, design and executing the experimental efforts to study the crack propagation and the fatigue strength of such complex welded components involves an accurate simulation of these loading conditions. The requirement of excessive time and cost allocations for experimental efforts motivates the application of more practical alternatives, such as numerical methods.

Through a detailed finite element (FE) model of a bridge, in addition to identifying stress variations, the characteristics of crack propagation can be investigated through a careful simulation of the crack. Extended research has been done on simulating multiple crack types and crack propagation via FE models to estimate the remaining fatigue life of the cracked component (2) (3) (4). These studies are frequently limited to local FE models of welded components due to the high computational costs of applying fine mesh sizes and higher dimensional elements, which are essential for a precise fatigue crack simulation. Fatigue performance assessment of complex structural components necessitates considering a global FE model of bridges to compute the stresses at the crack tip and the crack propagation details under a precise loading and boundary conditions of the component.

Limited research investigated the fatigue performance of cracked structural components using the global FE model of bridges. Aygül et al. created a global FE model of a railway bridge to investigate distortion-induced fatigue cracks growth at welded components of steel bridges considering two different crack propagation models (5). The study concluded that the variable amplitude loading could cause a shortened fatigue life as compared to the constant amplitude loading conditions, which necessitates being considered in crack propagation simulations and the concluding fatigue responses. Albuquerque et al. investigated fatigue assessment of cracked welded components of a case-study railway bridge. This study considered a global FE model for considering traffic loads and the local substructure model of a critical fracture element for simulating crack propagation. They also considered the dynamic traffic load effects using the model superposition method (6).

Irfaee and Mahmoud recently addressed a study on fracture performances, a box girder bridge of a mixed-mode propagated crack, using a multi-scale FE model of the bridge (7). The fatigue results of the study were obtained based on the numerical stresses of the multi-scale FE model under a constant amplitude static load. The details about the rate and direction of crack propagation were not clearly explained. In fatigue crack propagation studies, the concentrated stresses at the weld area of structural components have a direct influence on the crack propagation properties, which is required to be precisely computed. The crack-tip stresses for the propagated crack in the weld can conveniently be obtained through considering the weld geometry in the FE model. In addition, modeling the weld geometry in an FE model allows expanding fatigue crack propagation studies by simulating weld defects as well as the initiated crack due to the existing defect.

In this study, the fatigue performance of complex welded components of steel bridges is concerned. A multi-scale FE model is created for a case-study bridge to investigate candidate fatigue prone areas for crack initiation as well as the crack propagation properties under the variable amplitude traffic loads. The created model considers higher dimensional elements to model the concerning welded components and a three-dimensional crack propagation mechanism. The case-study is the Memorial Bridge, a vertical lift steel bridge in Portsmouth, NH. The bridge includes a novel gusset-less connection that consists of a complex web geometry, which is welded to cold-bent flange welds through curved geometry fillet welds. The stress variation under a dynamic truck load is considered in crack propagation simulations. Linear elastic fracture mechanics (LEFM) method is utilized to estimate the variations in fatigue remaining cycles of the gusset-less connection due to the crack growth.

8.3 Methodology

Fatigue in welded structural components consists of two phases of crack initiation and crack propagations. These two phases can influence the material and structural properties of the cracked component at the microstructure and macrostructural levels, respectively. The continuity of crack propagation, which is driven by cyclic concentrated stresses at the cracked area, can lead to the fracture of the component. The finite remaining service life of a cracked component in an elastic material is dependent on the crack propagation activity. Linear elastic fracture mechanics (LEFM) method extensively deals with fatigue strength of cracked steel components through considering material properties, geometric characteristics, and loading conditions (8). LEFM method characterizes the crack propagations details into three recognized modes, Mode I, Mode II, and Mode III, shown in Figure 8-1. An initiated fatigue crack may propagate following one or

combinations of modes. Complex welded structural components of long-span bridges are often involved in complicated loading and boundary conditions, which may trigger a mixed-mode crack at the welded area of the component (9). A precise crack propagation performance assessment of a welded component is primarily dependent on thorough knowledge about the loading conditions and induced stresses at the welded area.

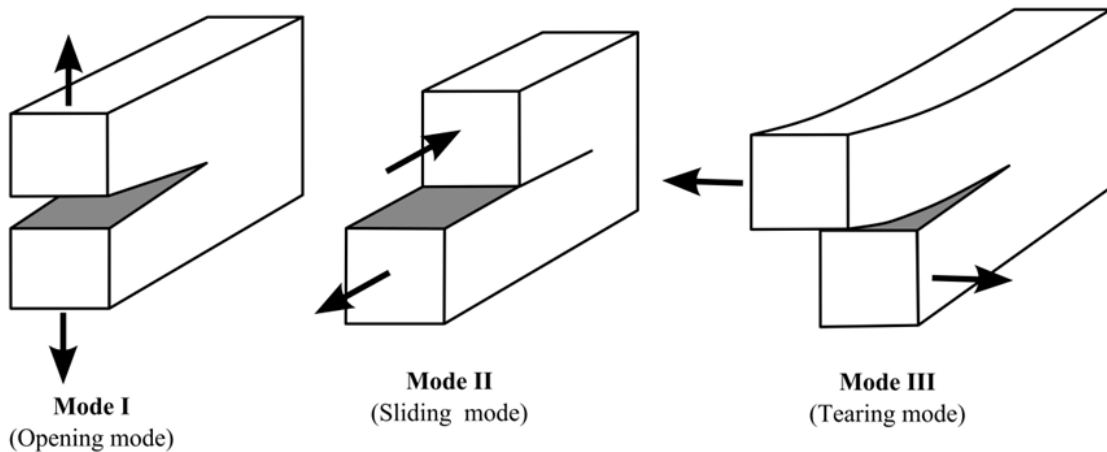


Figure 8-1 The three loading conditions/modes in fracture mechanics (112)

8.3.1 Fatigue crack under mixed mode loading

Using the LEFM method, the remaining fatigue cycles of the welded component due to an initiated fatigue crack can be estimated through the Paris law (10). The Paris law relies on the crack propagation relationship, requiring initial and final crack sizes to determine the remaining fatigue cycles through Eq. (8.1).

$$\frac{da}{dN} = C(\Delta K)^m \quad \text{Eq. (8.1)}$$

where C and m are material properties. da defines the crack length increment and dN expresses the number of cycles to failure corresponding to the crack increase. ΔK is defined as the stress intensity

factor (SIF) changes with crack increment, showing the crack growth rate and estimated via Eq (8.2).

$$\Delta K = K_{max} - K_{min} = f(a) \cdot \Delta\sigma \cdot \sqrt{\pi \cdot a} \quad \text{Eq. (8-2)}$$

where $\Delta\sigma$ depicts the stress ranges, applied for fatigue assessment. $f(a)$ is defined as the function of geometry, load and crack shape, which is addressed the available literature (11). SIF is also considered as the criterion for crack propagation and fracture, when compared to the threshold value of SIF (K_{th}), critical value of SIF (K_{IC}) via Eq.(8-3a) and Eq.(8-3b), respectively.

$$\Delta K \geq K_{th} \quad \text{Eq. (8-3a)}$$

$$\Delta K \geq K_{IC} \quad \text{Eq.(8-3b)}$$

The Paris law is primarily developed for the first mode crack, under a tensile loading condition. However, the method can be adjusted to be applied for the mixed-mode crack condition. In the mixed mode crack conditions, the equivalent SIF, ΔK_{eq} is required to be measured and implemented in the Paris's Law, Eq. (8.1). ΔK_{eq} is estimated through the SIF of the three modes, K_I, K_{II}, K_{III} , as expressed in Eq.8-4.

$$\Delta K_{eq} = \sqrt{K_I^2 + K_{II}^2 + (1 + \vartheta)K_{III}^2}, \quad \text{Eq. (8-4)}$$

where ϑ is the Poisson's ratio. Accurate computation of SIF is one of the fundamental steps in LEFM method. The J-integral method is a recognized method that is utilized to estimate the stress state and resulting SIF at the crack tip, particularly for complex details that experience mixed-mode crack conditions. For the mixed crack mode, the corresponding J-integral can be expressed as Eq. (8-5):

$$J = \frac{1}{E} (K_I^2 + K_I^2) + \frac{1}{2E} (K_{II}^2) \quad \text{Eq.(8-5)}$$

where E and G is the Elasticity. In addition to fatigue life prediction, the compute stress state at the crack tip is utilized to determine the details of crack propagation.

8.3.2 Estimating fatigue crack direction

Crack propagation may have a variable and less predictable direction, depending on the crack type and crack tip stress state variations. Mixed mode cracks may have a more complex crack propagation trend that changes in the direction and rate of propagation (12). In numerical fatigue assessment applications, crack direction must be accurately estimated to determine fatigue strength of the cracked component. There are multiple methods to measure crack propagation direction. The maximum tangential stress (MTS) criterion proposed by Erdogan and Sih (13), is one of the two recognized methods in giving acceptable responses, which are based on SIF criterion. The MTS method relies on the radial direction (θ_c) from the crack tip, where the tangential stress (σ_θ) reaches to the maximum value, as shown in Figure 8-2. Consequently, an unstable fracture condition can occur at the critical value of the tangential stress. The crack extension direction, θ_c , is obtained through maximizing the σ_θ corresponding to θ , in a local polar coordinate system ($\partial\sigma_{\theta,max}/\partial\theta$) at the crack tip, which is expressed in Eq. (8-6).

$$K_I \sin \theta_c + K_{II} (3 \cos \theta_c - 1) = 0 \quad \text{Eq. (8-6)}$$

θ_c that is extracted through (Eq.5-6) can be shown as:

$$\theta_c = 2 \tan^{-1} \left[\frac{1}{4} \frac{K_I}{K_{II}} - \frac{1}{4} \sqrt{\left(\frac{K_I}{K_{II}} \right)^2 + 8} \right] \text{ for } K_{II} > 0 \quad \text{Eq. (5-7a)}$$

$$\theta_c = 2 \tan^{-1} \left[\frac{1}{4} \frac{K_I}{K_{II}} + \frac{1}{4} \sqrt{\left(\frac{K_I}{K_{II}} \right)^2 + 8} \right] \text{ for } K_{II} < 0 \quad \text{Eq. (5-7b)}$$

The positive direction of θ_c is defined in the counterclockwise direction, measured from the initial crack orientation.

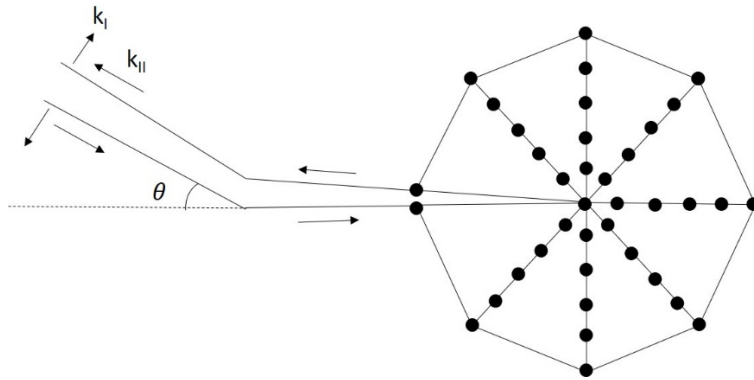


Figure 8-2 Determining Crack propagation direction in a radially meshed FE model

8.3.2.1 Through-the-thickness crack propagation

In reasonably thick plates, fatigue crack may not propagate through the entire thickness of the plate at the early stages of an initiated crack. Therefore, under the cyclic stresses, the crack will gradually propagate in the planar and out-of-plane direction of the welded component. Given the large thickness of the plate, the final crack size as the fracture criterion can be defined to be less than the plate thickness. The crack direction is determined using the principal stress vector direction at the crack tip.

8.3.3 Loading conditions during crack propagation

In the available experimental fatigue propagation studies, constant amplitude cyclic loading is frequently considered. However, it is indicated that the variable amplitude traffic-induced stress ranges in steel bridges can have a direct impact on the fatigue crack growth rate. In numerical fatigue crack propagation efforts, simulating the variable amplitude traffic loads at the bridge can impose high computation cost. Recently, some studies considered variable amplitude stress ranges in fatigue crack propagation assessment using theoretical and numerical methods in

local models having a limited number-of-degrees of freedom (14). The resulting stress ranges are implemented to compute the SIF and to determine the crack direction (15) (10). Alternatively, the equivalent stress ranges (*S_{eq}*) can be implemented to compute the SIF and subsequently to the Paris law to estimate the remaining fatigue life (16). In the current study, the dominant stress ranges that are experienced at the case-study bridge are simulated via the multi-scale model.

8.3.4 Crack propagation modeling using finite element method

A validated FE model of a bridge can be utilized as a significant tool to investigate fatigue propagation variations under the cyclic loads. The resulting numerical stresses are implemented in the Paris' law to estimate the remaining fatigue life of the cracked component. With recent ease-of-application of higher dimensional elements, mixed mode cracks that result in complex fracture planes can be accurately simulated, using appropriate modeling techniques. However, an accurate FE modeling relies on multiple key features, which include selection of elements, meshing (size and layout), crack propagation pattern, crack opening and crack closure. In this section, one of efficient method in creating an appropriate FE model for crack propagation modeling is addressed.

8.4 The case-study bridge

Memorial Bridge carries US Route 1 across the Piscataqua River connecting Portsmouth, NH with Kittery, ME, shown in Figure 8-3(a). The new Memorial Bridge was opened to traffic in July 2013. The new Memorial Bridge includes an innovative “gusset-less” truss connection as shown in Figure 8-3(b). The bridge is equipped with an array of sensors that report the structural responses due to traffic load and lift action excitations.

In this study, fatigue performance of the gusset-less connections under the cyclic traffic loads at the Memorial Bridge is concerned. The complex geometry of the connection and the

impact on the fatigue performance of the gusset-less connection, makes the connection an appropriate example to address the objectives of this study. Fatigue crack initiation and crack propagation of the gusset-less connection is investigated using a numerical FE model.

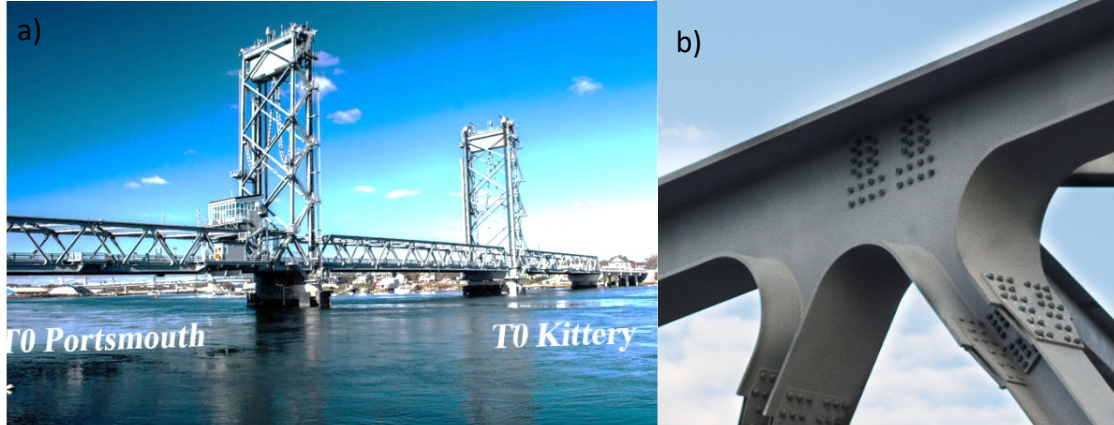


Figure 8-3. a) The Memorial Bridge, Portsmouth, NH(Left), b) The gusset-less connection of the Memorial Bridge (Right)

8.5 FE modeling of Memorial Bridge

In this section, a global FE model of the Memorial Bridge is created to investigate the structural performance of the gusset-less connection, under simulated traffic loads. The global FE model can provide a more realistic loading and boundary conditions for the objective component, as compared to the local FE models. Through the stress results of the model, the candidate location for fatigue crack initiation is identified.

8.5.1 Multi-scale global FE model

In this study, the restriction of modeling three-dimensional crack propagation in a global FE model is addressed through creating a multi-scale (M-S) model. A multi-scale model takes multiple dimensions of elements in a single FE model, corresponding to the expected structural responses. In a global FE model, the dimension of elements is selected based on the performance of the structural members. The differing elements are coupled together at the interface point. The

Multi-point constraint (MPC) equation is implemented to couple different dimensions of elements in this M-S model (Chapter4). In the previous studies, M-S models were created for the fatigue assessment of cracked structural components of bridges (17). However, the existing studies did not necessarily consider three-dimensional crack propagation under dynamic traffic loads. In addition, the weld geometry was not included in the models. The model is created in LUSAS, a commercial FE software, which is appropriate for modeling of large-scale structures including long-span bridges.

Three different dimensions of elements are considered in the M-S model, including solid elements, shell elements, and beam elements. The objective gusset-less connection that is selected for fatigue crack propagations is located in the middle of the bridge. This gusset-less connection is modeled via three-dimensional tetrahedral solid elements to accommodate the complex geometry of the component. The gusset-less connection has 5/8“fillet welds, connecting the flanges to the web of the connection. The weld geometry is also modeled through the solid elements to accommodate through-the-thickness crack propagation. A range of mesh sizes is considered for the solid elements, depending on the location of the crack. The adjacent elements to the crack tip are finely meshed (0.1 inches), while the mesh sizes gradually grow with the distance to the crack.

The remainder gusset-less connections of the bridge are modeled using three-dimensional thick shell elements. The deck of the bridge is also modeled via similar shell elements. Identical mesh size and mesh layout are considered for the gusset-less connections (2 inches). The long members are modeled with three-dimensional thick beam elements that include the braces, diagonals, floor beams, top and bottom chords. The minimum allowable size of the mesh is considered for the beam members. The properties of the model are detailed in Table 8-1. In Figure

8-4, the global M-S model of the bridge is shown for the healthy condition of the bridge. The model is validated through the truck load test results that were implemented in quasi-static and dynamic conditions, expressed in (18).

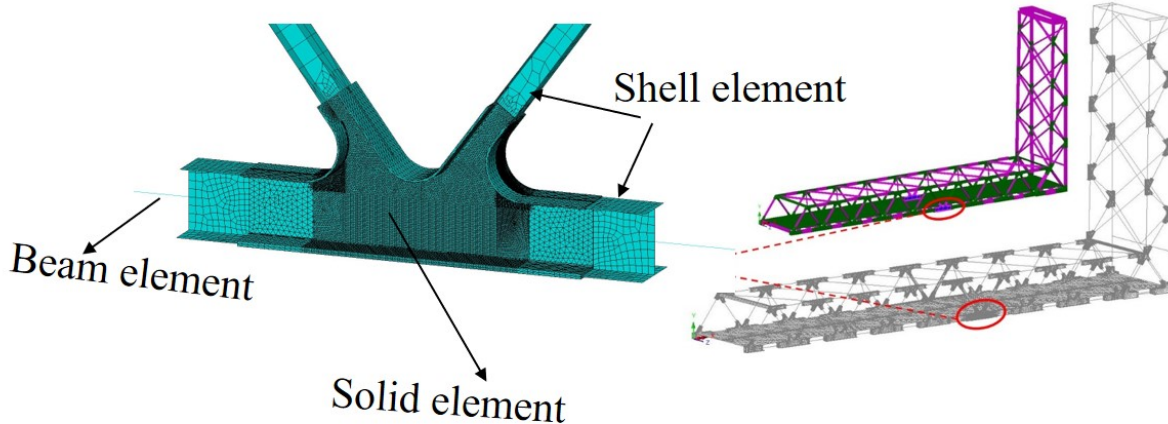


Figure 8-4 The MS global model of the Memorial Bridge created in LUSAS

Table 8-1 The characteristics of the M-S model

Model properties	Solid element	Shell element	Beam element
Number of elements	94257852	158993	5160
Maximum mesh size(in)	3	10	11
Minimum mesh size(in)	0.1	1	5
Modules of elasticity (psi)		29.0	6

8.5.1.1 Coupling of multiple dimensions

The MPC equations are implemented to couple beam to shell and beam to solid elements. These equations are addressed in Chapter 4 and Chapter 7 and, therefore, are not repeated in this chapter. In addition, due to the included weld geometry of the gusset-less connection in the M-S model via solid elements, the direct coupling of solid to beam elements is prohibited in the M-S model. Therefore, the lower chord is exclusively modeled with shell elements to provide solid to shell and shell to beam elements coupling. The simulated crack or other weld defects is

recommended to be at a considerable distance to the interface location to prevent any stress concentration at the interface. Changing the interface location may require an extension in solid elements and an increase in the DOF of the M-S model, which imposes high computation costs.

8.6 The structural analysis results

The M-S model is validated through the recorded stress responses during the load test. Based on the inspection results, the gusset-less connection at the Memorial Bridge does not include any detected damage to be implemented to the M-S model. Therefore, prior to launch crack simulation, the possible location for crack initiation is investigated using the structural analysis results. In this section, the numerical responses of the M-S model are utilized to investigate the structural performance of the gusset-less connection, under the passage of a single truck. The load test truck (Chapter 3) is implemented to the deck of the M-S model as a dynamic moving load. The time-history of moments and loads (axial and shear) are obtained, at the boundary of the gusset-less connection, connected to the other members, simultaneously. Under the moving load, the implemented load combination to the gusset-less connection is evaluated, and the dominant loading case is determined. In Figure 8-5, the boundary locations are shown.

Floor beams transfer the load of the truck at the deck to the connection. These floor beams are not involved in load transformation until the truck is positioned directly at the top of the member. Therefore, the load is significantly transferred to the gusset-less connection through *bottom chords*, as well as *diagonals*. In this case, the transferred axial loads are dominant, which cause stress concretions at the toe of the curved welds (at the left and right sides of the connection). The out-of-plane bending, and shear loads are transferred to connection when the truck is located at the closest position to the connection. These bending moments and shear loads

become the dominant loads, as compared to the axial loads that are transferred from the in-plane members (diagonal and bottom chord). In this case, the stress concentration area at the curved weld toe becomes closer to the bottom chord.

Consequently, a possible crack at the weld toe can be a mixed of Mode I and Mode II cracks that propagate in the plane and through-the-thickens of the web of the gusset-less connection. The middle-curve weld is significantly influenced by the shear loads that are transferred via the floor beam that is connected to the inner stiffener of the gusset-less connection (Figure 8-5). Therefore, a possible fatigue crack at the middle-curved may follow crack mode II pattern. These resulting information on the fatigue crack mode and the candidate crack ignition locations are implemented in the flowing section for crack simulations.

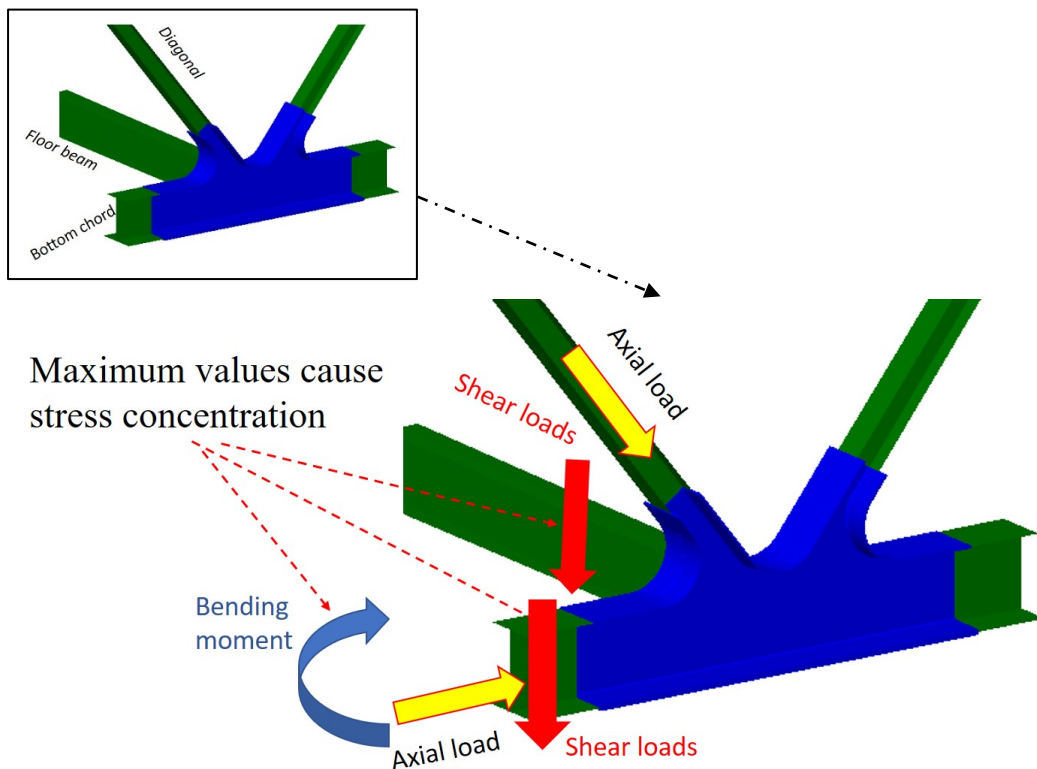


Figure 8-5 The connected members to the gusset-less connection

8.7 Modeling fatigue crack via M-S model

8.7.1 Meshing layout

An appropriate mesh layout is one of the significant steps to obtain a precise FE model in crack propagation simulation. In the available literature, a radial meshing is proposed at the crack tip (19). This meshing system allows computing *J-integral* and SIF in a cylindrical coordinate system. Also, such radial meshing allows determining the crack propagation direction for the surface crack. This meshing system is only proposed for the surface of the plate, which assumes the crack is initiated and propagated through the entire thickness. In three-dimensional crack propagation, the direction of the crack in the out-of-plane direction (through-the-thickness) must be estimated based on the resulting out-of-plane stresses at the crack tip. In this section, a three-dimensional mesh layout is proposed at the crack tip, which allows predicting the crack direction in the plane and out-of-plane direction of the plate, as shown in Figure 8-6.

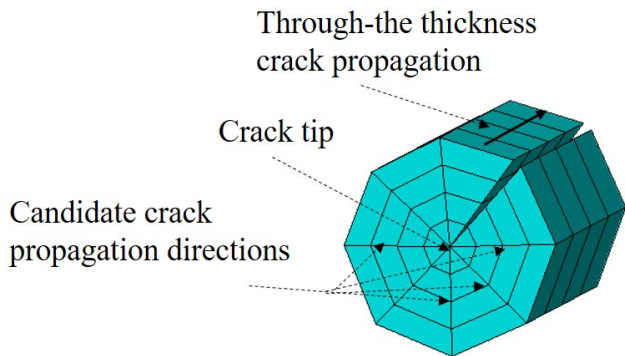


Figure 8-6 Meshing at the crack tip to predict fatigue crack direction

8.7.2 Crack initiation at weld toe of gusset-less connection

At the toe of welds, small crack sizes may occur at the intersection of the fusion line and the plate surface, which are too small to be detected via the routine inspections. Therefore, the

assumptions for the initial crack size may not be available for simulation. Similarly, the weld defects might not be successfully detected through visual inspections to be considered in the model, particularly in large size welds. Therefore, in this study, the initiated crack details in terms of crack type and locations are based on the obtained numerical results of the model.

In this section, the results through evaluating the gusset-less connection performance in section 8-6 are utilized for crack initiation. Based on the resulting numerical stresses at the gusset-less connection, a mixed-mode crack type is selected. Consequently, the crack propagation is performed at the planar and out-of-plane direction of the web surface of the gusset-less connection. The location of the crack at the weld toe of the gusset-less connection is determined based on the structural analysis results of the model, as shown in Figure 8-7. The initial crack length, a_i is selected to have 0.5" length in the planar direction. The direction on the initiated crack is determined to be perpendicular to the principal stress, which is obtained through the structural analysis of the M-S model. At the crack tip, the mesh is modified, as shown in Figure 8-7, to transform the crack singularity to a smooth surface.

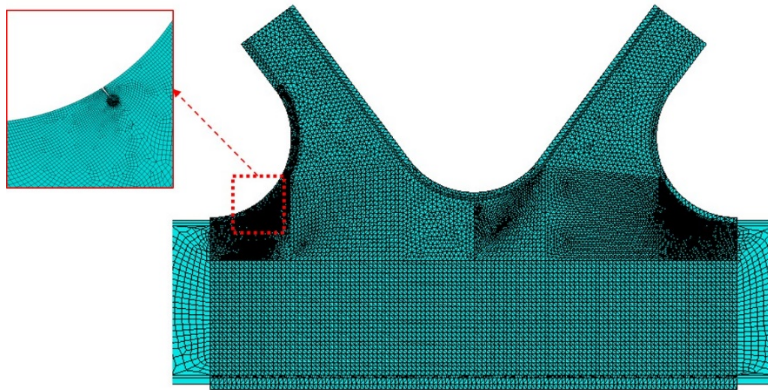


Figure 8-7 Selected location for crack initiation at weld toe of the gusset-less connection

8.7.3 Crack propagation at weld toe of gusset-less connection

Crack propagation relies on the computed stresses and the resulting SIF at the crack tip. If the resulting SIF at the crack tip is less than the critical value (K_{th}), the crack will not propagate. In this section, the M-S model is loaded via the overload trucks (Class 13 truck) to obtain the above threshold stress state at the crack tip. Three different traffic scenarios that consist of the overload truck vehicle classes are implemented to the M-S model when the truck travels at the northbound, southbound, and both lanes (not simultaneously). The resulting SIF at the crack tip is computed using the three induced stress ranges from each traffic scenario, using equivalent stress ranges (S_{eq}) (5).

In addition, in earlier studies, the crack propagation rate was provided through experimental or theoretical studies while considering the material degradation is considered at the process zone near the crack tip to predict the crack propagation rate (20). In this section, crack growth is simulated through a stepwise effort. In addition, earlier studies considered the entire thickness of the plate was considered during the surface crack propagation (21). Given the 1.25" thickness of the gusset plates, the initiated crack might not initially penetrate through the entire thickness. Therefore, four steps of crack propagations are considered for through-the-thickness direction (0.3", 0.625", 0.925", 1.25"). This is performed through an iterative algorithm.

8.8 Numerical results under crack propagation

In this section, the structural analysis results are investigated due to crack propagation of the global M-S model. In Figure 8-8, the stress contours of the gusset-less connection at the maximum crack size is shown for two crack cases varying in crack size. The stress contours at the cracked area are shown at the crack tip in the plane and out-of-plane directions of the connection.

It is demonstrated that the induced stresses at the crack tip, are not uniform in the planer and out-of-plane directions.

In Figure 8-8a, the smaller crack size, the resulting stress concentration at the crack tip is less significant as compared to the larger crack size. In Figure 8-8b, the larger crack size, the stress concentrations are induced at the two tips of the crack that are in the weld geometry and the web of the gusset-less connection. Consequently, the stress concentration may not be entirely transferred at the uncracked part of the plate, when the simulated crack is not propagated through the entire thickness of the plate. The resulting stress state and SIF at the crack tip may not be identical in the out-of-plane direction. However, to compute the K_{eq} , the maximum stress state of the crack tip is considered for each iteration of crack propagation.

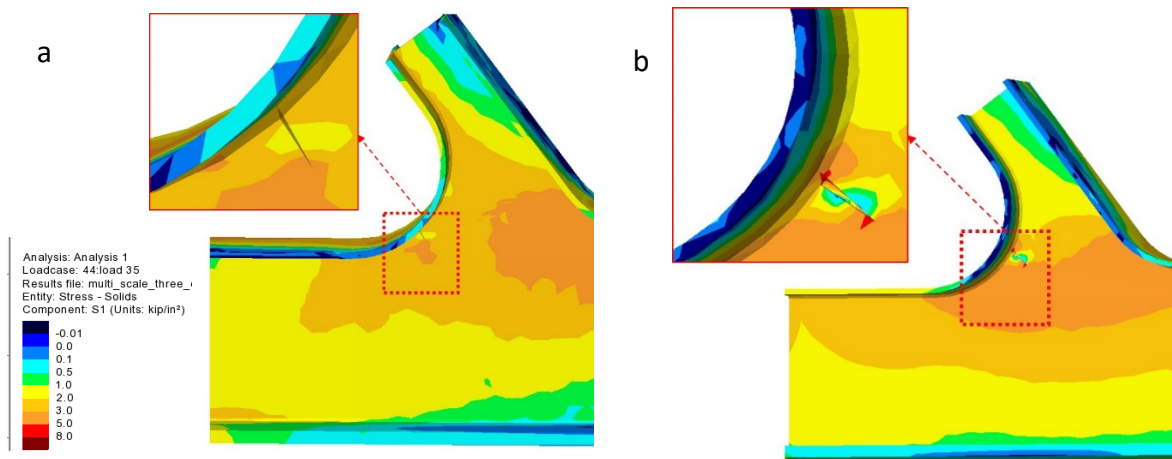


Figure 8-8 Stress contours at the cracked area of the gusset-less connection for a)75 mm crack, b) 125mm crack

In Figure 8-9, the time history stress results at the crack tip are shown in for four crack-size steps in the surface direction of the connection. Considerable changes in the peak value of the responses are observed with the increase in the crack size. The resulting numerical stress ranges

are extracted from the time-history stress responses to estimate K_{eq} . To compute K_{eq} , K_I and K_{II} are obtained exclusively for each step of crack propagation.

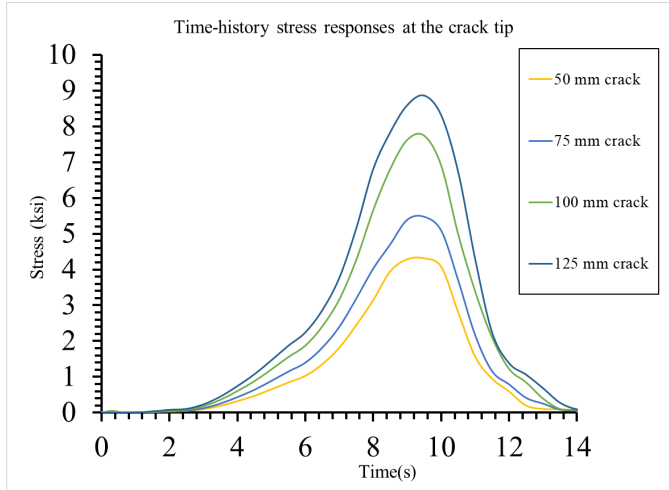


Figure 8-9 Time-history stress at the crack tip for four crack sizes

In Figure 8-10, the measured K_{eq} and K_I variations are shown, corresponding to the crack lengths in the planar direction of the web surface. The K_{th} is also determined in the graph. In the early iterations of crack propagation, the resulting K_I is demonstrated to be below the K_{th} , and technically the initiated crack may not propagate, as opposed to K_{eq} results. The observed difference highlights the significance of computing K_{eq} in fatigue crack propagation of complex welded structural components.

However, a similar trend is observed for the two crack modes, showing in the measured K_{eq} , the K_I is dominant as compared to K_{II} . In addition, it is illustrated that changes in the K_{eq} due to the crack increase in length is more significant, as compared to the through-the-thickness direction. In addition, the trend of SIF changes with the increase in the crack is not uniform throughout the entire crack propagation length. In practice, during the service life of the structural component, the crack growth rate will increase due to the material degradations. The computed

SIF (K_{eq} and K_I) will be utilized in the next section to evaluate the fatigue life of the concerning component under the propagated crack.

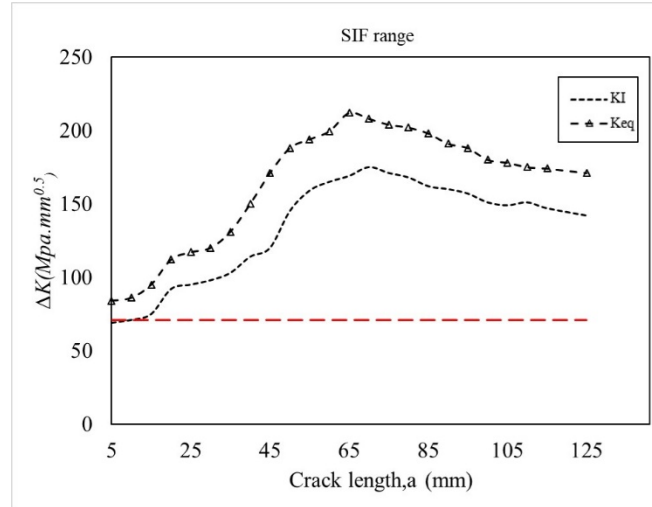


Figure 8-10 SIF variation in crack propagation considering mode I and mixed-mode crack conditions

8.9 Fatigue life prediction results using numerical data

The SIF values are obtained for different crack lengths. For each crack length, fatigue response of the gusset-less connection is calculated, using Paris's law. In Table 8-2, the details of Paris's law parameters are shown for the considered cracks at the gusset-less connection, recommended by IIW (22). In Figure 8-11, the resulting stress cycle variations are shown versus the increase in the crack size. The fatigue cycles are calculated for two crack modes, Mode I crack and mixed-mode crack. It is demonstrated that mixed mode fatigue crack propagates with a higher growth rate, as compared to the mode I crack. Consequently, a shorter fatigue remaining life can be estimated in using the mixed mode crack. However, in simulating the fatigue crack and fatigue life cycle estimation, it is essential to ensure that the mixed mode crack is more likely to happen, otherwise, the fatigue results can be overestimated.

The resulting trend of stress cycles can be utilized as a tool to determine the required inspection intervals of the component in the maintenance program of the bridge. The resulting remaining life of the component has also, a decisive impact on obtaining an efficient inspection program and determine the inspection intervals. During each inspection, the crack is required to be accurately computed and included in the M-S model to update the model and the resulting fatigue responses. Additionally, the stress cycles are required to be determined for the high stress ranges, causing a finite fatigue life.

Table 8-2 The LEFM properties applied for fatigue assessment of the gusset-less connection

m	C $(Mpa.mm^{0.5})$	K_{th} $(Mpa.mm^{0.5})$	a_i (mm)	a_f (mm)
3	5.21E13	63	5	125

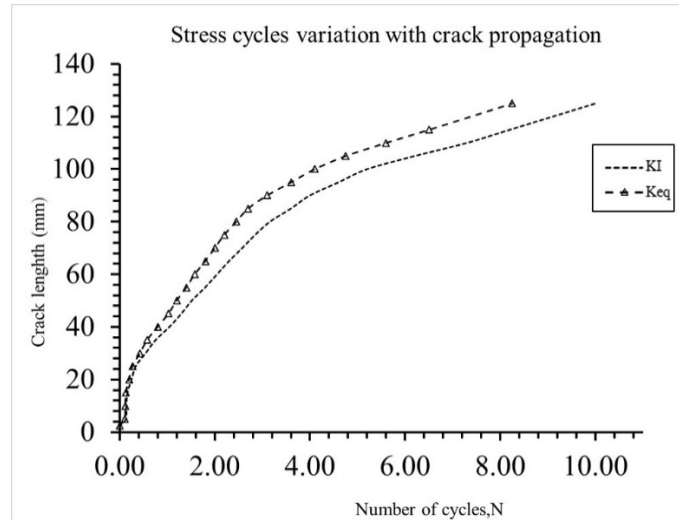


Figure 8-11 Fatigue cycle variation in crack propagation for two crack modes

8.10 Conclusion

In this study, a multi-scale global model is created to simulate crack propagation in the welded structural components. Through the multi-scale model, the crack-induced stress ranges can be obtained through the implemented dynamic traffic scenarios. It is demonstrated that the M-S model is an efficient tool in providing valuable information on structural degradations that occurs due to crack propagation. Therefore, it is recommended for a detected crack, develop a validated M-S FE model to precisely compute the stresses at the crack tip and the remaining fatigue cycles. In addition, in the design and implementation of a novel welded structural component, a validated M-S model allows for an understanding of the structural performance of the component and the candidate locations that are prone to fatigue. These locations can be prioritized for instrumentation in the structural health monitoring program of bridges. Other concluding remarks of the study are expressed in the following:

- Simulations of existing crack propagation for in-service welded structural components are dependent on the intuition of the structural behavior of the component, material properties, and welding history.
- The restricted information, however, may raise uncertainty in the obtained responses for measured stress intensity factors and fatigue life. For complex structural components, this information can be more restricted.
- The obtained fatigue responses through numerical stresses are required to be implemented with caution in bridge management program of in-service bridges having a detected fatigue crack, since the residual stresses at the welded area are not considered in the numerical results.

- The stress concentration area may not be captured through the installed strain rosettes at the gusset-less connection. Therefore, the nominal recorded strain at the bridge may not be applicable in fracture mechanics methods.

References

- 1) AASHTO. 2017. *ASHTO LRFD bridge design specifications, 8th ed.* Washington, DC: AASHTO.
- 2) Singh, I.V., Mishra, B.K., Bhattacharya,S., Patil, R.U. 2012. "The numerical simulation of fatigue crack growth using extended finite element method." *International Journal of Fatigue* 36: 109-119.
- 3) Wang, Y. , Wang, Z., and Zheng, Y. 2019. "Analysis of Fatigue Crack Propagation of an Orthotropic Bridge Deck Based on the Extended Finite Element Method." *Advances in Civil Engineering* 2019: 1-14.
- 4) Camas, D., Garcia-Manrique, J., Perez-Garcia, F., Gonzalez-Herrera, A. 2020, . "Numerical modelling of three-dimensional fatigue crack closure: Plastic wake simulation." *International Journal of Fatigue* In press.
- 5) Aygül, M., Al-Emrani,M., Barsoum, M. Leander, J. 2014. "An investigation of distortion-induced fatigue cracking under variable amplitude loading using 3D crack propagation analysis." *Engineering Failure Analysis* 45: 151-163
- 6) Albuquerque, C., Silva, A.L.L. M.P.de Jesus,A., Calçadaa, R. 2015. "An efficient methodology for fatigue damage assessment of bridge details using modal superposition of stress intensity factors." *International Journal of Fatigue* 61-77.
- 7) Irfae, M., Mahmoud, H.,. 2019. "Mixed-Mode Fatigue and Fracture Assessment of a Steel Twin Box-Girder Bridge." *Journal of Bridge Engineering* 24 (7): 04019056.
- 8) Andersson, T.L. 2005. *Fracture Mechanics: Fundamentals and Applications, Third edition* New York, USA: CRC Press Taylor and Francis Group.
- 9) Burdekin, F. M., and G. J. Yang. 1997. "Failure assessment diagrams for mixed mode loading and cracked tubular joints." *9th International Conference on Fracture*. Oxford, UK: Pergamon.: Advances in Fracture Research. 27-37.
- 10) Paris, P., and Erdogan, F. 1963. "A Critical Analysis of Crack Propagation Laws." *Journal of Basic Engineering* 85 (4): 528-533.
- 11) Radaj, D., Sonsino, C.M., Fricke,W. 2006. *Fatigue Assessment of Welded Joints by Local Approaches*. Edited by 2. Cambridge: Woodhead Publishing.
- 12) Sajith, S., Murthy, K.S.R.K., Robi,P.S. 2020. "Experimental and numerical investigation of mixed mode fatigue crack growth models in aluminum 6061-T6." *International Journal of Fatigue* 120: In Press.
- 13) Erdogan, F., and Sih, G. C. 1963. "On the Crack Extension in Plates Under Plane Loading and Transverse Shear." *J. Basic Eng.* 85 (4): 519-525.
- 14) Floros, D.,Ekberg, A., Larsson, F. 2019. "Evaluation of crack growth direction criteria on mixed-mode fatigue crack growth experiments." *International Journal of Fatigue* 129: In Press.
- 15) Venkatesan, K.R. 2016. *Subcycle Fatigue Crack Growth Formulation for Constant and Variable Amplitude Loading*. ARIZONA STATE UNIVERSITY.
- 16) Pais, M.J., and Kim, N.M. 2015. "Predicting fatigue crack growth under variable amplitude loadings with usage monitoring data." *Advances in Mechanical Engineering* 7 (12): 1-11.
- 17) Aygül,, M. 2013. *Fatigue evaluation of welded details –using the finite element method*. Gothenburg, Sweden: CHALMERS UNIVERSITY OF TECHNOLOGY.
- 18) Mashayekhi, M., Santini-Bell, E. 2018. "Three-dimensional multiscale finite element models for in-service performance assessment of bridges." *Computer-Aided Civil and Infrastructure Engineering* 34 (5): 385-401.
- 19) Maligno, A.R., Rajaratnam, S., Leen, S.B. , Williams, E.J. 2010. "A three-dimensional (3D) numerical study of fatigue crack growth using remeshing techniques." *Engineering Fracture Mechanics* 77: 94-111.

- 20) Wang, W., Hsu,C.T. T. 1994. "Fatigue crack growth rate of metal by plastic energy damage accumulation theory." *Journal of Engineering Mechanics* 120 (4): 776-795.
- 21) Beden, S. M., S. Abdullah, and A. K. A. Mohd Ihsan. 2009. "Review of fatigue crack propagation models for metallic components." *European Journal of Scientific Research* 28 (3): 364-397.
- 22) Hobbacher, A. 2008. *Recommendation for Fatigue Design of Welded Joints and Components*. Paris, France: The International Institute of Welding.

Chapter 9

CONCLUSIONS AND FUTURE WORK

The conclusions in this chapter express the findings of the study, presented in the previous chapters. In this study, a fatigue performance assessment protocol is developed for complex structural components of steel bridges. Multiple fatigue assessment methods were implemented in this protocol to evaluate the efficacy of each method in estimating the fatigue performance of complex components. The protocol is deployed to a case-study complex welded component, the gusset-less connection at the Memorial Bridge. The following results are obtained:

9.1 Fatigue assessment using nominal stress method

Complex structural components frequently experience complex loading conditions. However, the existing S-N curves are created based on the experimental fatigue tests under nominal stresses. Therefore, application of existing S-N curves for the fatigue assessment of complex structural components may result in overestimated fatigue lives. It is suggested to consider local fatigue assessment methods at welded areas of a target component for fatigue assessment. The local concentrated stresses at weld toes can be obtained through well-developed FE models.

9.1.1 Using SHM data

The SHM data are beneficial tools in reporting traffic conditions of bridges and resulting variable amplitude stress cycles at an investigating component, which are essential for fatigue assessment. However, current SHM data only notify surface strains. Therefore, the application of

SHM data for fatigue assessment becomes limited when through-the-thickness stresses (normal and shear) are considerable. As a consequence, SHM data may underestimate the vulnerability of complex structural components by overestimating the fatigue life of the component. It is recommended to consider field-collected SHM data as a supplementing source for the fatigue assessment of complex structural components.

9.1.2 Using numerical data

In this study, the field-collected SHM data are supplemented with numerical data for fatigue assessment application. A set of M-S global FE models are developed and implemented to model the Memorial Bridge to obtain the desired numerical stress responses, with reduced computational time. However, it was illustrated that the M-S global FE models require significant time and effort to create and the level of complexity of these models may preclude them for use in structural design. The inclusion of multiple element types and dimension requires appropriate coupling to capture both in-plane and out-of-plane structural performance. Also, the value of the structural responses of the M-S models are dependent on the defined coupling system, and the interface locations between the opposing dimensional elements. The efficient position of interfaces requires a thorough understanding of the structural performance of the bridge.

These complexities can make the M-S modeling more complicated and less practical for bridge design or condition assessment efforts. In addition, validating and updating an M-S model can be time-consuming and complicated, as compared to the simplified beam models. The complex M-S models of this study are recommended for research efforts. However, for practical applications, it is recommended to simplify the M-S model by considering a conservative distance for interface location from the stress concentrated areas. In a simplified M-S model, only a single

target structural component can be modeled using three-dimensional elements, while the remainder of members are modeled with simplified beam models. This simplified M-S model is suggested for modeling the details (e.g., bolts and weld sizes) in novel design of structural components. Additional challenges in the use of M-S models for fatigue assessment is the modeling of the complex weld geometry. The limited field-collected SHM data that report nominal stresses may not be applicable in the verification of hotspot stresses at a weld toe. Therefore, for in-service bridges, it is recommended to temporarily instrument welded area (e.g., with DIC cameras) to obtain the concentrated stresses along the weld toe for model validation purposes.

Traffic load simulation through a global FE model requires a comprehensive database of traffic information including the quantity, size, weight, speed of trucks. This information should be readily available from the bridge owner. . Alternatively, in this study, field-collected SHM data is integrated with traffic camera records at the Memorial Bridge for simulating traffic scenarios. However, in modeling large scale bridges with multiple lanes, simulation of traffic scenarios can be a more complicated task, which requires more specific information about the traveling trucks. In addition, the numerical time-history stress responses may not indicate the vehicle-deck interactions that exist in the field-collected SHM data. This interaction is not considered as part of this work.

In addition, integrating numerical and field-collected time-history responses for fatigue assessment and/or fatigue crack prediction requires quantification of existing random noises in the field-collected SHM data. It is necessary to clarify whether the detected random noises can influence the measured fatigue responses or not. Modification of numerical time-history stress responses with random noises can be an alternative that is suggested in integrating numerical and field-collected SHM data for fatigue assessment. However, the type and frequency of the

implemented noise are required to be consistent with the observed noises in the field-collected SHM data.

9.2 Fatigue assessment using hotspot stress method

Hotspot stresses at the gusset-less connection are obtained in this study, using SCF and interpolation of reference points. It is observed that a variable set of SCFs is obtained along radius of the weld toe of the gusset-less connection. Therefore, an exclusive SCF is required to be determined, corresponding to the direction of the installed strain gage (collecting nominal stresses). Consequently, the resulting hotpot stress may not be the maximum hotspot stress along the weld toe of the component, when the strain gage is not installed at the maximum critical location of the connection. However, SCF can be implemented to the field-collected SHM data for a quick estimate of fatigue responses at the weld toe.

The M-S model is created in this study to considering the requirements of the hotspot stress method at the gusset-less connection. The validated M-S model may better reflect the complex geometric impacts of the component on the resulting hotspot stresses at the weld toe. The model allows to evaluate the induced hotspot stresses under multiple traffic situations. The proposed M-S model can also be utilized during the design process of complex structural components of bridges to consider hotspot stresses in fatigue design of a complex welded component. In addition, for complex structural components with undetermined fatigue category, application of different nominal and hotspot fatigue categories may result in inconsistent fatigue responses for the component. As a consequence, it is recommended to consider multiple fatigue categories to find the appropriate category, which is more compatible with the characteristics of the component.

9.3 Fatigue response estimation due to an induced crack

9.3.1 Using SHM data

It is demonstrated that the measured fatigue responses, using field-collected strain responses of multiple strain gages of a component can have an exclusive and predictable correlation, which report the healthy condition of the component. Therefore, an irregular fatigue response that does not follow the determined correlation between the responses of the strain gages can alarm for a possible crack. A predicted crack can be reported to bridge managers for more detailed inspection, using non-destructive testing (NDT) methods. It is also illustrated that crack-induced fatigue responses can be predicted in the trend of measured fatigue responses using field-collected SHM data

However, successful damage detection is dependent on the damage's size, location, and distance to the installed strain gages. The created mathematical model in this study can be utilized in the management program of bridges to determine the inspection interval of a cracked component. However, insufficient strain gages may not successfully capture the deviant fatigue responses at the early stages of a fatigue crack. Therefore, for components with a detected crack, it is recommended to collect additional fatigue responses close to the crack tip, using temporarily installed sensors.

9.3.2 Using numerical model

Additionally, fatigue crack initiation and crack propagation can be investigated through a validated FE model. The M-S global model was created to consider fatigue crack in a global model. Simulation of fatigue crack propagation requires some necessary information of the crack type, rate of crack propagation, and material properties changes. However, in complex structural

components, this information may not be available. In addition, the crack propagation simulation can be based on the designer's assumptions, if the model is created during the design of the structural component. For in-service bridges, a more accurate investigation on crack propagation characteristics can be implemented, using the inspection results. In this case, visual inspection reports, or NDT results can be considered in the FE model to obtain a more accurate estimation of fatigue remaining cycles of a cracked component.

9.4 Suggestions for future research

Some related subjects are suggested to be considered in future studies for fatigue assessment of complex structural components in steel bridges, as expressed in the following:

- Investigate the geometric impacts of the complex component on the induced hotspot stresses and the fatigue responses by changing the properties of the weld, weld size, and the plate thickness through an M-S global model.
- Consider variable amplitude dynamic traffic loads and dynamic crack propagation process in estimating fatigue response.
- Simulate possible weld defects in an M-S model and investigate the crack propagation properties and the resulting fatigue response.
- Through a short-term instrumenting of the investigating connection (via e.g., DIC camera), provide information on the variability of the hotspot stress responses along the weld toe for more accurate model calibration.
- Implement other local fatigue assessment methods, including the notch stress methods, and compare the fatigue results.